CORROSION ON NOBLE, ACTIVE, AND PASSIVATING METALS

GALVANICALLY COUPLED TO ALUMINUM

A THESIS SUBMITTED TO THE GRADUATE DIVISION OF THE
UNIVERSITY OF HAWAI‘I AT MĀNOA

MASTER OF SCIENCE

IN

MECHANICAL ENGINEERING

MAY 2018

By

Sonya Ling

Thesis Committee:

Lloyd Hihara, Chairperson

Scott Miller

Weilin Qu

Acknowledgements

I would like to thank Dr. Lloyd Hihara for his support and guidance throughout my graduate program and this project. I am grateful for the opportunity to have worked in a lab that is supportive and studies relevant issues here in Hawaii, and these are a result of his encouraging attitude and knowledge.

I would also like to extend my gratitude toward Dr. Scott Miller and Dr. Weilin Qu for their feedback and assistance in the writing of my thesis, as well as their insight throughout my undergraduate and graduate programs.

To all the current and past members of the Hawai‘i Corrosion Lab, I am so astounded by the support and knowledge of each person and each member has made me a better researcher and person.

My predecessor and friend, Ms. Kate Quaimbao, I am eternally grateful for her support and confidence in my abilities to complete the project that she had worked so hard on. She is my role model and makes me strive to do thorough and insightful work.

Many thanks to my co-workers at Pearl Harbor Naval Shipyard and IMF for allowing me the time to pursue my educational and academic goals. I am grateful for the understanding and accommodations that helped facilitate the completion of my program and thesis.

Finally, my family and friends that have watched me grow as student, researcher and person. I am thankful for the words and acts of encouragement: the coffee, the food, and sustenance to fuel my body and mind. Mr. Daniel Wacek and Mr. Michael Coffman for assisting me in production and formatting of many of the figures and tables, this helped put my mind to

ease. To my parents, thank you for supporting me in all my academic endeavors and dreams. I would not be who I am and would not have accomplished this without their love and support.

Abstract

Aluminum is a readily available metal and can be alloyed to produce a material suitable for many applications. Its material properties and corrosion resistance has made it a popular alloy, especially for applications requiring lightweight materials. However, due to its active location in the galvanic series and EMF series, it can be very susceptible to galvanic corrosion. Hence, there have been many studies on the galvanic corrosion of aluminum coupled to more noble metals in the galvanic and EMF series. It is generally assumed that the noble metal in the galvanic couple with aluminum is cathodically protected and immune to corrosion. In an extensive galvanic corrosion study that was recently conducted (in diverse environments in Hawaii and in an accelerated corrosion test chamber) on aluminum coupled to noble (copper and silver) metals, various noble passivating (316 stainless steel and titanium 6Al-4V) alloys, a non-passivating (1018 carbon steel) alloy, significant amounts of corrosion product from plain carbon steel and even noble silver and copper metals were found on aluminum. In this study, the corrosion of the cathodic metals in the couple (i.e., silver, copper, 316 SS, Ti-6Al-4V, and 1018 mild steel), which have often been neglected, have been studied using 3-dimensional profilometry, x-ray diffraction, and weight loss to determine the extent of corrosion. Even miniscule amounts of corrosion product produced by the cathode can have significant effects on the corrosion of the anode aluminum.

Table of Contents

Table of Figures

List of Tables

List of Abbreviations

Al: Aluminum Alloy 6061-T6

Ag: pure Silver

Cu: pure Copper

CCTC: Cyclic Corrosion Test Chamber

LA: Lyon Arboretum

KIL: Kilauea

MCBH: Marine Corp Base Hawaii

1018 carbon steel: mild steel

SS: 316 Stainless Steel

Ti: Titanium Alloy 6Al-4V

w/: with

w/o: without

XRD: X-Ray Diffraction

1 Introduction

Industry always has to consider material properties when selecting building materials. With the wide array and availability of metals and numerous alloys, materials can be selected or mixed to optimize strength, durability, and cost-effectiveness. Aluminum has been used extensively in various applications for its ability to alloy with other metals to obtain desired material properties (e.g. strength and corrosion resistance) and relatively low cost. It also is a passivating metal, creating a protective layer once exposed to oxygen, allowing it to be corrosion resistant. This research focuses primarily on the corrosion of passivating metals (316 stainless steel and titanium alloy 6Al-4V), non-passivating active metals (1018 mild steel), and noble metals (copper and silver) when galvanically coupled to aluminum alloy 6061-T6. The corrosion of the cathodic metals in the galvanic couple is often neglected, but can have significant effects on the corrosion of the anode aluminum even if miniscule amounts of corrosion product produced by the cathode contaminates the anode aluminum surface.

1.1 Theory

Corrosion is a phenomena that affects metals when a difference in potential or environmental contributions are present. The galvanic cell, the foundation of galvanic corrosion, was discovered by Luigi Galvani, a Italian physician, in the eighteenth century during his studies of bimetallic materials [1]. The galvanic cell is comprised of a cathode and an anode, and converts chemical energy into electrical energy. Later in the nineteenth century, British chemist, Sir Humphry Davy, pioneered work in cathodic protection utilizing the theory behind the phenomena of galvanic corrosion. Iron and zinc were used to protect the copper lining of ship's hulls against the corrosive nature of seawater [2]. Sir Davy's protégé, Michael Faraday, discovered that the amount of reactant was proportional to the current times the duration of time

that the current flowed, modern day referred to as Faraday's Law [3]. The galvanic cell converts chemical energy to electrical energy. The effects of this phenomena occurs when two dissimilar metals form a circuit that allows electrons to flow from the anode to the cathode, called galvanic current. The electro-potential differences is the driving force for galvanic current that allows for oxidation and reduction reactions to occur and resulting in an increase in corrosion rate of the anode. In addition to corrosion induced by galvanic current, local corrosion can occur on the surface of the anode due to local cathodic sites formed as a result of the galvanic current. Thus, total corrosion rate, i_{total}, of the anode can be determined by the following equation

$$i_{total} = i_{galv} + i_{local} \quad \text{(Eq. 1)}$$

where i_{galv} is the corrosion rate due to galvanic coupling and i_{local} is the corrosion rate due to local cathodic sites. Local corrosion generally has been estimated by the taking the corrosion rate of the uncoupled metal.

Faraday's Law is used to determine the Galvanic corrosion of the anode by using the current flow.

$$\partial m = \frac{W\,\Delta t\,\Sigma_j I_j}{nF} \quad \text{(Eq. 2)}$$

where W is the atomic weight of the anode, Δt is time increment of each I, I is the galvanic current, j is the number of measurement iterations taken of I, n is the number of electrons transferred determined by the half-cell reaction, and F is Faraday's number (96,487 Coulombs).

Utilizing similar parameters from Equation 2, the penetration rate (PR) due to galvanic current can be calculated using the following equation

$$PR = \frac{Q\,W}{n\,F\,\rho\,t_{\text{exposure}}\,\alpha} \quad \text{(Eq. 3)}$$

where Q is the charge, ρ is the density of the anode, $t_{exposure}$ is the total exposure time, and α is the surface area of the anode exposed. Charge, Q, is calculated using the current and exposure time as follows:

$$Q = \Sigma_j \, I_j \, \Delta t \quad \text{(Eq. 4)}$$

Corrosion rate (CR) measures the mass loss due corrosion and is calculated from

$$CR = \frac{\partial m}{\alpha \, t_{exposure}} \quad \text{(Eq. 5)}$$

where $\delta m = m_{initial} - m_{final}$, the difference in mass of the sample prior to and post exposure, α is the surface area exposed, and $t_{exposure}$ is the time that the sample is exposed to the corrosive environment. Furthermore, penetration rate (PR) can be determined using the following relationship with corrosion rate

$$PR = \frac{CR}{\rho_{metal}} \quad \text{(Eq. 6)}$$

where ρ_{metal} is the density of the metal or alloy.

1.2 Background

The EMF Series gives standard potentials for pure metals and the Galvanic Series gives corrosion potentials for alloys that allows for the determination of the cathode and anode when two metals are compared or paired. On both series, Ti, Fe, Cu, and Ag have higher potentials compared to Al, indicating that these metals act as the cathode when coupled to Al.

The metals and alloys studied are categorized into three types: passivating, non-passivating active, and noble. Passivating metals are metals that form a protective layer on the surface of the metal when exposed to passivating environments, resulting in corrosion resistance.

Aluminum, as well as titanium and stainless steels, are known for their passivating behavior that lends them to be utilized in moist environments. Non-passivating (active) metals are those metals and alloys that react with water and undergoes significant oxidation resulting in corrosion. 1018 steel is susceptible to corrosion while exposed to moist environments. Noble metals resist corrosion and oxidation and are considered stable. Copper and silver are considered noble metals due to their positive position in the EMF Series.

The composition of the cathode alloy is important to consider in local corrosion of the anode due to the effects of leaching. When an alloy corrodes, the alloying elements may leach to the surface of the metal, creating local cathodic sites, hence increasing the corrosion rate.

Table 1: Elemental composition of the alloys used in this study.

Aluminum Alloy 6061-T6		316 Stainless Steel		Titanium Alloy 6Al-4V		1018 Carbon Steel	
Si	0.4-0.8%	Cr	18%(max)	Al	6%	C	0.14-0.20%
Mg	0.8-1.2%	Ni	14%(max)	V	4%	Mn	0.60-0.90%
Cu	0.15-0.4%	Mo	3%(max)	Fe	0.25%(max)	P	0.040%(max)
Fe	0.7%(max)	Mn	2%(max)	O	0.2%(max)	S	0.050%(max)
Zn	0.25%(max)	Si	1%(max)				
Mn	0.15%(max)	Cr	0.08%(max)				
Ti	0.15%(max)	P	0.045%(max)				
Cr	0.04-0.35%	S	S 0.03%(max)				

Furthermore, the environmental conditions that metal is exposed to is another factor that can affect the corrosion properties of a metal. An example of this effect of halogen ions on normally passivating metals. The most aggressive halogen ion, Chloride (Cl^-), penetrates the passive film, and by doing so results in pitting corrosion.

1.3 Research Objectives

The following research focused on how passivating (316 stainless steel and titanium alloy 6Al-4V), non-passivating active (1018 mild steel), and noble metals (Cu and Ag) behaved when coupled to aluminum alloy 6061-T6. This study investigates the effects of galvanic corrosion on the aforementioned metals and alloys when coupled to the aluminum alloy 6061-T6 and exposed to different environments. Hawaii's diverse microclimates allows for thorough and centralized studies; the four exposure sites are as follows: Lyon Arboretum, a rainforest environment; Marine Corp Base Hawaii (MCBH), a highly corrosive marine environment; Kilauea, a volcanic and high altitude environment; and the Cyclic Corrosion Test Chamber (CCTC), a standard of testing accelerated outdoor corrosion.

Corrosion of the cathodic samples were noted when the samples were collected from the exposure site. The preliminary observation of corrosion on the cathode was unexpected due the theory behind corrosion and galvanic corrosion as previously covered. Simultaneously, there was indication of potential contamination by the cathode corrosion by-product onto the anode. Thus, the cathodic samples were further investigated to obtain and determine quantitative data on the actual corrosion damage incurred on the cathodic samples.

Experimental procedures that were employed following the exposure of the sample couplings include the standardized cleaning and development of cleaning procedure for silver to determine mass loss, calculations of mass loss, corrosion rates, and penetration rates, and the surface analysis by utilizing a X-Ray Diffraction (XRD) machine in conjunction with the powder diffraction X-ray (PDXL) software and a 3-D Profilometer.

The data collected for the aluminum alloy and anodic samples from this study has been analyzed in a written thesis by Ms. Kathleen Quiambao.

2 Literature Review

2.1 Galvanic Corrosion in Atmospheric Environment

Field studies and experiments were performed to gain more insight on the relationship between Aluminum alloy 1050 when galvanically coupled with various metals and the effects of environmental atmosphere on the corrosion rates by Doyle and Wright. The alloys and metals that were coupled to AA1050 were mild steel, copper, lead, monel, graphite, 304 stainless steel, chromium plated steel, and galvanized steel. The experimental set up utilized a fastener made of the aforementioned cathodic metals and a wire produced from AA1050 was wrapped around the threads of the fastener. These metal couples were then exposed to various environments across Canada, North Carolina, USA, and North Africa, in aggressive marine and industrial conditions. Corrosion rate was determined by the mass loss of the anode . Doyle and Wright ranked the environments based on the resulting mass loss and determined that the marine environment yielded greater corrosion rates. Furthermore, the proximity to the ocean was determined to be a contributing factor as well. The samples that were exposed 250 meters away from the ocean experienced a drastic decrease in the effects of galvanic corrosion when compared to those samples that were 25 meters away from the ocean [4].

2.2 Galvanic Corrosion in Immersion Environment

Galvanic corrosion studies have been done on various metal couplings. Notably, Mansfeld and Kenkel galvanically coupled Aluminum alloy 6061 to copper and titanium alloy 6Al-4V and exposed those couples to 3.5% NaCl, tap water, and distilled water. The weight loss data was taken to determine the galvanic effects on corrosion. For AA 6061, the samples experienced the most galvanic effects when coupled to copper and the least when coupled to Ti 6Al-4V in all three solutions [5].

Another study was performed on high alloy stainless steels (i.e., 316 stainless steel, 22% Cr duplex stainless steel, alloy 825) in sea water. High alloy stainless steels was studied when coupled to other metals (carbon steel, copper alloys, nickel based alloys, titanium, graphite) and the corrosion rate was determined from various other studies. The effects on these metals when used in different components within a sea water system was addressed and means of protection were discussed. Coatings, inserts to prevent contact between dissimilar metals, and sacrificial parts were recommended as preventive actions for the different components (valves, heat exchangers, piping) in order to prolong the system operationality. Furthermore, Francis determined that the effects of galvanic corrosion when coupled to other passive alloys could be negated, however, the metals are still susceptible to crevice corrosion. Furthermore, he discusses the behavior of these high alloy stainless steels as similar when exposed to sea water [6].

3 Materials and Methods

There were various configurations that were used when exposing the metals and alloys of interest (i.e., AA 6061-T6, pure Cu, pure Ag, Ti 6Al-4V, 316 stainless steel, 1018 carbon steel). The samples were prepped to be 2 inch by 1 inch with varying thicknesses, depending on the metal. Those samples that were coupled had a hole with diameter of 0.25 inch drilled in the center of the crevice area (a section 1inch by 1 inch). The couples were fastened together using a non-conductive, glass reinforced polyurethane fastener. Loggers were attached to a few of the coupled samples. Those samples that had loggers attached also had a non-conductive, sheet of G10 fiberglass to prevent metal-to-metal contact. For the environmental exposure sites (i.e., Lyon Arboretum, MCBH, Kilauea), four uncoupled samples were exposed along with four sets of coupled samples, without loggers attached and in configurations of the AA 6061-T6 was on top and with the cathodic metal on top, for each cathodic metal of interest. In addition, three sets of coupled samples were exposed at these sites with the cathodic metal on top of the AA6061-T6 sample and a logger attached.

Detailed description of the experimental set up can be found in a thesis written by Quiambao [7].

3.1 Experimental Procedures

The methods utilized include X-Ray Diffraction (XRD) machine in conjunction with the powder diffraction X-ray (PDXL) software and a 3-D Profilometer.

3.1.1 XRD Method

A Rigaku MiniFlex II Desktop XRD was utilized to obtain the surface composition. The parameters used for the XRD when performing scans were taken in counts-per-second and

continuous. The start angle was 3 degrees and stop angle was set to 90 degrees with a sampling power at 30kV and 15 mA.

3.1.2 3-D Profilometer Method

A Micro Photonics micro measure system, 3-D profilometer, was used to take the surface roughness of the selected sample. An area 1 mm by 50 mm was taken along the length of the sample on side opposite of the pin stamp markings and starting in the crevice region. For the 3-D profilometer, the scanning was performed using a micromeasure optical pen with a measurement range of 3 mm, spot diameter of 25 μm, accuracy of 600 nm, and minimum measurable thickness of 220 μm at a scanning velocity of about 2 mm/second.

3.2 Test Sites

The four test sites utilized for this study were Lyon Arboretum, Marine Corp Base Hawaii, Kilauea, and Cyclic Corrosion Test Chamber. The variation in test sites allowed for data to be collect for different effects of the atmosphere on the galvanic couples.

3.2.1 Lyon Arboretum

Located in Manoa on Oahu, Lyon Arboretum is a rainforest type environment where moist and wet conditions exist for most of the year. The constant moisture allowed for the analysis of the effect of water and organic materials on galvanic couples. The temperature at this location for the duration of the exposure ranged from 15°C to 40°C.

3.2.2 Marine Corp Base Hawaii

The Marine Corp Base Hawaii in Kaneohe exposure site is on the coastline. This close proximity to the ocean and the high level of chlorides classifies the location as a severe marine

environment. Also, the location exposes the samples to sea salt from the wave breaks and in the air. The location's temperature ranged from 15°C to 37°C.

3.2.3 Kilauea

The exposure location on Kilauea is located in Hawaii Volcanoes National Park on the Big Island. This site subjects the samples to the natural release of sulfur from the volcano, as well as the chlorides in the air from the ocean. The temperatures during the deployment time ranged from 11°C to 39°C. Kilauea does not have much vegetation around the exposure site or any other means of providing shade.

3.2.4 Cyclic Corrosion Test Chamber

The samples to undergo the CCTC were subjected to an accelerated corrosion test in accordance with the GM-9540P, a standardized corrosion test. The test comprised of salt solutions of sodium chloride, calcium chloride, and sodium bicarbonate. The samples were placed horizontally. Each cycle of the GM-9540P test takes 24-hours and cycles through a series of the aforementioned salt sprayed onto the surface at room temperature. Following the spray was an eight-hour period of 100% humidity at 49°C. Finally, a dry period at 60°C occurred prior to repeating the cycle. This cycle was repeated for a total of 30 cycles.

4 Results

4.1 Penetration Rate and Mass Loss

The exposed specimen were collected, cleaned, and weighed to determine mass loss. 316 SS (Stainless Steel), AA 6061-T6, and pure Cu species were cleaned in chemical solutions in accordance with the ASTM G1 “Standard Practice for Preparing, Cleaning, and Evaluating Corrosion Test Specimens”. The cleaning mechanism employed for AA6061-T6 was a solution of phosphoric acid and chromium trioxide. pure copper was cleaned in a solution of hydrochloric acid and distilled water. 316 SS was dipped into a cleaning solution comprised of nitric acid and water. Whereas the other metal specimens were cleaned chemically, the Ti 6Al-4V samples ultrasonically cleaned in de-ionized water at room temperature for 15 minutes to remove the corrosion product. Furthermore, 1018 steel samples were glass bead blast to remove corrosion product. However, due to the absence of a standard method by which to clean pure Ag, Goddards Silver Dip™, a commercial silver cleaner, was employed to remove the impurities. A preliminary test of the silver dip was performed in order to determine whether significant mass loss would be experienced. Virgin pure silver pieces were weighed then submerged and soaked in the silver dip for one minute intervals, washed in liquinox soapy water, rinsed with de-ionized water, dried with a paper towel, and placed in a dry box for 30 minutes and reweighed. This process was repeated three times, with no significant mass change—less than 0.001 grams in mass change. The fourth and final time the process was repeated with a 15 minute soak period vice the one minute interval. Similarly, the resulting mass difference was insignificant, it being less than 0.001 grams in mass change. The pure Ag samples were then cleaned by first sonicating the samples for ten minutes, drying them with a paper towel and then placed into the dry box for 30 minutes. Next, the samples were soaked in the silver dip for 15 minutes, rinsed with tap

water, sonicated for five minutes, rinsed with de-ionized water, dried with a paper towel, and then placed in the dry box for an hour. The samples were then re-weighed and the process was repeated until the mass change was less than 0.001 grams.

The average penetration rate was calculated for each of the metals and alloys (Ti 6Al-4V, 316 stainless steel, 1018 steel, pure Cu, and pure Ag) for the four environments. Within each environment, the penetration rate was determined for the multiple configurations; each location had an uncoupled, coupled on top of AA6061-T6 with logger attached, coupled on top of AA6061-T6 without logger attached, and coupled below AA6061-T6 without logger attached. For CTCC, the configuration of metal coupled with AA6061-T6 on top with a logger attached was also included.

Mass loss was determined by taking the difference between the initial and post exposure mass for each cleaned sample. Penetration rate was calculated utilizing Equation 6 and parameters in

Table 7 for each cleaned sample, where density for pure Cu and pure Ag were taken from the periodic table. The average of the three cleaned samples was taken for each configuration (uncoupled, Al-on top, X-on top) to determine the average PR. Surface area, α, for the uncoupled samples was treated as a rectangular piece, whereas the coupled samples took account for the decrease due to the hole created for the fastener. The average penetration rates for each metal and alloy are dictated on

Table 2 thru Table 6.

Table 2: Average penetration rate of pure Cu coupled to AA6061-T6 in mm per year.

Exposure site	Uncoupled	Coupled with logger		Coupled without logger	
		AA6061-T6 on top	Pure Cu on top	AA 6061-T6 on top	Pure Cu on top
	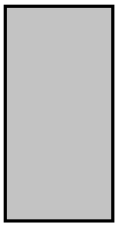	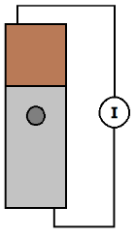	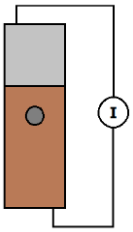	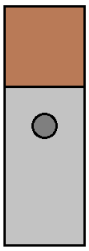	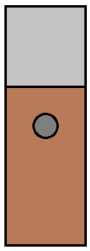
CCTC	2.74E-02	1.55E-02	1.61E-02	1.26E-02	1.10E-02
MCBH	1.32E-02		6.98E-03	7.08E-03	7.74E-03
LA	2.97E-03		1.39E-03	9.79E-04	1.33E-03
KIL	4.39E-03		2.34E-03	2.27E-03	2.18E-03

Table 3: Average penetration rate of pure Ag coupled to AA 6061-T6 in mm per year.

Exposure site	Uncoupled	Coupled with logger		Coupled without logger	
		AA 6061-T6 on top	Pure Ag on top	AA 6061-T6 on top	Pure Ag on top
	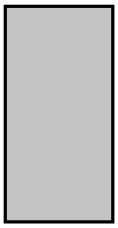	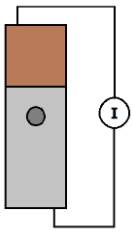	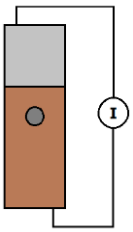	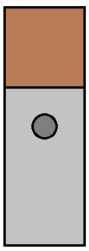	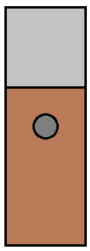
CCTC	2.51E-03	1.67E-03	1.24E-03	4.10E-03	2.35E-03
MCBH	8.01E-04		3.46E-04	2.26E-04	2.61E-04
LA	8.70E-04		2.51E-04	2.03E-04	2.45E-04
KIL	1.47E-03		3.71E-04	4.32E-04	3.74E-04

Table 4: Average penetration rate of Ti 6Al-4V coupled to AA 6061-T6 in mm per year.

Exposure site	Uncoupled	Coupled with logger		Coupled without logger	
		AA 6061-T6 on top	Ti 6Al-4V on top	AA 6061-T6 on top	Ti 6Al-4V on top
	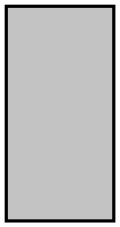	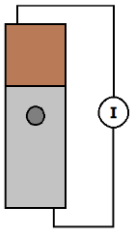	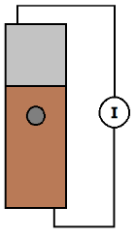	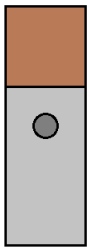	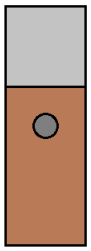
CCTC	-9.10E-04	-6.58E-03	-3.22E-03	-1.48E-02	-5.00E-03
MCBH	-2.89E-05		-2.41E-04	-7.96E-04	-9.79E-04
LA	-6.50E-05		-1.17E-04	-9.79E-04	-5.04E-04
KIL	0.00E+00		-1.48E-05	-6.75E-04	-5.19E-04

Table 5: Average penetration rate of 316 Stainless Steel coupled to AA 6061-T6 in mm per year.

Exposure site	Uncoupled	Coupled with logger		Coupled without logger	
		AA 6061-T6 on top	316 SS on top	AA 6061-T6 on top	316 SS on top
	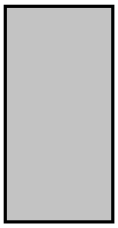	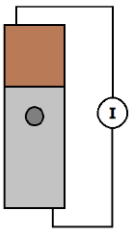	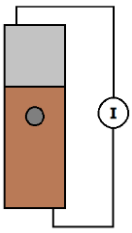	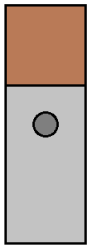	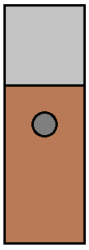
CCTC	1.26E-04	1.45E-04	9.08E-05	1.09E-04	7.27E-05
MCBH	1.48E-04		2.02E-05	2.81E-02	-1.65E-03
LA	2.00E-05		2.42E-05	2.42E-05	3.23E-05
KIL	5.67E-05		5.74E-05	4.92E-05	4.10E-05

Table 6: Average penetration rate of 1018 steel coupled to AA 6061-T6 in mm per year.

Exposure site	Uncoupled	Coupled with logger		Coupled without logger	
		AA 6061-T6 on top	1018 Steel on top	AA 6061-T6 on top	1018 Steel on top
	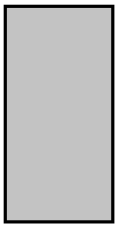	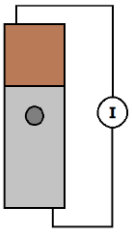	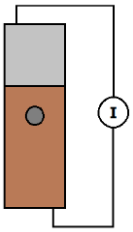	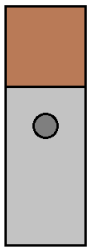	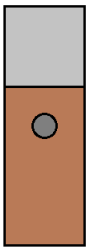
CCTC	2.65E+00	1.34E+00	1.52E+00	1.90E+00	1.76E+00
MCBH	1.07E+00		5.53E-01	6.23E-01	5.68E-01
LA	9.03E-02		1.14E-01	1.22E-01	1.21E-01
KIL	9.93E-02		7.44E-02	8.00E-02	7.74E-02

Table 7: Parameters used to calculate mass loss and penetration rate.

	316 Stainless Steel	Ti 6Al-4V	1018 Steel	Pure Cu	Pure Ag
$\alpha_{uncoupled}$ [cm^2]	28.01	28.23	30.65	28.36	27.43
$\alpha_{coupled}$ [cm^2]	27.67	27.91	30.65	28.06	27.01
ρ [g/cm^2]	8.00 [8]	4.42 [9]	7.87 [10]	8.94	10.49
t_{CTCC} [days]	30	30	30	30	30
t_{KIL} [days]	133	133	133	133	133
$t_{LA/MCBH}$ [days]	135	135	135	135	135

4.2 Corrosion morphology

The corrosion morphology was of interest for the cathodic samples and both the macroscopic and microscopic aspects were addressed. The coupons were scanned post-exposure and again after cleaning. An XRD with the PDXL software was utilized to analyze the surface of the uncleaned specimen to determine the compound make up on interfacial area. Additionally, a 3D micro-measurement was taken of a small area, one millimeter wide along the length of the

sample. This was done to obtain the surface roughness and topography of a small cross-section of each sample. Surface analysis utilizing the XRD was performed on one sample of the uncoupled, coupled without logger with AA 6061-T6 on top, and coupled without logger with X-on top configurations from each of the locations. Each of these samples was left with corrosion product and environmental impact intact, without cleaning. The topography measurements were taken on cleaned samples, one for each configuration. The samples that were measured was determined by taking the samples that exhibited the greatest mass loss percentage.

4.2.1 Macroscopic

The exposed samples were scanned for pure Cu, pure Ag, 316 stainless steel, 1018 steel, and AA 6061-T6 and are on Table 8 through Table 35**Error! Reference source not found.**; Ti 6Al-4 was not scanned prior to cleaning. Similarly, once the samples were cleaned, they were scanned again and documented on Table 36 through Table 55. The tables show the samples from the various configurations: uncoupled, coupled with loggers AA 6061-T6 on top or X-on top, and coupled without loggers AA 6061-T6 on top or X-on top.

4.2.1.1 Post Exposure Specimen

Samples were documented after collection from the exposure sites. The metal samples in the following tables include: pure Cu, pure Ag, 316 stainless steel, 1018 steel, and AA 6061-T6. The post exposure scans for AA 6061-T6 coupons that were coupled to pure Cu, pure Ag, and 1018 steel were included to provide more insight in the reaction of these combinations.

Table 8: Pure copper samples exposed to Lyon Arboretum pre-cleaning. First row: 1C1, 1CL1, 1CX1, 1CX5 Front and back. Second row: 1C2, 1CL2, 1CX2,1CX6 Front and back. Third row: 1C3, 1CL3, 1CX3, 1CX7 Front and back.

Pure Copper: Lyon Arboretum							
Uncoupled Front	Uncoupled Back	Coupled w/ Logger Front Cu on top	Coupled w/ Logger Back Cu on top	Coupled w/o Logger Front AA 6061-T6 on top	Coupled w/o Logger Back AA 6061-T6 on top	Coupled w/o Logger Front Cu on top	Coupled w/o Logger Back Cu on top
							
							
							

Table 9: Pure copper samples exposed to Marine Corp Base Hawaii pre-cleaning. First row: 2C1, 2CL1, 2CX1, 2CX5 Front and back. Second row: 2C2, 2CL2, 2CX2, 2CX6 Front and back. Third row: 2C3, 2CL3, 2CX3, 2CX7 Front and back.

Pure Copper: MCBH							
Uncoupled Front	Uncoupled Back	Coupled w/ Logger Front Cu on top	Coupled w/ Logger Back Cu on top	Coupled w/o Logger Front AA 6061-T6 on top	Coupled w/o Logger Back AA 6061-T6 on top	Coupled w/o Logger Front Cu on top	Coupled w/o Logger Back Cu on top
							
							
							

Table 10: Pure copper samples exposed to Kilauea pre-cleaning. First row: 3C1, 3CL1, 3CX1, 3CX5 Front and back. Second row: 3C2, 3CL2, 3CX2, 3CX6 Front and back. Third row: 3C3, 3CL3, 3CX3, 3CX7 Front and back.

Pure Copper: Kilauea							
Uncoupled Front	Uncoupled Back	Coupled w/ Logger Front Cu on top	Coupled w/ Logger Back Cu on top	Coupled w/o Logger Front AA 6061-T6 on top	Coupled w/o Logger Back AA 6061-T6 on top	Coupled w/o Logger Front Cu on top	Coupled w/o Logger Back Cu on top
							
	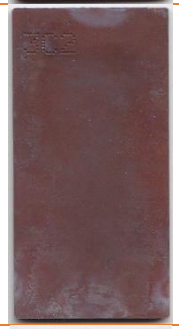						
							

Table 11: Pure copper samples exposed to CCTC pre-cleaning. First row: 4C1, 4CL4, 4CX1, 4CX5, 4CL1 Front and back. Second row: 4C2, 4CL5, 4CX2, 4CX6, 4CL2 Front and back. Third row: 4C3, 4CL6, 4CX3, 4CX7, 4CL3 Front and back.

Pure Copper: CCTC									
Uncoupled Front	Uncoupled Back	Coupled w/ Logger Front Cu on top	Coupled w/ Logger Back Cu on top	Coupled w/o Logger Front AA6061-T6 on top	Coupled w/o Logger Back AA6061-T6 on top	Coupled w/o Logger Front Cu on top	Coupled w/o Logger Back Cu on top	Coupled w/ Logger Front AA6061-T6 on top	Coupled w/ Logger Back AA6061-T6 on top
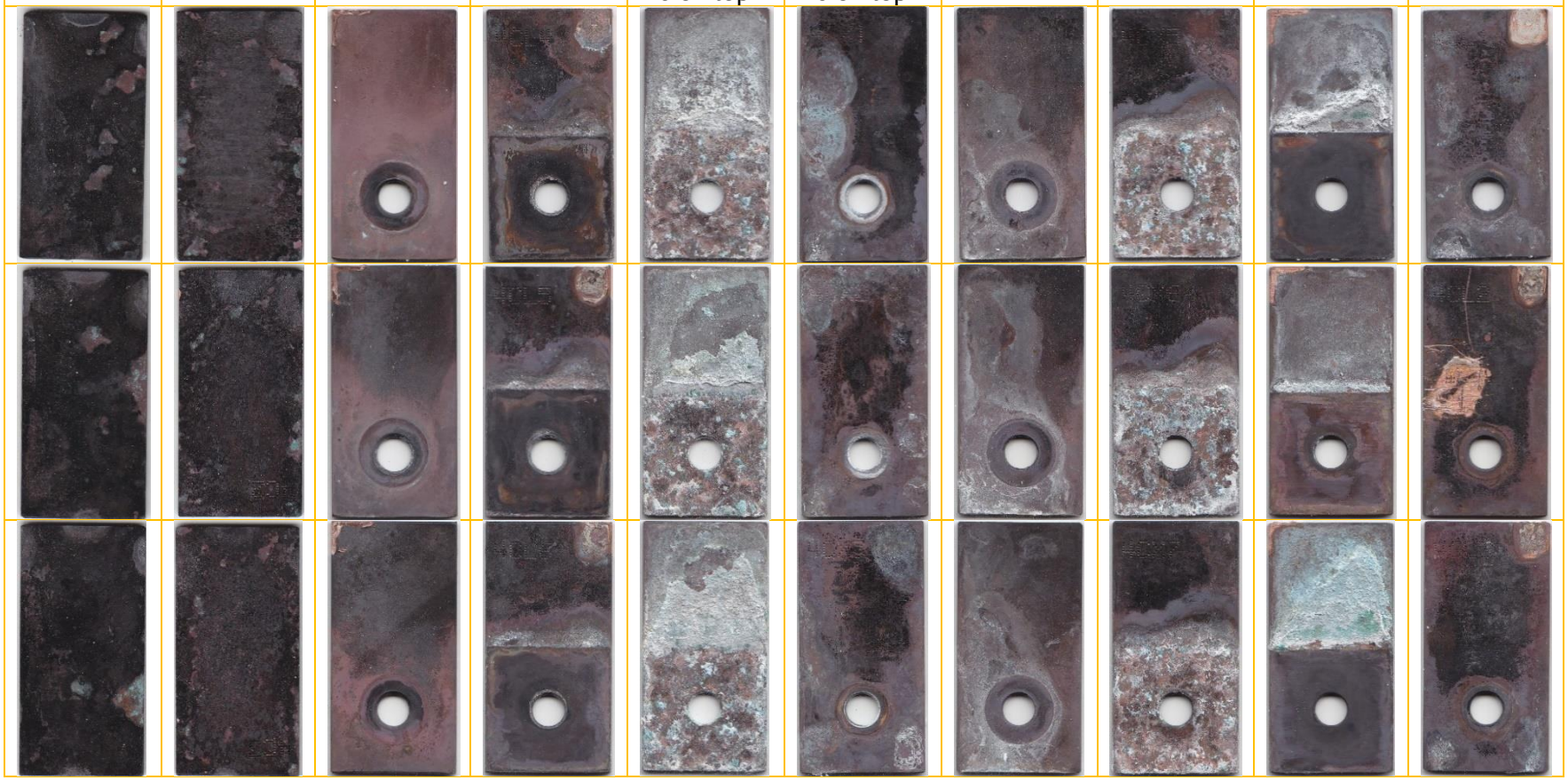									

Table 12: Pure silver (Ag) samples exposed to Lyon Arboretum pre-cleaning. First row: 1B1, 1BL1,1BX1, 1BX5 Front and back. Second row: 1B2, 1BL2, 1BX2, 1BX6 Front and back. Third row: 1B3, 1BL3, 1BX3, 1BX7 Front and back.

Pure Silver: Lyon Arboretum							
Uncoupled Front	Uncoupled Back	Coupled w/ Logger Front Ag on top	Coupled w/ Logger Back Ag on top	Coupled w/o Logger Front AA 6061-T6 on top	Coupled w/o Logger Back AA 6061-T6 on top	Coupled w/o Logger Front Ag on top	Coupled w/o Logger Back Ag on top
							
							
							

Table 13: Pure silver (Ag) samples exposed to Marine Corp Base Hawaii pre-cleaning. First row: 2B1, 2BL1,2BX1, 2BX5 Front and back. Second row: 2B2, 2BL2, 2BX2, 2BX6 Front and back. Third row: 2B3, 2BL3, 2BX3, 2BX7 Front and back.

Pure Silver: MCBH							
Uncoupled Front	Uncoupled Back	Coupled w/ Logger Front Ag on top	Coupled w/ Logger Back Ag on top	Coupled w/o Logger Front AA 6061-T6 on top	Coupled w/o Logger Back AA 6061-T6 on top	Coupled w/o Logger Front Ag on top	Coupled w/o Logger Back Ag on top
							
							
							

Table 14: Pure silver (Ag) samples exposed to Kilauea pre-cleaning. First row: 3B1, 3BL1, 3BX1, 3BX5 Front and back. Second row: 3B2, 3BL2, 3BX2, 3BX6 Front and back. Third row: 3B3, 3BL3, 3BX3, 3BX7 Front and back.

Pure Silver: Kilauea							
Uncoupled Front	Uncoupled Back	Coupled w/ Logger Front Ag on top	Coupled w/ Logger Back Ag on top	Coupled w/o Logger Front AA 6061-T6 on top	Coupled w/o Logger Back AA 6061-T6 on top	Coupled w/o Logger Front Ag on top	Coupled w/o Logger Back Ag on top
							
							
							

Table 15: Pure silver (Ag) samples exposed to CCTC pre-cleaning. First row: 4B1, 4BL4, 4BX1, 4BX5, 4BL1 Front and back. Second row: 4B2, 4BL5, 4BX2, 4BX6, 4BL2 Front and back. Third row: 4B3, 4BL6, 4BX3, 4BX7, 4BL3 Front and back.

Pure Silver: CCTC									
Uncoupled Front	Uncoupled Back	Coupled w/ Logger Front Ag on top	Coupled w/ Logger Back Ag on top	Coupled w/o Logger Front AA 6061-T6 on top	Coupled w/o Logger Back AA 6061-T6 on top	Coupled w/o Logger Front Ag on top	Coupled w/o Logger Back Ag on top	Coupled w/ Logger Front AA 6061-T6 on top	Coupled w/ Logger Back AA 6061-T6 on top
									
									
									

Table 16:316 Stainless Steel (SS) samples exposed to Lyon Arboretum pre-cleaning. First row: 1E1, 1EL1, 1EX1, 1EX5 front and back. Second row: 1E2, 1EL2, 1EX2, 1EX6 front and back. Third row: 1E3, 1EL3, 1EX3, 1EX7 Front and back.

316 Stainless Steel: Lyon Arboretum							
Uncoupled Front	Uncoupled Back	Coupled w/ Logger Front 316 SS on top	Coupled w/ Logger Back 316 SS on top	Coupled w/o Logger Front AA 6061-T6 on top	Coupled w/o Logger Back AA 6061-T6 on top	Coupled w/o Logger Front 316 SS on top	Coupled w/o Logger Back 316 SS on top
							
							
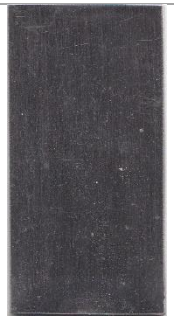							

Table 17: 316 Stainless Steel (SS) samples exposed to MCBH pre-cleaning. First row: 2E1, 2EL1 ,2EX1, 2EX5 front and back. Second row: 2E2, 2EL2, 2EX2, 2EX6 front and back. Third row: 2E3, 2EL3, 2EX3, 2EX7 front and back.

316 Stainless Steel: MCBH							
Uncoupled Front	Uncoupled Back	Coupled w/ Logger Front 316 SS on top	Coupled w/ Logger Back 316 SS on top	Coupled w/o Logger Front AA 6061-T6 on top	Coupled w/o Logger Back AA 6061-T6 on top	Coupled w/o Logger Front 316 SS on top	Coupled w/o Logger Back 316 SS on top
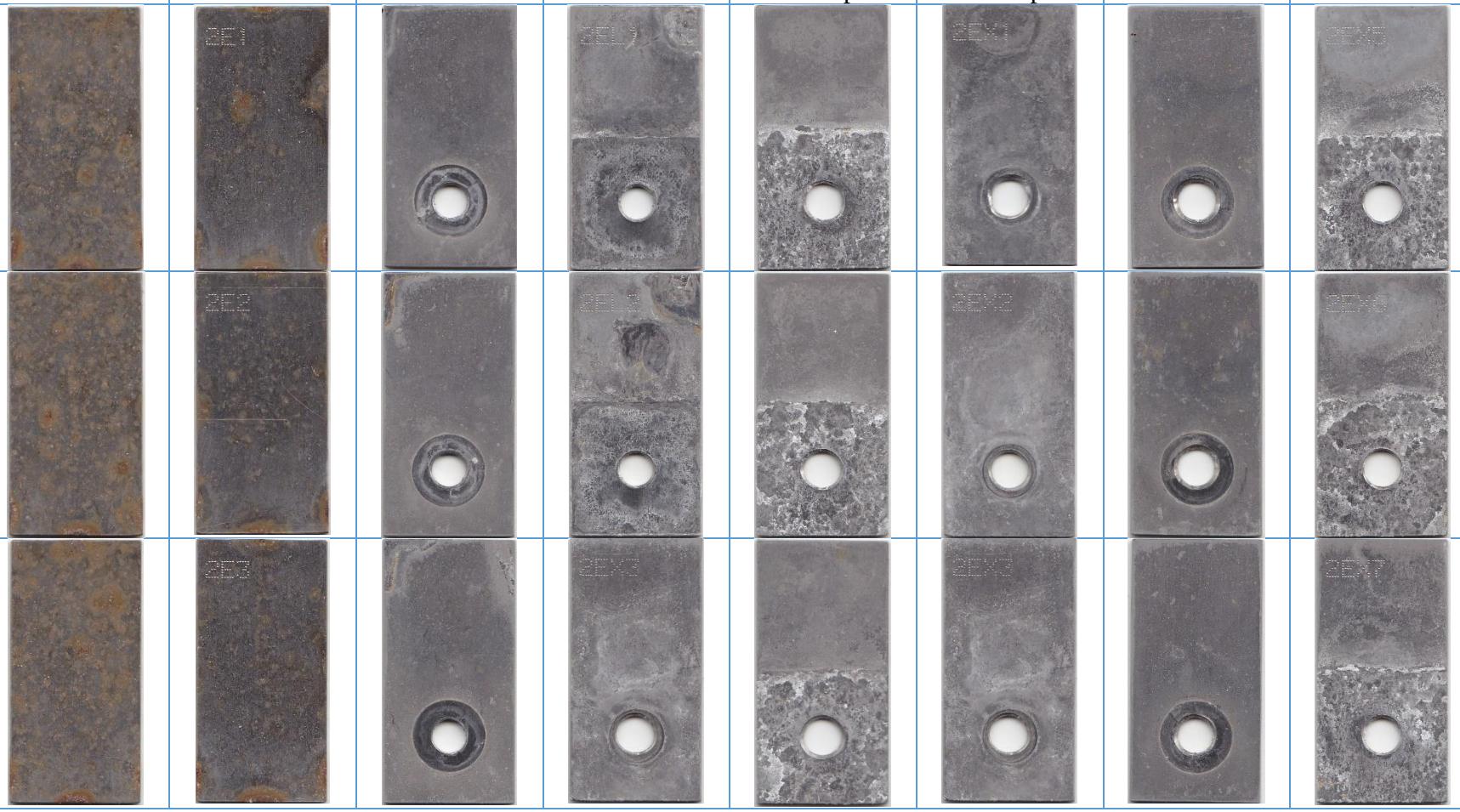							

Table 18: 316 Stainless Steel (SS) samples exposed to Kilauea pre-cleaning. First row: 3E1, 3EL1, 3EX1, 3EX5 front and back. Second row: 3E2, 3EL2, 3EX2, 3EX6 front and back. Third row: 3E3, 3EL3, 3EX3, 3EX7 front and back.

316 Stainless Steel: Kilauea							
Uncoupled Front	Uncoupled Back	Coupled w/ Logger Front 316 SS on top	Coupled w/ Logger Back 316 SS on top	Coupled w/o Logger Front AA 6061-T6 on top	Coupled w/o Logger Back AA 6061-T6 on top	Coupled w/o Logger Front 316 SS on top	Coupled w/o Logger Back 316 SS on top
							
							
							

Table 19: 316 Stainless Steel (SS) samples exposed to CCTC pre-cleaning. First row: 4E1, 4EL4, 4EX1, 4EX5, 4EL1 front and back. Second row: 4D2, 4DL5, 4DX2, 4DX6, 4EL2 front and back. Third row: 4D3, 4DL6, 4DX3, 4DX7, 4EL3 front and back.

Stainless Steel: CCTC									
Uncoupled Front	Uncoupled Back	Coupled w/ Logger Front 316 SS on top	Coupled w/ Logger Back 316 SS on top	Coupled w/o Logger Front AA 6061-T6 on top	Coupled w/o Logger Back AA 6061-T6 on top	Coupled w/o Logger Front 316 SS on top	Coupled w/o Logger Back 316 SS on top	Coupled w/ Logger Front AA 6061-T6 on top	Coupled w/ Logger Back AA 6061-T6 on top
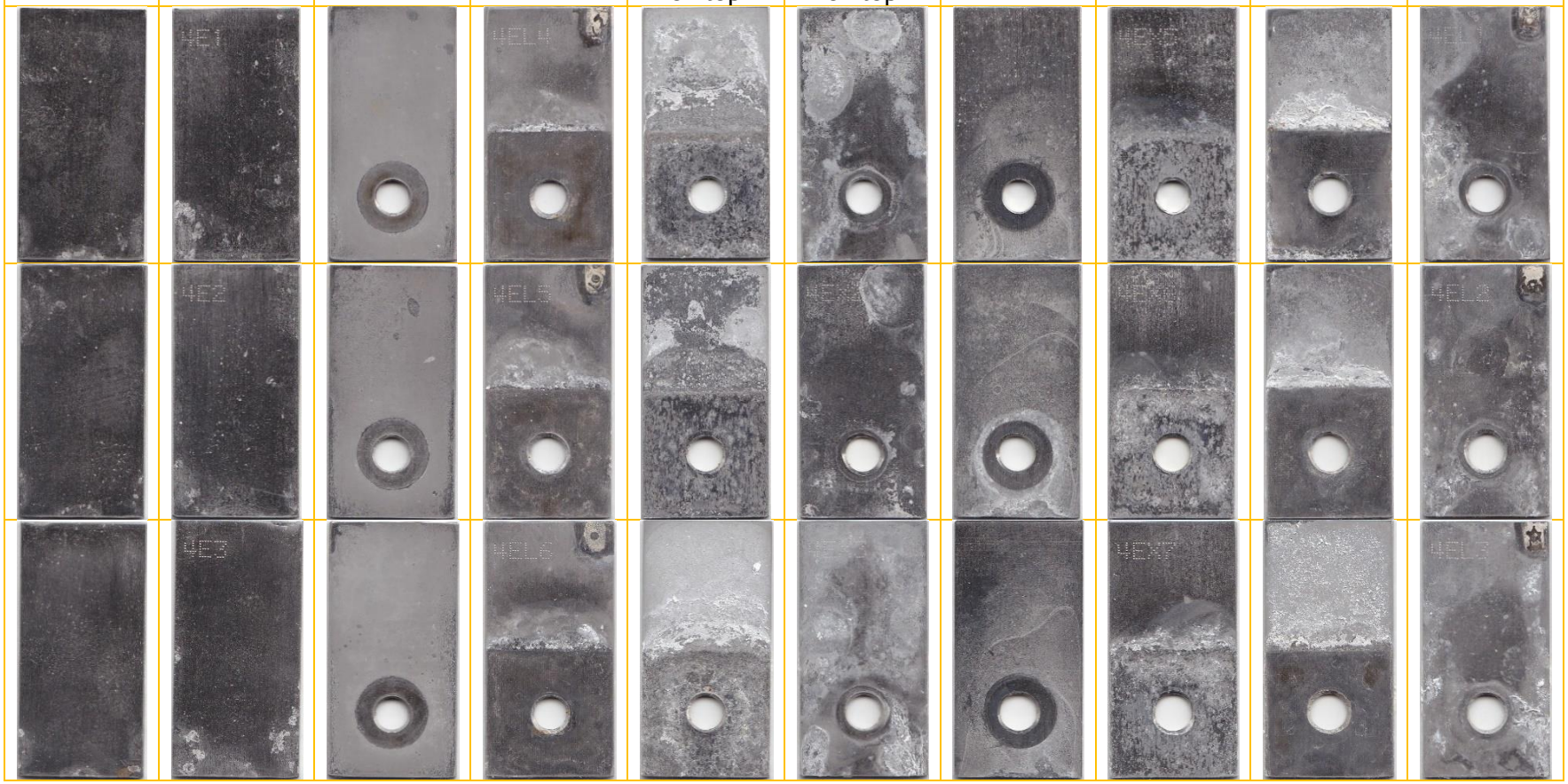									

Table 20: 1018 steel samples exposed to Lyon Arboretum pre-cleaning. First row: 1F1, 1FL1, 1FX1, 1FX5 front and back. Second row: 1F2, 1FL2, 1FX2,1FX6 front and back. Third row: 1F3, 1FL3, 1FX3, 1FX7 Front and back.

1018 Steel: Lyon Arboretum							
Uncoupled Front	Uncoupled Back	Coupled w/ Logger Front 1018 Steel on top	Coupled w/ Logger Back 1018 steel on top	Coupled w/o Logger Front AA 6061-T6 on top	Coupled w/o Logger Back AA 6061-T6 on top	Coupled w/o Logger Front 1018 steel on top	Coupled w/o Logger Back 1018 steel on top
							
							
							

Table 21: 1018 steel samples exposed to Marine Corp Base Hawaii pre-cleaning. First row: 2F1, 2FL1, 2FX1, 2FX5 Front and back. Second row: 2F2, 2FL2, 2FX2, 2FX6 Front and back. Third row: 2F3, 2FL3, 2FX3, 2FX7 Front and back

1018 Steel: MCBH							
Uncoupled Front	Uncoupled Back	Coupled w/ Logger Front 1018 steel on top	Coupled w/ Logger Back 1018 steel on top	Coupled w/o Logger Front AA 6061-T6 on top	Coupled w/o Logger Back AA 6061-T6 on top	Coupled w/o Logger Front 1018 steel on top	Coupled w/o Logger Back 1018 steel on top
							
							
							

Table 22: 1018 steel samples exposed to Kilauea pre-cleaning. First row: 3F1, 3FL1, 3FX1, 3FX5 Front and back. Second row: 3F2, 3FL2, 3FX2, 3FX6 Front and back. Third row: 3F3, 3FL3, 3FX3, 3FX7 Front and back.

1018 Steel: Kilauea							
Uncoupled Front	Uncoupled Back	Coupled w/ Logger Front 1018 steel on top	Coupled w/ Logger Back 1018 steel on top	Coupled w/o Logger Front AA6061-T6 on top	Coupled w/o Logger Back AA6061-T6 on top	Coupled w/o Logger Front 1018 steel on top	Coupled w/o Logger Back 1018 steel on top
							
							
							

Table 23: 1018 steel samples exposed to CCTC pre-cleaning. First row: 4F1, 4FL4, 4FX1, 4FX5, 4FL1 Front and back. Second row: 4F2, 4FL5, 4FX2, 4FX6, 4FL2 Front and back. Third row: 4F3, 4FL6, 4FX3, 4FX7, 4FL3 Front and back.

1018 Steel: CTCC									
Uncoupled Front	Uncoupled Back	Coupled w/ Logger Front 1018 steel on top	Coupled w/ Logger Back 1018 steel on top	Coupled w/o Logger Front AA6061-T6 on top	Coupled w/o Logger Back AA6061-T6 on top	Coupled w/o Logger Front 1018 steel on top	Coupled w/o Logger Back 1018 steel on top	Coupled w/ Logger Front AA6061-T6 top	Coupled w/ Logger Back AA6061-T6 top
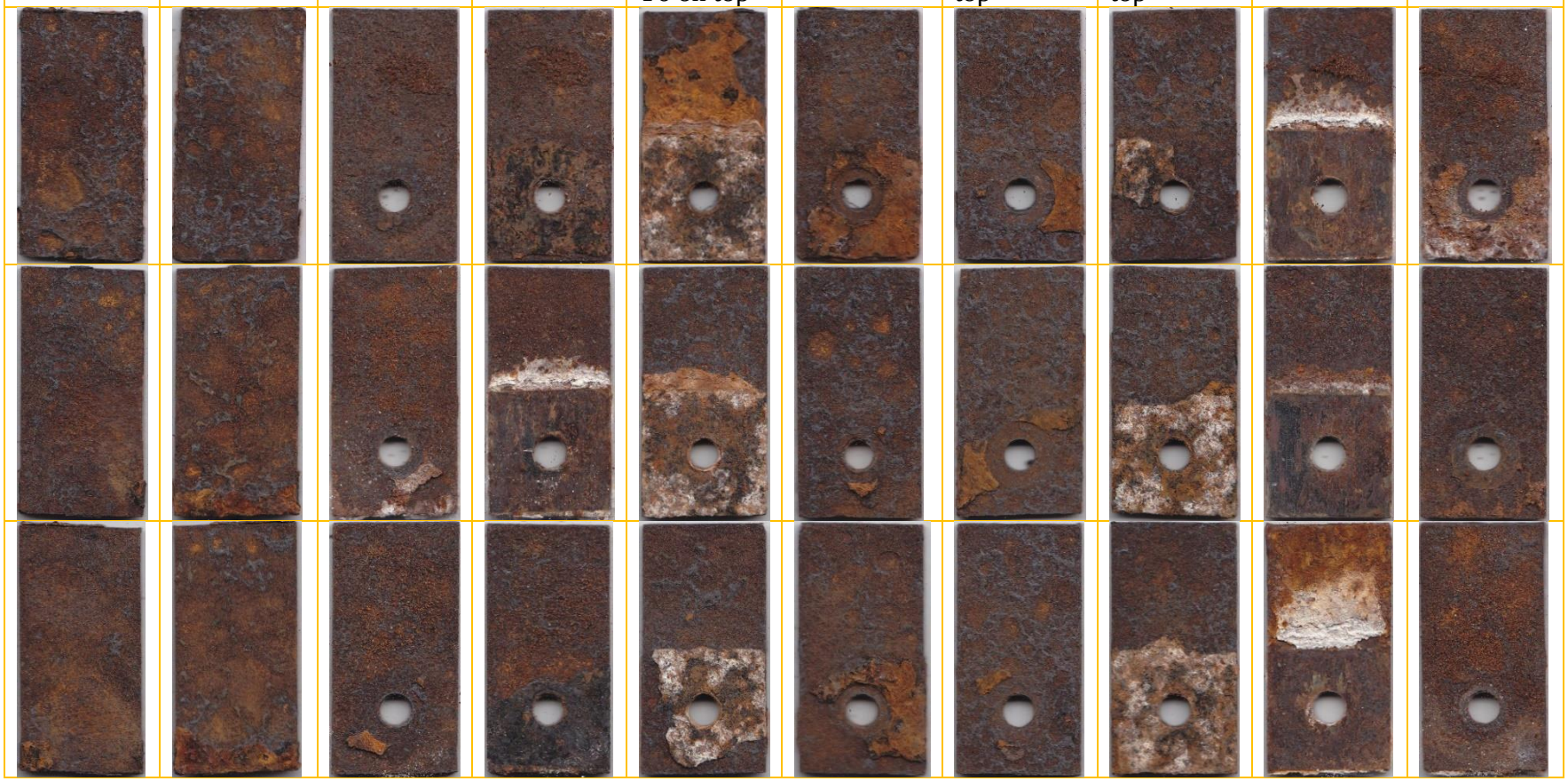									

Table 24: AA 6061-T6 coupled to pure Cu samples exposed to Lyon Arboretum pre-cleaning. First row: 1A1, 1ALC1, 1AC1, 1AC5 front and back. Second row: 1A2, 1ALC2, 1AC2, 1AC6 front and back. Third row: 1A3, 1ALC3, 1AC3, 1AC7 Front and back.

AA 6061-T6-pure Copper: Lyon Arboretum							
Uncoupled Front	Uncoupled Back	Coupled w/ Logger Front pure Cu on top	Coupled w/ Logger Back pure Cu on top	Coupled w/o Logger Front AA6061-T6 on top	Coupled w/o Logger Back AA6061-T6 on top	Coupled w/o Logger Front pure Cu on top	Coupled w/o Logger Back pure Cu on top
							
							
							

Table 25: AA6061-T6 coupled to pure Cu samples exposed to MCBH pre-cleaning. First row: 2A1, 2ALC1, 2AC1, 1AC5 front and back. Second row: 2A2, 2ALC2, 2AC2, 2AC6 front and back. Third row: 2A3, 2ALC3, 2AC3, 2AC7 Front and back.

AA 6061-T6-pure Copper: MCBH							
Uncoupled Front	Uncoupled Back	Coupled w/ Logger Front pure Cu on top	Coupled w/ Logger Back pure Cu on top	Coupled w/o Logger Front AA6061-T6 on top	Coupled w/o Logger Back AA6061-T6 on top	Coupled w/o Logger Front pure Cu on top	Coupled w/o Logger Back pure Cu on top
							
							
							

Table 26: AA 6061-T6 coupled to pure Cu samples exposed to Kilauea pre-cleaning. First row: 3A1, 3ALC1, 3AC1, 3AC5 front and back. Second row: 3A2, 3ALC2, 3AC2, 3AC6 front and back. Third row: 3A3, 3ALC3, 3AC3, 3AC7 Front and back.

AA 6061-T6-pure Copper: Kilauea							
Uncoupled Front	Uncoupled Back	Coupled w/ Logger Front pure Cu on top	Coupled w/ Logger Back pure Cu on top	Coupled w/o Logger Front AA6061-T6 on top	Coupled w/o Logger Back AA6061-T6 on top	Coupled w/o Logger Front pure Cu on top	Coupled w/o Logger Back pure Cu on top
							
							
							

Table 27: AA 6061-T6 coupled to pure Cu samples exposed to CCTC pre-cleaning. First row: 4A1, 4ALC4, 4AC1, 4AC5, 4ALC1 front and back. Second row: 4A2, 4ALC5, 4AC2, 4AC6, 4ALC2 front and back. Third row: 4A3, 4ALC6, 4AC3, 4AC7, 4ALC3 Front and back.

AA 6061-T6-pure Copper: CCTC									
Uncoupled Front	Uncoupled Back	Coupled w/ Logger Front pure Cu on top	Coupled w/ Logger Back pure Cu on top	Coupled w/o Logger Front AA6061-T6 on top	Coupled w/o Logger Back AA6061-T6 on top	Coupled w/o Logger Front pure Cu on top	Coupled w/o Logger Back pure Cu on top	Coupled w/ Logger Front AA6061-T6 on top	Coupled w/ Logger Back AA6061-T6 on top
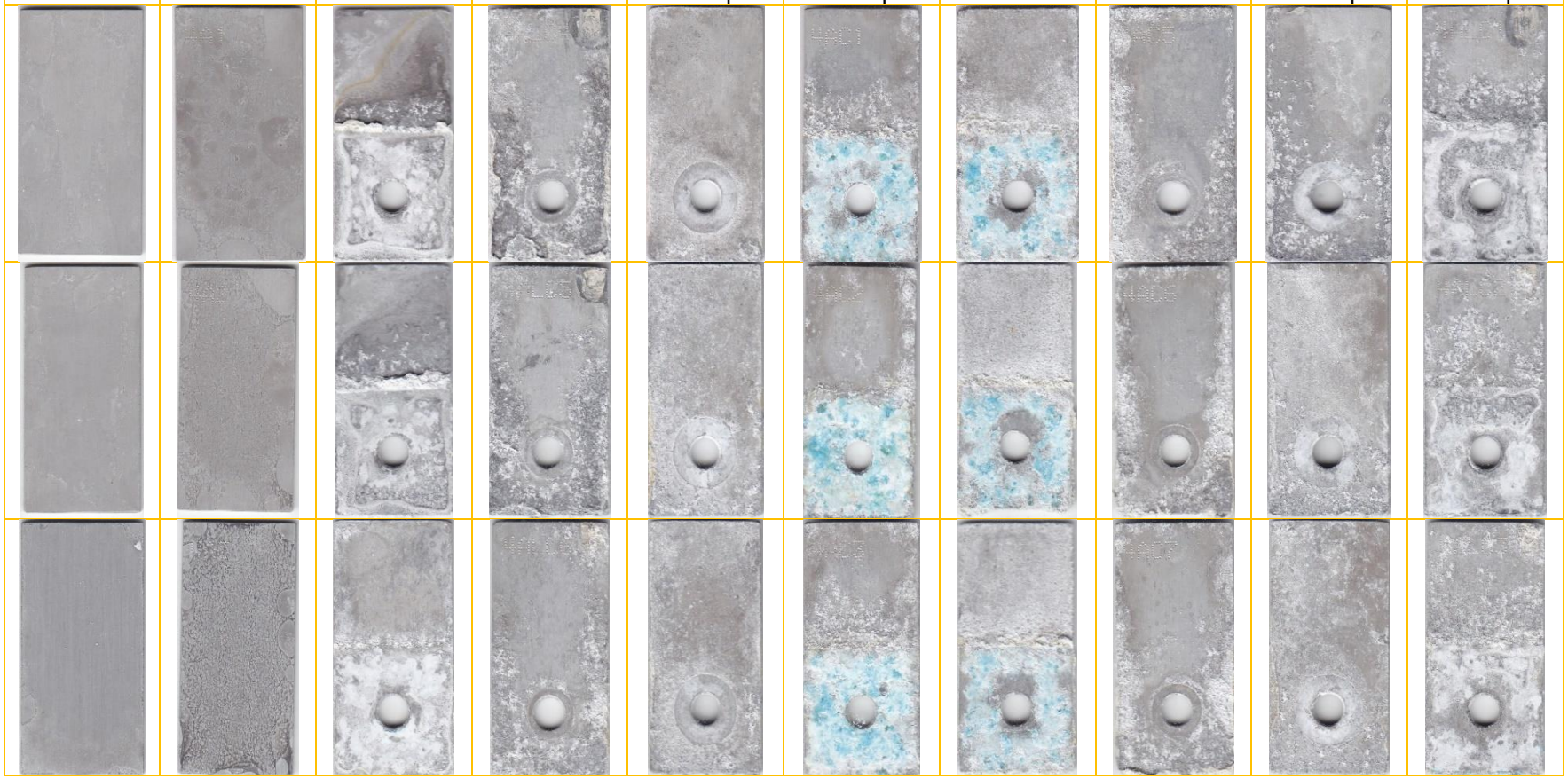									

Table 28: AA6061-T6 coupled to pure Ag samples exposed to Lyon Arboretum pre-cleaning. First row: 1A1, 1ALB1, 1AB1, 1AB5 front and back. Second row: 1A2, 1ALB2, 1AB2, 1AB6 front and back. Third row: 1A3, 1ALB3, 1AB3, 1AB7 Front and back.

AA 6061-T6-pure Silver: Lyon Arboretum							
Uncoupled Front	Uncoupled Back	Coupled w/ Logger Front Ag on top	Coupled w/ Logger Back Ag on top	Coupled w/o Logger Front AA6061-T6 on top	Coupled w/o Logger Back AA6061-T6 on top	Coupled w/o Logger Front Ag on top	Coupled w/o Logger Back Ag on top
							
							
							

Table 29: AA 6061-T6 coupled to pure Ag samples exposed to Lyon Arboretum pre-cleaning. First row: 2A1, 2ALB1, 2AB1, 2AB5 front and back. Second row: 2A2, 2ALB2, 2AB2, 2AB6 front and back. Third row: 2A3, 2ALB3, 2AB3, 2AB7 Front and back.

AA 6061-T6-pure Silver: MCBH							
Uncoupled Front	Uncoupled Back	Coupled w/ Logger Front Ag on top	Coupled w/ Logger Back Ag on top	Coupled w/o Logger Front AA6061-T6 on top	Coupled w/o Logger Back AA6061-T6 on top	Coupled w/o Logger Front Ag on top	Coupled w/o Logger Back Ag on top
							
							
							

Table 30: AA 6061-T6 coupled to pure Ag samples exposed to Kilauea pre-cleaning. First row: 3A1, 3ALB1, 3AB1, 3AB5 front and back. Second row: 3A2, 3ALB2, 3AB2, 3AB6 front and back. Third row: 3A3, 3ALB3, 3AB3, 3AB7 Front and back.

AA 6061-T6-pure Silver: Kilauea							
Uncoupled Front	Uncoupled Back	Coupled w/ Logger Front Ag on top	Coupled w/ Logger Back Ag on top	Coupled w/o Logger Front AA6061-T6 on top	Coupled w/o Logger Back AA6061-T6 on top	Coupled w/o Logger Front Ag on top	Coupled w/o Logger Back Ag on top
							
							
							

Table 31: AA 6061-T6 coupled to pure Ag samples exposed to CCTC pre-cleaning. First row: 4A1, 4ALB4, 4AB1, 4AB5, 4ALB1 front and back. Second row: 4A2, 4ALB5, 4AB2, 4AB6, 4ALB2 front and back. Third row: 4A3, 4ALB6, 4AB3, 4AB7, 4ALB3 Front and back.

AA 6061-T6-pure Silver: CCTC									
Uncoupled Front	Uncoupled Back	Coupled w/ Logger Front Ag on top	Coupled w/ Logger Back Ag on top	Coupled w/o Logger Front AA6061-T6 on top	Coupled w/o Logger Back AA6061-T6 on top	Coupled w/o Logger Front Ag on top	Coupled w/o Logger Back Ag on top	Coupled w/ Logger Front AA6061-T6 on top	Coupled w/ Logger Back AA6061-T6 on top
									
									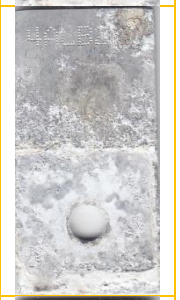
		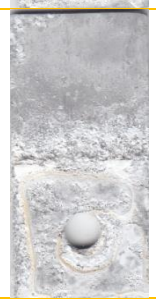							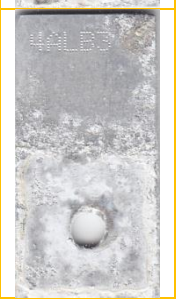

Table 32: AA 6061-T6 coupled to 1018 steel samples exposed to Lyon Arboretum pre-cleaning. First row: 1A1, 1ALF1, 1AF1, 1AF5 front and back. Second row:1A2, 1ALF2, 1AF2, 1AF6 front and back. Third row: 1A3, 1ALF3, 1AF3, 1AF7 Front and back.

AA 6061-T6 -1018 Steel: Lyon Arboretum							
Uncoupled Front	Uncoupled Back	Coupled w/ Logger Front 1018 steel on top	Coupled w/ Logger Back 1018 steel on top	Coupled w/o Logger Front AA6061-T6 on top	Coupled w/o Logger Back AA6061-T6 on top	Coupled w/o Logger Front 1018 steel on top	Coupled w/o Logger Back 1018 steel on top
							
							
							

Table 33: AA 6061-T6 coupled to 1018 steel samples exposed to MCBH pre-cleaning. First row: 2A1, 2ALF1, 2AF1, 2AF5 front and back. Second row:2A2, 2ALF2, 2AF2, 2AF6 front and back. Third row: 2A3, 2ALF3, 2AF3, 2AF7 Front and back.

AA 6061-T6-1018 Steel: MCBH							
Uncoupled Front	Uncoupled Back	Coupled w/ Logger Front 1018 steel on top	Coupled w/ Logger Back 1018 steel on top	Coupled w/o Logger Front AA6061-T6 on top	Coupled w/o Logger Back AA6061-T6 on top	Coupled w/o Logger Front 1018 steel on top	Coupled w/o Logger Back 1018 steel on top
							
							
							

Table 34: AA 6061-T6 coupled to 1018 steel samples exposed to Kilauea pre-cleaning. First row: 3A1, 3ALF1, 3AF1, 3AF5 front and back. Second row:3A2, 3ALF2, 3AF2, 3AF6 front and back. Third row: 3A3, 3ALF3, 3AF3, 3AF7 Front and back.

AA 6061-T6-1018 Steel: Kilauea							
Uncoupled Front	Uncoupled Back	Coupled w/ Logger Front 1018 steel on top	Coupled w/ Logger Back 1018 steel on top	Coupled w/o Logger Front AA6061-T6 on top	Coupled w/o Logger Back AA6061-T6 on top	Coupled w/o Logger Front 1018 steel on top	Coupled w/o Logger Back 1018 steel on top
							
							
							

Table 35: AA 6061-T6 coupled to 1018 steel samples exposed to CCTC pre-cleaning. First row: 4A1, 4ALF4, 4AF1, 4AF5, 4ALF1 front and back. Second row: 4A2, 4ALF5, 4AF2, 4AF6, 4ALF2 front and back. Third row: 4A3, 4ALF6, 4AF3, 4AF7, 4ALF3 Front and back.

AA 6061-T6-1018 Steel: CCTC									
Uncoupled Front	Uncoupled Back	Coupled w/ Logger Front 1018 steel on top	Coupled w/ Logger Back 1018 steel on top	Coupled w/o Logger Front AA6061-T6 on top	Coupled w/o Logger Back AA6061-T6 on top	Coupled w/o Logger Front 1018 steel on top	Coupled w/o Logger Back 1018 steel on top	Coupled w/ Logger Front AA6061-T6 on top	Coupled w/ Logger Back AA6061-T6 on top
									

4.2.1.2 Cleaned Specimen

The exposed coupons were separated and cleaned according to their respective process. The resulting cleaned metal was laid out to visually inspect the sets of samples based off their configuration and location. The cleaned scans were done on pure Cu, pure Ag, Ti 6Al-4V, 316 stainless steel, and 1018 steel.

Table 36: Pure copper samples exposed to Lyon Arboretum post-cleaning. First row: 1C1, 1CL1, 1CX1, 1CX5 Front and back. Second row: 1C2, 1CL2, 1CX2, 1CX6 Front and back. Third row: 1C3, 1CL3, 1CX3, 1CX7 Front and back.

Pure Copper: Lyon Arboretum							
Uncoupled Front	Uncoupled Back	Coupled w/ Logger Front Cu on top	Coupled w/ Logger Back Cu on top	Coupled w/o Logger Front AA6061-T6 on top	Coupled w/o Logger Back AA6061-T6 on top	Coupled w/o Logger Front Cu on top	Coupled w/o Logger Back Cu on top
							
							
							

Table 37: Pure copper samples exposed to Marine Corp Base Hawaii post-cleaning. First row: 2C1, 2CL1, 2CX1, 2CX5 Front and back. Second row: 2C2, 2CL2, 2CX2, 2CX6 Front and back. Third row: 2C3, 2CL3, 2CX3, 2CX7 Front and back.

Pure Copper: MCBH							
Uncoupled Front	Uncoupled Back	Coupled w/ Logger Front Cu on top	Coupled w/ Logger Back Cu on top	Coupled w/o Logger Front AA6061-T6 on top	Coupled w/o Logger Back AA6061-T6 on top	Coupled w/o Logger Front Cu on top	Coupled w/o Logger Back Cu on top
							
							
							

Table 38: Pure copper samples exposed to Kilauea post-cleaning. First row: 3C1, 3CL1, 3CX1, 3CX5 Front and back. Second row: 3C2, 3CL2, 3CX2, 3CX6 Front and back. Third row: 3C3, 3CL3, 3CX3, 3CX7 Front and back.

Pure Copper: Kilauea							
Uncoupled Front	Uncoupled Back	Coupled w/ Logger Front Cu on top	Coupled w/ Logger Back Cu on top	Coupled w/o Logger Front AA6061-T6 on top	Coupled w/o Logger Back AA6061-T6 on top	Coupled w/o Logger Front Cu on top	Coupled w/o Logger Back Cu on top
							
							
							

Table 39: Pure copper samples exposed to CCTC post-cleaning. First row: 4C1, 4CL4, 4CX1, 4CX5, 4CL1 Front and back. Second row: 4C2, 4CL5, 4CX2, 4CX6, 4CL2 Front and back. Third row: 4C3, 4CL6, 4CX3, 4CX7, 4CL3 Front and back.

Pure Copper: CCTC									
Uncoupled Front	Uncoupled Back	Coupled w/ Logger Front Cu on top	Coupled w/ Logger Back Cu on top	Coupled w/o Logger Front AA6061-T6 on top	Coupled w/o Logger Back AA6061-T6 on top	Coupled w/o Logger Front Cu on top	Coupled w/o Logger Back Cu on top	Coupled w/ Logger Front AA6061-T6 on top	Coupled w/ Logger Back AA6061-T6 on top
									

Table 40: Pure silver (Ag) samples exposed to Lyon Arboretum post-cleaning. First row: 1B1, 1BL1,1BX1, 1BX5 Front and back. Second row: 1B2, 1BL2, 1BX2, 1BX6 Front and back. Third row: 1B3, 1BL3, 1BX3, 1BX7 Front and back.

Pure Silver: Lyon Arboretum							
Uncoupled Front	Uncoupled Back	Coupled w/ Logger Front Ag on top	Coupled w/ Logger Back Ag on top	Coupled w/o Logger Front AA6061-T6 on top	Coupled w/o Logger Back AA6061-T6 on top	Coupled w/o Logger Front Ag on top	Coupled w/o Logger Back Ag on top
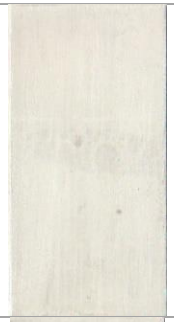							
							
							

Table 41: Pure silver (Ag) samples exposed to Marine Corp Base Hawaii post-cleaning. First row: 2B1, 2BL1, 2BX1, 2BX5 Front and back. Second row: 2B2, 2BL2, 2BX2, 2BX6 Front and back. Third row: 2B3, 2BL3, 2BX3, 2BX7 Front and back.

Pure Silver: MCBH							
Uncoupled Front	Uncoupled Back	Coupled w/ Logger Front Ag on top	Coupled w/ Logger Back Ag on top	Coupled w/o Logger Front AA6061-T6 on top	Coupled w/o Logger Back AA6061-T6 on top	Coupled w/o Logger Front Ag on top	Coupled w/o Logger Back Ag on top
							
							
	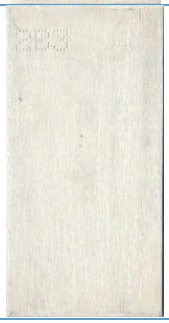						

Table 42: Pure silver (Ag) samples exposed to Kilauea post-cleaning. First row: 3B1, 3BL1, 3BX1, 3BX5 Front and back. Second row: 3B2, 3BL2, 3BX2, 3BX6 Front and back. Third row: 3B3, 3BL3, 3BX3, 3BX7 Front and back.

Pure Silver: Kilauea							
Uncoupled Front	Uncoupled Back	Coupled w/ Logger Front Ag on top	Coupled w/ Logger Back Ag on top	Coupled w/o Logger Front AA6061-T6 on top	Coupled w/o Logger Back AA6061-T6 on top	Coupled w/o Logger Front Ag on top	Coupled w/o Logger Back Ag on top
							
							
							

Table 43: Pure silver (Ag) samples exposed to CCTC post-cleaning. First row: 4B1, 4BL4, 4BX1, 4BX5, 4BL1 Front and back. Second row: 4B2, 4BL5, 4BX2, 4BX6, 4BL2 Front and back. Third row: 4B3, 4BL6, 4BX3, 4BX7, 4BL3 Front and back.

Pure Silver: CCTC									
Uncoupled Front	Uncoupled Back	Coupled w/ Logger Front Ag on top	Coupled w/ Logger Back Ag on top	Coupled w/o Logger Front AA6061-T6 on top	Coupled w/o Logger Back AA6061-T6 on top	Coupled w/o Logger Front Ag on top	Coupled w/o Logger Back Ag on top	Coupled w/ Logger Front AA6061-T6 on top	Coupled w/ Logger Back AA6061-T6 on top
									
									
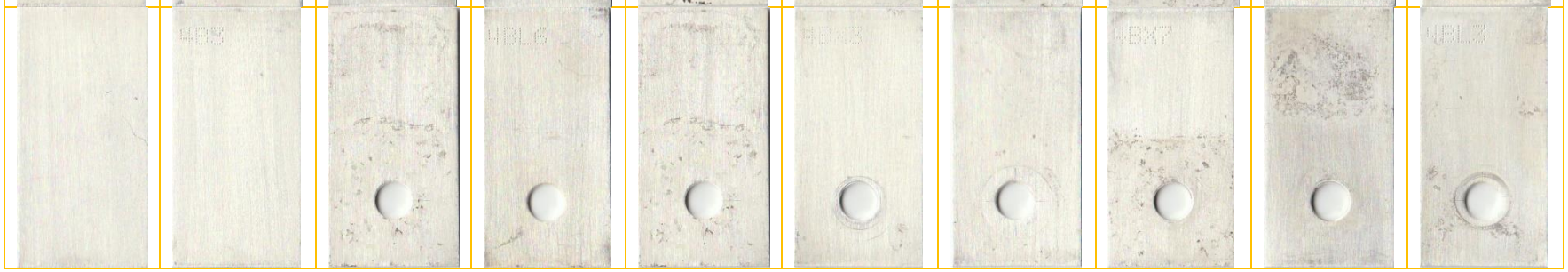									

Table 44: Ti 6Al-4V samples exposed to Lyon Arboretum post-cleaning. First row: 1D1, 1DL1,1DX1, 1DX5 Front and back. Second row: 1D2, 1DL2, 1DX2, 1DX6 Front and back. Third row: 1D3, 1DL3, 1DX3, 1DX7 Front and back.

Ti 6Al-4V: Lyon Arboretum							
Uncoupled Front	Uncoupled Back	Coupled w/ Logger Front Ti 6Al-4V on top	Coupled w/ Logger Back Ti 6Al-4V on top	Coupled w/o Logger Front AA6061-T6 on top	Coupled w/o Logger Back AA6061-T6 on top	Coupled w/o Logger Front Ti 6Al-4V on top	Coupled w/o Logger Back Ti 6Al-4V on top
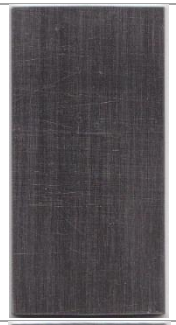							
							
							

Table 45: Ti 6Al-4V samples exposed to MCBH post-cleaning. First row: 3D1, 3DL1, 3DX1, 3DX5 Front and back. Second row: 3D2, 3DL2, 3DX2, 3DX6 Front and back. Third row: 3D3, 3DL3, 3DX3, 3DX7 Front and back.

Ti 6Al-4V: MCBH							
Uncoupled Front	Uncoupled Back	Coupled w/ Logger Front Ti 6Al-4V on top	Coupled w/ Logger Back Ti 6Al-4V on top	Coupled w/o Logger Front AA6061-T6 on top	Coupled w/o Logger Back AA6061-T6 on top	Coupled w/o Logger Front Ti 6Al-4V on top	Coupled w/o Logger Back Ti 6Al-4V on top
	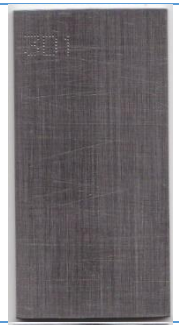						
							
							

Table 46: Ti 6Al-4V samples exposed to Kilauea post-cleaning. First row: 2D1, 2DL1,2DX1, 2DX5 Front and back. Second row: 2D2, 2DL2, 2DX2, 2DX6 Front and back. Third row: 2D3, 2DL3, 2DX3, 2DX7 Front and back.

Ti 6Al-4V: Kilauea							
Uncoupled Front	Uncoupled Back	Coupled w/ Logger Front Ti 6Al-4V on top	Coupled w/ Logger Back Ti 6Al-4V on top	Coupled w/o Logger Front AA6061-T6 on top	Coupled w/o Logger Back AA6061-T6 on top	Coupled w/o Logger Front Ti 6Al-4V on top	Coupled w/o Logger Back Ti 6Al-4V on top
							
							
							

Table 47: Ti 6Al-4V samples exposed to CCTC post-cleaning. First row: 4D1, 4DL4, 4DX1, 4DX5 Front and back. Second row: 4D2, 4DL5, 4DX2, 4DX6 Front and back. Third row: 4D3, 4DL6, 4DX3, 4DX7 Front and back.

Ti 6Al-4V: CCTC									
Uncoupled Front	Uncoupled Back	Coupled w/ Logger Front Ti 6Al-4V on top	Coupled w/ Logger Back Ti 6Al-4V on top	Coupled w/o Logger Front AA6061-T6 on top	Coupled w/o Logger Back AA6061-T6 on top	Coupled w/o Logger Front Ti 6Al-4V on top	Coupled w/o Logger Back Ti 6Al-4V on top	Coupled w/ Logger Front AA6061-T6 on top	Coupled w/ Logger Back AA6061-T6 on top
									
									
									

Table 48: 316 Stainless Steel (SS) samples exposed to Lyon Arboretum post-cleaning. First row: 1E1, 1EL1, 1EX1, 1EX5 front and back. Second row: 1E2, 1EL2, 1EX2, 1EX6 front and back. Third row: 1E3, 1EL3, 1EX3, 1EX7 Front and back.

316 Stainless Steel: Lyon Arboretum							
Uncoupled Front	Uncoupled Back	Coupled w/ Logger Front 316 SS on top	Coupled w/ Logger Back 316 SS on top	Coupled w/o Logger Front AA6061-T6 on top	Coupled w/o Logger Back AA6061-T6 on top	Coupled w/o Logger Front 316 SS on top	Coupled w/o Logger Back 316 SS on top
							
							
							

Table 49: 316 Stainless Steel (SS) samples exposed to MCBH post-cleaning. First row: 2E1, 2EL1 ,2EX1, 2EX5 front and back. Second row: 2E2, 2EL2, 2EX2, 2EX6 front and back. Third row: 2E3, 2EL3, 2EX3, 2EX7 front and back.

316 Stainless Steel: MCBH							
Uncoupled Front	Uncoupled Back	Coupled w/ Logger Front 316 SS on top	Coupled w/ Logger Back 316 SS on top	Coupled w/o Logger Front AA6061-T6 on top	Coupled w/o Logger Back AA6061-T6 on top	Coupled w/o Logger Front 316 SS on top	Coupled w/o Logger Back 316 SS on top
							
							
							

Table 50: 316 Stainless Steel (SS) samples exposed to Kilauea post-cleaning. First row: 3E1, 3EL1, 3EX1, 3EX5 front and back. Second row: 3E2, 3EL2, 3EX2, 3EX6 front and back. Third row: 3E3, 3EL3, 3EX3, 3EX7 front and back.

316 Stainless Steel: Kilauea							
Uncoupled Front	Uncoupled Back	Coupled w/ Logger Front 316 SS on top	Coupled w/ Logger Back 316 SS on top	Coupled w/o Logger Front AA6061-T6 on top	Coupled w/o Logger Back AA6061-T6 on top	Coupled w/o Logger Front 316 SS on top	Coupled w/o Logger Back 316 SS on top
							
							
							

Table 51: 316 Stainless Steel (SS) samples exposed to CCTC post-cleaning. First row: 4E1, 4EL4, 4EX1, 4EX5, 4EL1 front and back. Second row: 4D2, 4DL5, 4DX2, 4DX6, 4EL2 front and back. Third row: 4D3, 4DL6, 4DX3, 4DX7, 4EL3 front and back.

316 Stainless Steel: CCTC									
Uncoupled Front	Uncoupled Back	Coupled w/ Logger Front 316 SS on top	Coupled w/ Logger Back 316 SS on top	Coupled w/o Logger Front AA6061-T6 on top	Coupled w/o Logger Back AA6061-T6 on top	Coupled w/o Logger Front 316 SS on top	Coupled w/o Logger Back 316 SS on top	Coupled w/ Logger Front AA6061-T6 on top	Coupled w/ Logger Back AA6061-T6 on top
									
									
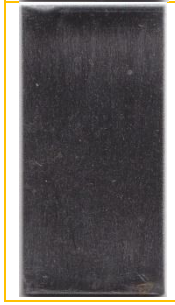									

Table 52: 1018 steel samples exposed to Lyon Arboretum post-cleaning. First row: 1F1, 1FL1, 1FX1, 1FX5 front and back. Second row: 1F2, 1FL2, 1FX2,1FX6 front and back. Third row: 1F3, 1FL3, 1FX3, 1FX7 Front and back.

1018 Steel: Lyon Arboretum							
Uncoupled Front	Uncoupled Back	Coupled w/ Logger Front 1018 steel on top	Coupled w/ Logger Back 1018 steel on top	Coupled w/o Logger Front AA6061-T6 on top	Coupled w/o Logger Back AA6061-T6 on top	Coupled w/o Logger Front 1018 steel on top	Coupled w/o Logger Back 1018 steel on top
							
							
							

Table 53: 1018 steel samples exposed to Marine Corp Base Hawaii post-cleaning. First row: 2F1, 2FL1, 2FX1, 2FX5 Front and back. Second row: 2F2, 2FL2, 2FX2, 2FX6 Front and back. Third row: 2F3, 2FL3, 2FX3, 2FX7 Front and back

1018 Steel: MCBH							
Uncoupled Front	Uncoupled Back	Coupled w/ Logger Front 1018 steel on top	Coupled w/ Logger Back 1018 steel on top	Coupled w/o Logger Front AA6061-T6 on top	Coupled w/o Logger Back AA6061-T6 on top	Coupled w/o Logger Front 1018 steel on top	Coupled w/o Logger Back 1018 steel on top
							
							
							

Table 54: 1018 steel samples exposed to Kilauea post-cleaning. First row: 3F1, 3FL1, 3FX1, 3FX5 Front and back. Second row: 3F2, 3FL2, 3FX2, 3FX6 Front and back. Third row: 3F3, 3FL3, 3FX3, 3FX7 Front and back.

1018 Steel: Kilauea							
Uncoupled Front	Uncoupled Back	Coupled w/ Logger Front 1018 steel on top	Coupled w/ Logger Back 1018 steel on top	Coupled w/o Logger Front AA6061-T6 on top	Coupled w/o Logger Back AA6061-T6 on top	Coupled w/o Logger Front 1018 steel on top	Coupled w/o Logger Back 1018 steel on top
							

Table 55: 1018 steel samples exposed to CCTC post-cleaning. First row: 4F1, 4FL4, 4FX1, 4FX5, 4FL1 Front and back. Second row: 4F2, 4FL5, 4FX2, 4FX6, 4FL2 Front and back. Third row: 4F3, 4FL6, 4FX3, 4FX7, 4FL3 Front and back.

1018 Steel: CTCC									
Uncoupled Front	Uncoupled Back	Coupled w/ Logger Front 1018 steel on top	Coupled w/ Logger Back 1018 steel on top	Coupled w/o Logger Front AA6061-T6 on top	Coupled w/o Logger Back AA6061-T6 on top	Coupled w/o Logger Front 1018 steel on top	Coupled w/o Logger Back 1018 steel on top	Coupled w/ Logger Front AA6061-T6 top	Coupled w/ Logger Back AA6061-T6 top
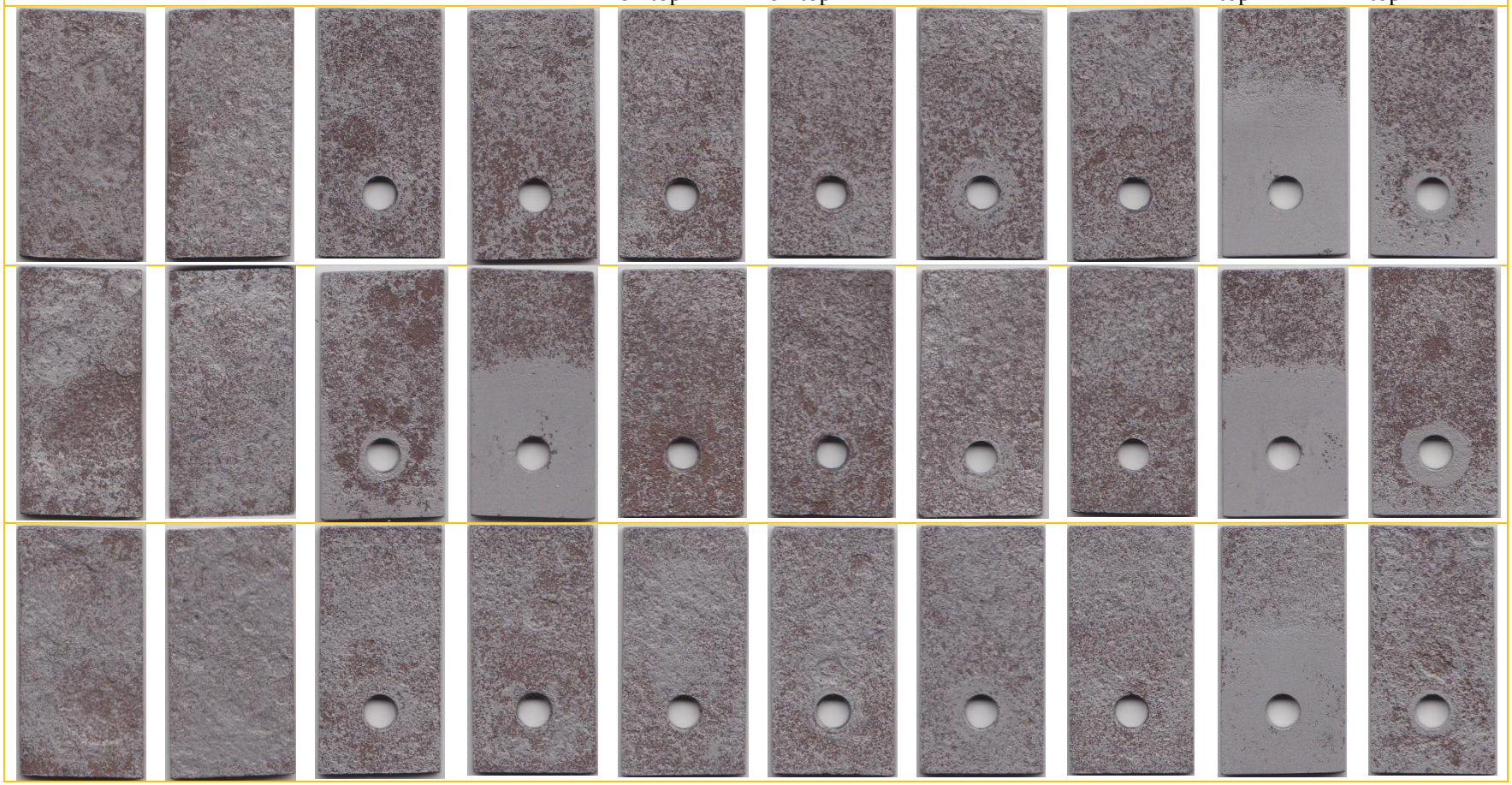									

4.2.2 X-Ray Diffraction

4.2.2.1 Lyon Arboretum

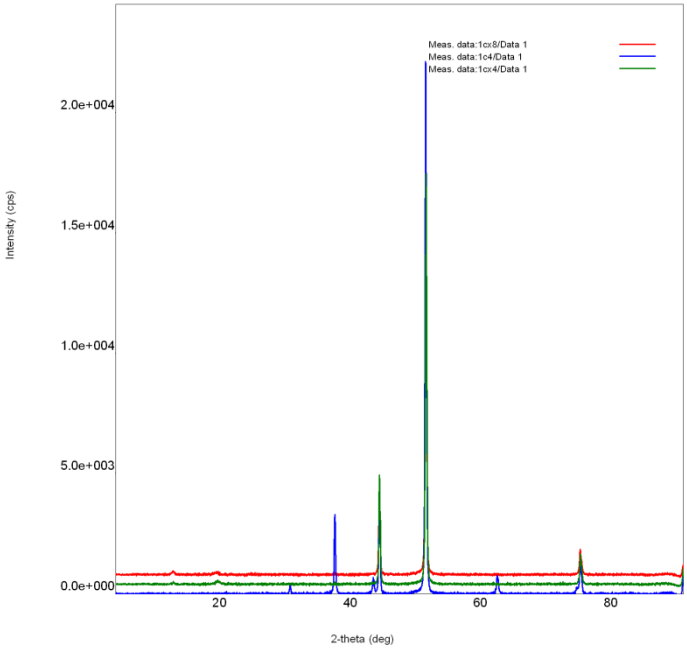

Figure 1: XRD spectra of pure Cu samples (LA) uncoupled 1C4 [blue], AA 6061 T6 on top 1CX4 [green], pure Cu on-top 1CX8 [red].

All three copper samples share the peaks at 43.4, 50.5, 74.2. These peaks correspond with Cu. The uncoupled sample had peaks at 29.7, 36.5, 42.4 and 61.5 that indicate copper oxide. The two coupled samples show small, wide peaks at 11.8 and 18.5 that were unable to be identified.

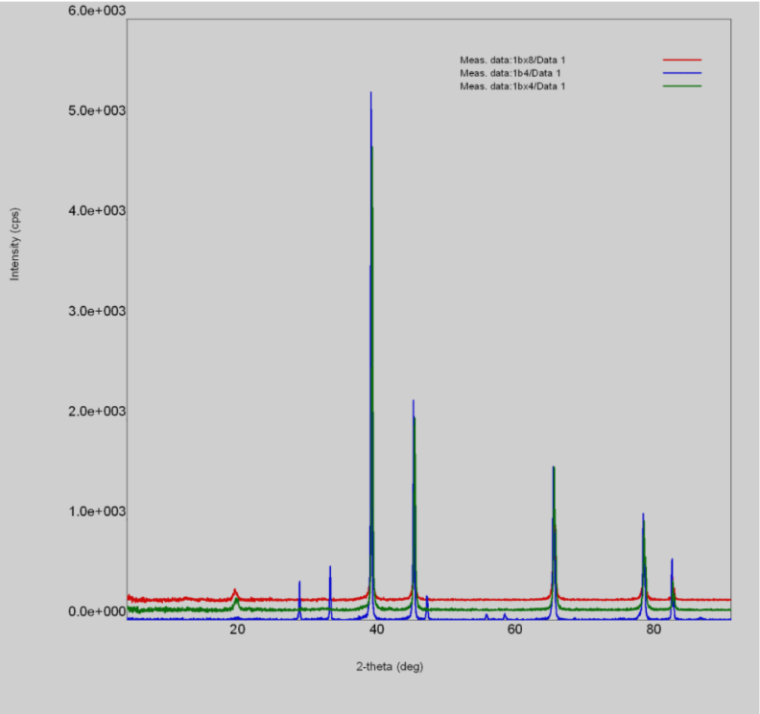

Figure 2: XRD spectra of pure Ag samples (LA) uncoupled 1B4 [blue], AA 6061 T6 on top 1BX4 [green], pure Ag on-top 1BX8 [red].

The XRD spectra pure Ag samples exposed at Lyon Arboretum indicate silver with corresponding peaks at 38.1, 44.2, 64.4, 77.3, 81.5 for all three coupons. The additional peaks on the uncoupled sample at 27.8, 32.2, 46.1, 54.7, 57.4 correspond to silver chloride (AgCl). An additional peak was observed on the coupled samples at 18.5 that could be attributed to aluminum hydroxide ($Al(OH)_3$) from the corrosion of AA 6061-T6 in the interfacial region of the couple.

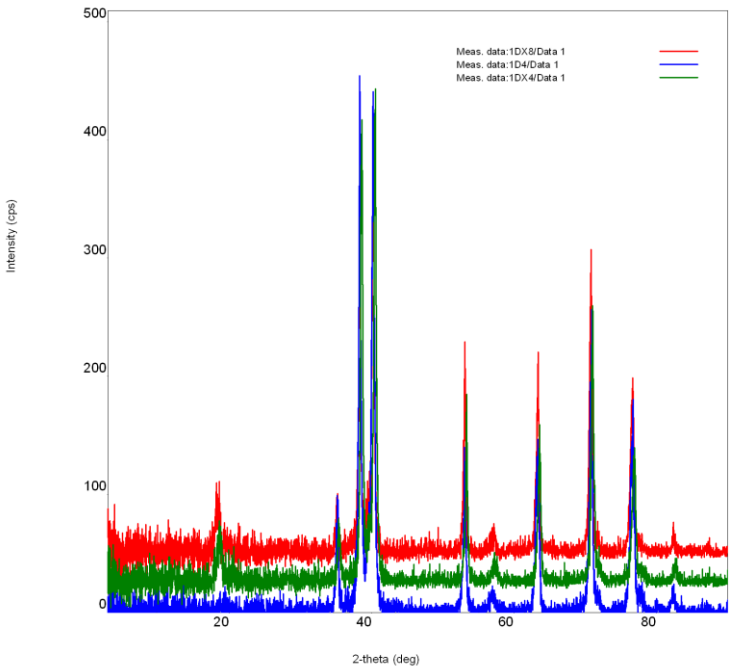

Figure 3: XRD spectra of Ti 6Al-4V (LA) uncoupled 1D4 [blue], AA 6061 T6 on top 1DX4 [green], Ti 6Al-4V on-top 1DX8 [red].

Titanium 6Al-4V samples at Lyon Arboretum exhibited XRD spectra that was less defined. However, the peaks ascertained from the spectra at 35.2, 38.3, 40.2, 53.1, 63.3, 70.8, 76.7, 82.2 corresponding to titanium. Those same peaks in addition to the peak at 18.5 for the coupled samples indicate titanium oxide (TiO).

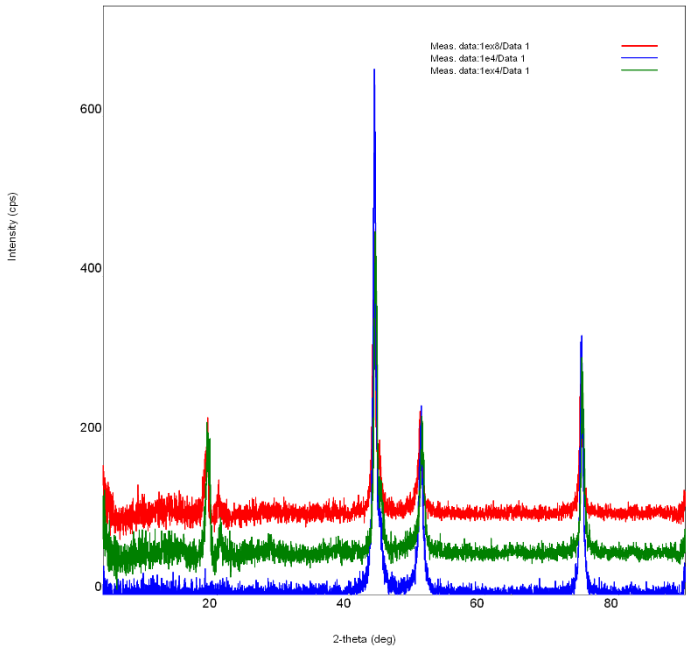

Figure 4: XRD spectra of 316 SS samples (LA) uncoupled 1E4 [blue], AA 6061 T6 on top 1EX4 [green], 316 SS on-top 1EX8 [red].

316 stainless steel indicated primarily the stainless steel from the XRD spectra with peaks at 43.5, 50.6, 74.5 for all samples. The additional peak for the coupled samples at 18.5 are suspected to be contamination of $Al(OH)_3$, similar to the peaks found on the pure copper at this same location.

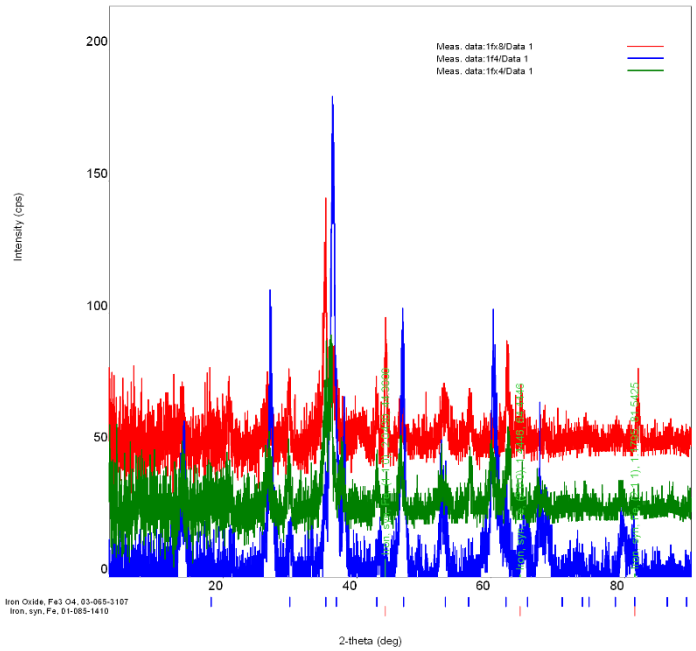

Figure 5: XRD spectra of 1018 steel samples (LA) uncoupled 1F4 [blue], AA 6061 T6 on top 1FX4 [green],1018 steel on-top 1FX8 [red].

The spectra for 1018 steel showed lower intensities for its peaks. The uncoupled sample had the most resulting peaks, that are associated with Lepidocrocite at 14.1, 27.2, 36.3, 38.0, 46.8, 60.4, 64.5, 67.8, 79.7. Whereas, the coupled samples produced less peaks only at 35.2, 44.3, 53.2, 62.4 for 1FX4 and 36.1, 56.8, 60.1, 62.8 for 1FX8. The peaks most likely indicating iron oxide (FeO_2) for 1FX4 and iron (Fe) or FeO_2 1FX8.

4.2.2.2 Marine Corp Base Hawaii

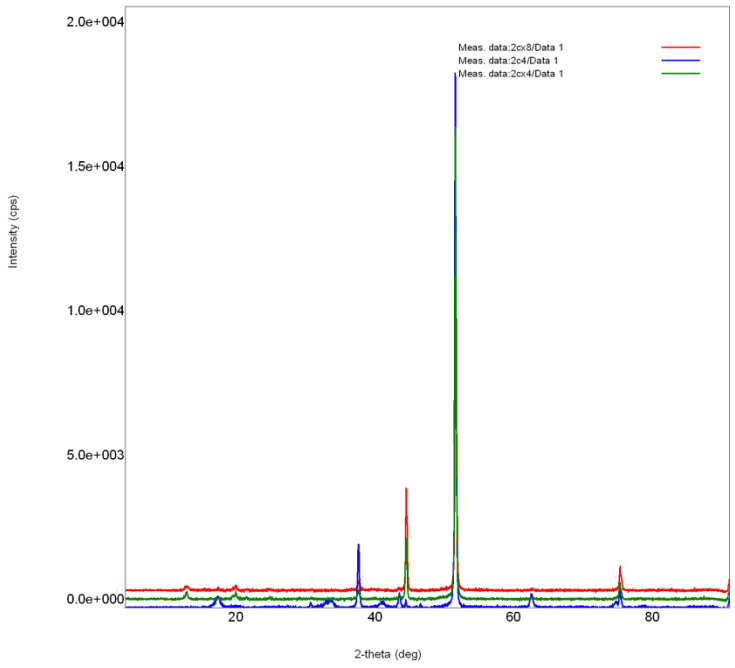

Figure 6: XRD spectra of pure Cu samples (MCBH) uncoupled 2C4 [blue], AA 6061 T6 on top 2CX4 [green], pure Cu on-top 2CX8 [red].

The common peaks between the three samples at 29.6, 36.5, 42.4, 50.5, 61.4, 73.6, 74.2 indicate copper oxide (CuO). However, many of those same peaks, 29.6, 36.5, 42.4, 61.4, also correspond to Cu. Additionally, the unidentified peaks on the uncoupled sample (19.1, 32.5, 40.0, 43.4, 45.5) are not exhibited on the coupled spectra. The coupled samples both had unidentified peaks at 11.8 and 18.9, which could be attributed to exchange between the AA 6061-T6 and pure copper samples.

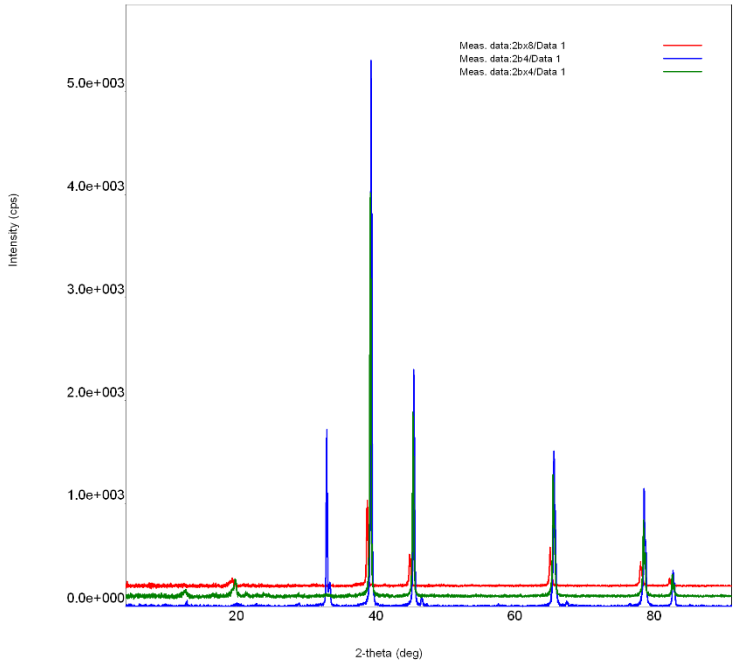

Figure 7: XRD spectra of pure Ag samples (MCBH) uncoupled 2B4 [blue], AA 6061 T6 on top 2BX4 [green], pure Ag on-top 2BX8 [red].

Spectra from Ag at MCBH demonstrated characteristic peaks for Ag at 38.1, 44.4, 64.5, 77.4, 81.6 for all samples. However, the uncoupled sample had additional unidentified peaks at 31.8, 32.3, 45.5, 66.3. Similarly, the peak at 18.5 for the coupled samples was not identified, though it is likely attributed to $Al(OH)_3$ on the interfacial area.

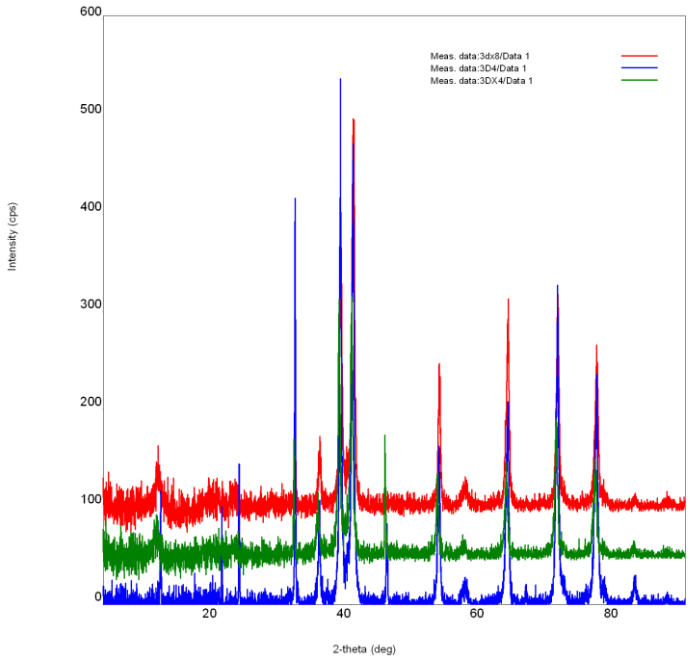

Figure 8: XRD spectra of Ti 6Al-4V (MCBH) uncoupled 3D4 [blue], AA 6061 T6 on top 3DX4 [green], Ti 6Al-4V on-top 3DX8 [red].

Spectra for Ti 6Al-4V samples display similar peaks at 11.6, 35.2, 38.4, 40.3, 52.2, 57.0, 63.5, 70.9, 76.5, 82.4 that are indicative of Ti 6Al-4V. The coupled spectra are nearly identical, whereas the uncoupled spectra shows sharp peaks at 20.7 and 23.3 that are not on the coupled spectra and were not identified in the library.

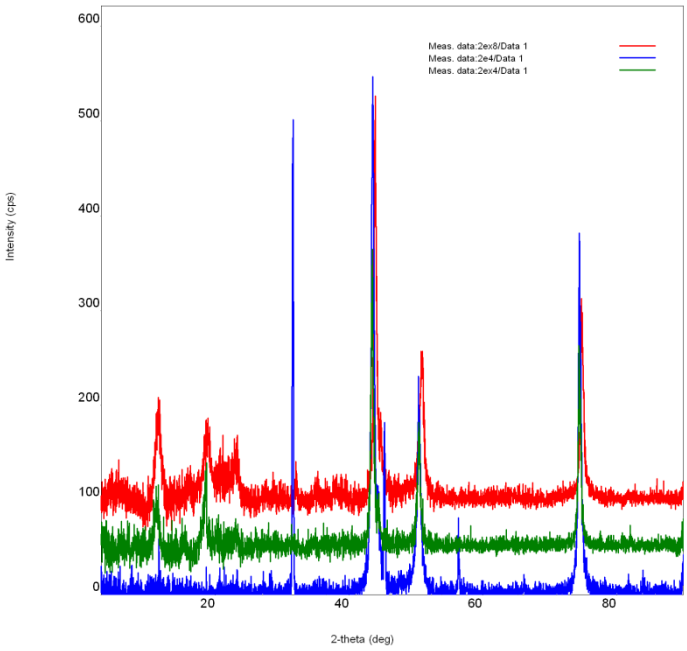

Figure 9: XRD spectra of 316 SS samples (MCBH) uncoupled 2E4 [blue], AA 6061 T6 on top 2EX4 [green], 316 SS on-top 2EX8 [red].

316 stainless steel at MCBH XRD spectra included several additional peaks on the uncoupled sample that correlated to salt (NaCl), not unusual to marine environments, and unidentified peaks at 31.6 and 31.7. However, the remaining peaks at 43.5, 50.6, 74.5 are correspondent to 316 stainless steel. Furthermore, the peak at 18.6 for both coupled samples are likely from $Al(OH)_3$ seen in other samples. Additionally, the peak for 2EX4 at 23.1 remains unidentified.

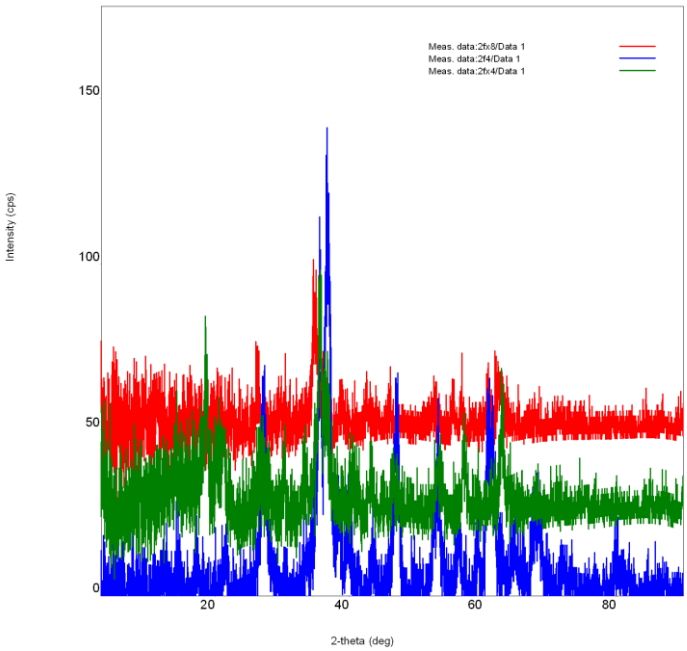

Figure 10: XRD spectra of 1018 steel samples (MCBH) uncoupled 2F4 [blue], AA 6061 T6 on top 2FX4 [green],1018 steel on-top 2FX8 [red].

1018 steel exhibited less intense peaks than other species in this environment. At MCBH, the uncoupled sample produced a spectra that had peaks associated with Lepidocrocite (FeO(OH)) at 27.4, 35.8, 36.9, 38.4, 47.1, 53.4, 56.3, 60.7, 68.1. 2FX4, the couple with AA6061-T6 on top, exhibited peaks at 18.5, 35.6, 57.2, 62.9 that may be attributed to goethite. Similarly, 2FX8, the couple with 1018 steel on top, produced two characteristic peaks at 34.7 and 62.3 that could be a result of iron hydroxide ($Fe(OH)_2$).

4.2.2.3 Kilauea

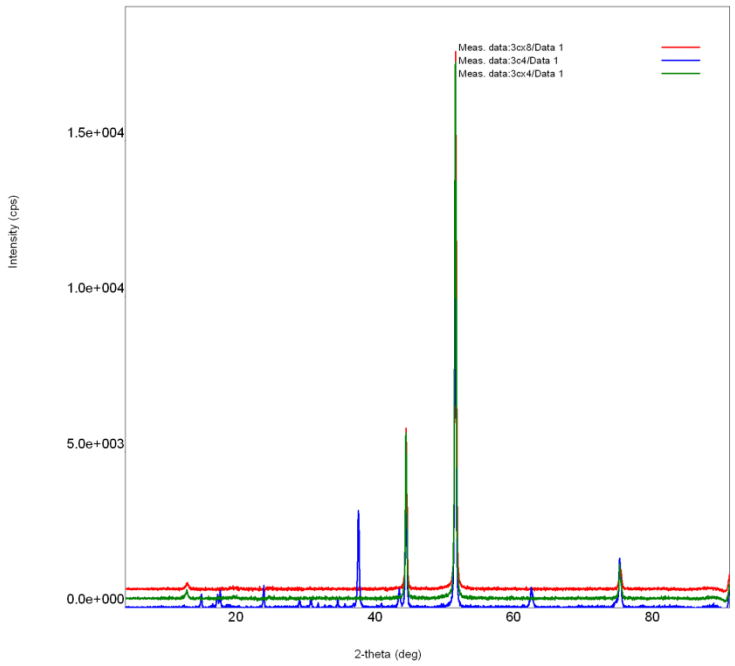

Figure 11: XRD spectra of pure Cu samples (KIL) uncoupled 3C4 [blue], AA 6061 T6 on top 3CX4 [green], pure Cu on-top 3CX8 [red].

All three pure Cu samples displayed peaks at 11.9, 43.4, 50.5, 74.2 that correspond to pure Cu. The coupled samples both indicated an extra peak at 11.9 that has not be identified. The uncoupled sample, however, had many additional peaks at 13.9, 16.2, 16.6, 22.9, 28.0, 29.6, 33.5, 36.5, 42.4, 61.5 that may be attributed to Brochontite, a copper sulfite.

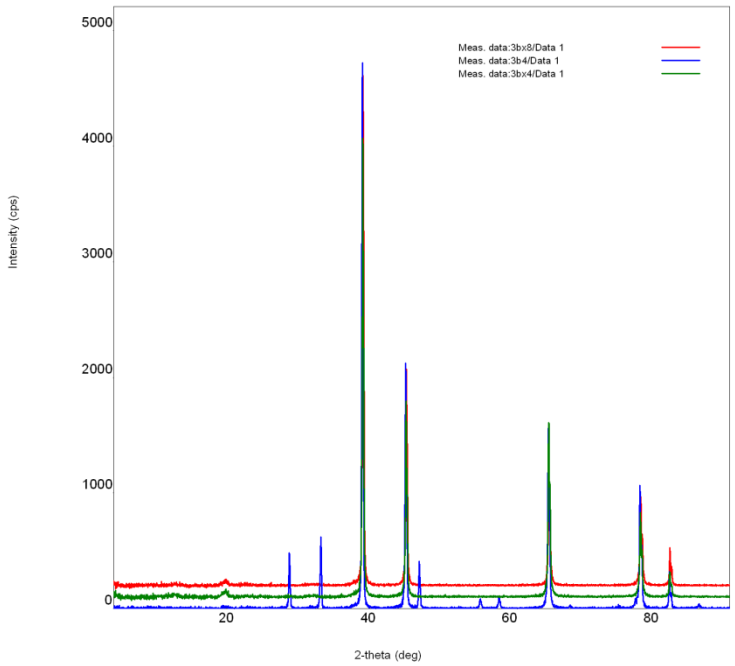

Figure 12: XRD spectra of pure Ag samples (KIL) uncoupled 3B4 [blue], AA 6061 T6 on top 3BX4 [green], pure Ag on-top 3BX8 [red].

The pure Ag spectra at Kilauea depicted clear common peaks for all three samples at 38.1, 44.3, 64.4, 77.3, 81.5 corresponding to pure Ag. The additional peaks on the uncoupled spectra 27.8, 32.2, 46.2, 54.7, 57.4, 67.4, 74.4, 76.8, 85.6 indicate silver chloride (AgCl). The coupled samples' spectra include just one additional peak at 18.9 that is unidentified.

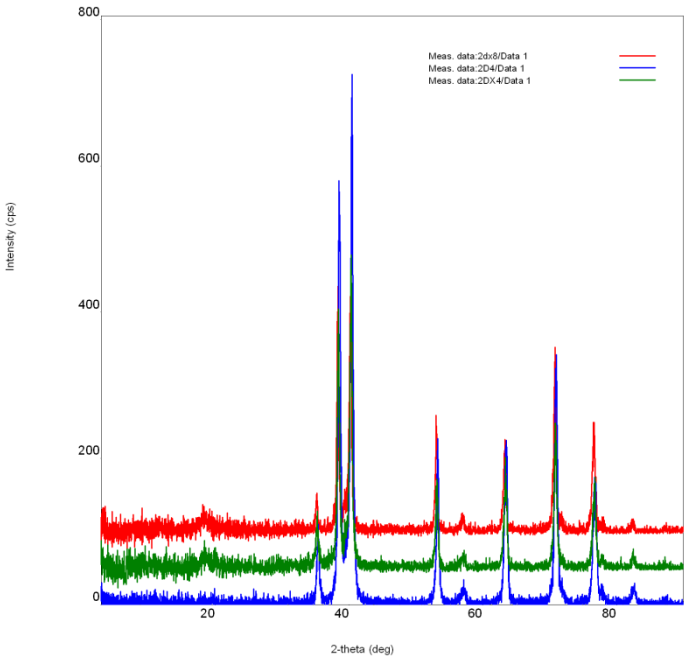

Figure 13: XRD spectra of Ti 6Al-4V (KIL) uncoupled 2D4 [blue], AA 6061 T6 on top 2DX4 [green], Ti 6Al-4V on-top 2DX8 [red].

The Ti 6Al-4V samples that were exposed to Kilauea exhibited spectra that indicated Ti 6Al-4V at peaks 35.4, 38.5, 40.5, 53.5, 63.5, 71.0, 76.8, 82.6 across all three coupons. The uncoupled coupon had an additional peak at 57.2, which is believed to be attributed to by an alloying component. For both coupled samples, an additional peak was observed at 18.5 and is suspected to be $Al(OH)_3$.

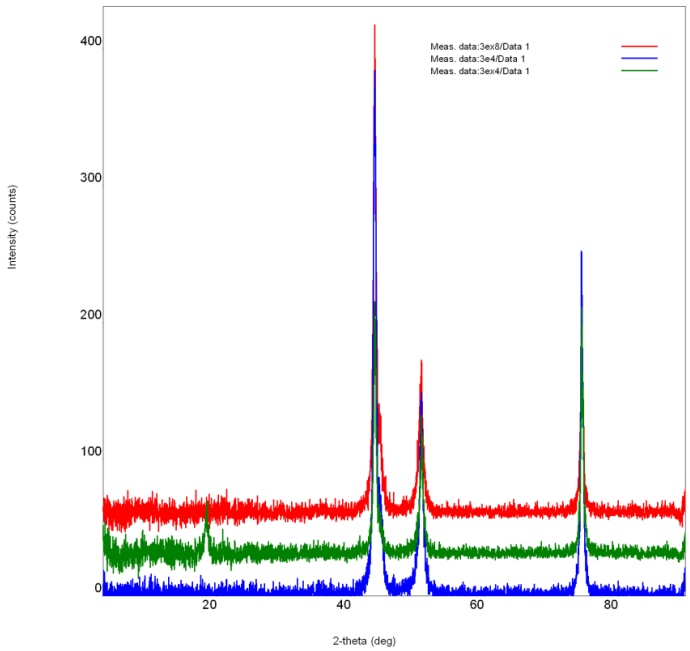

Figure 14: XRD spectra of 316 SS samples (KIL) uncoupled 3E4 [blue], AA 6061 T6 on top 3EX4 [green], 316 SS on-top 3EX8 [red].

All three spectra show clear peaks at 43.5, 50.6, 74.5 that are indicative of 316 stainless steel. However, the coupled sample 3EX4, displays an extra peak at 18.4 which is suspected to be $Al(OH)_3$ and contamination.

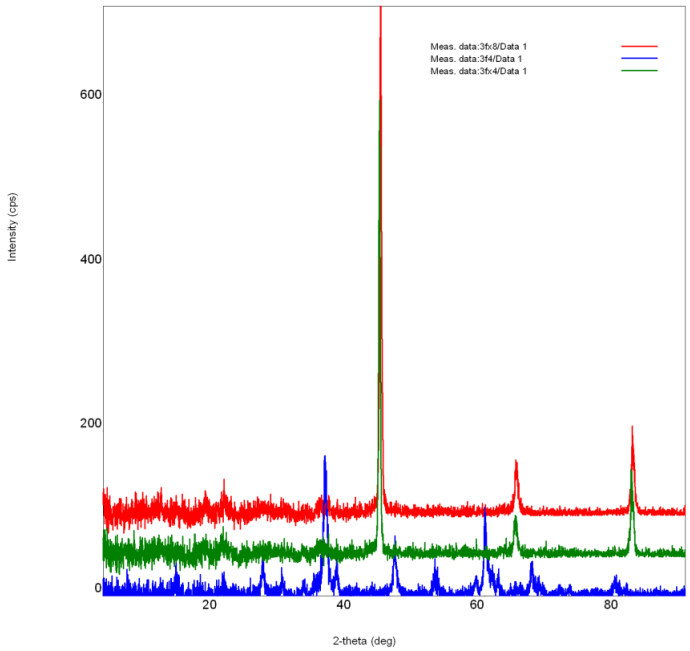

Figure 15: XRD spectra of 1018 steel samples (KIL) uncoupled 3F4 [blue], AA 6061 T6 on top 3FX4 [green],1018 steel on-top 3FX8 [red].

Major peaks indicated on the 1018 steel spectra for the uncoupled coupon are 27.7, 37.0, 38.8, 47.5, 53.3, 67.7, 69.0 that align with Lepidocrocite. Unlike the uncoupled coupon, there were less peaks and observed at 21.4, 35.5, 53.5, 52.6 that could indicate goethite.

4.2.2.4 Cyclic Corrosion Test Chamber

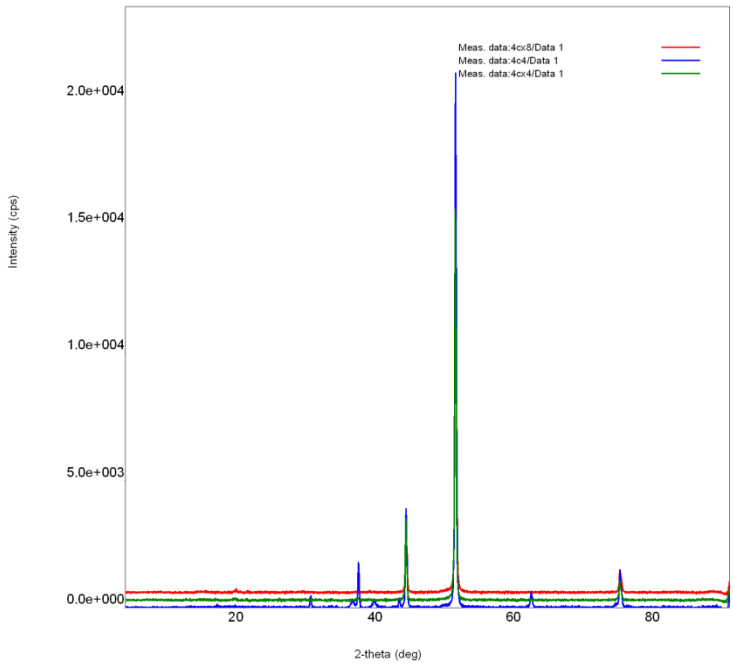

Figure 16: XRD spectra of pure Cu samples (CCTC) uncoupled 4C4 [blue], AA 6061 T6 on top 4CX4 [green], pure Cu on-top 4CX8 [red].

Pure Cu spectra show distinct peaks for all three samples at 43.4, 50.5, 74.2 matches to pure Cu. The additional peaks on the uncoupled sample at 29.6, 36.5, 42.4, 61.4 indicate CuO, though 16.2, and 38.7 were undetermined. Coupled sample, 4CX4, resulted in an extra peak at 19.0 that could be attributed to $Al(OH)_3$.

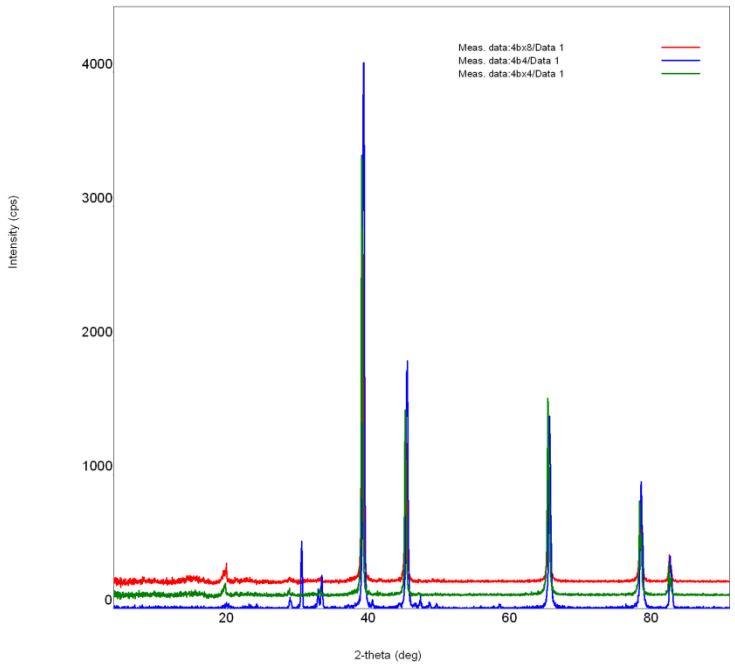

Figure 17: XRD spectra of pure Ag samples (CCTC) uncoupled 4B4 [blue], AA 6061 T6 on top 4BX4 [green], pure Ag on-top 4BX8 [red].

The pure Ag samples yielded peaks at 38.1, 44.3, 64.4, 77.4, 81.5 that match Ag. The uncoupled sample also produced peaks at 29.5, 39.5, 43.3, 46.3, 47.6 that could be attributed to either calcium carbonate ($CaCO_3$) or AgCl. The remaining peaks at 19.0, 32.4, 45.6, 57.5 were unable to be identified. Both coupled samples resulted in a peak at 18.8, also not identified.

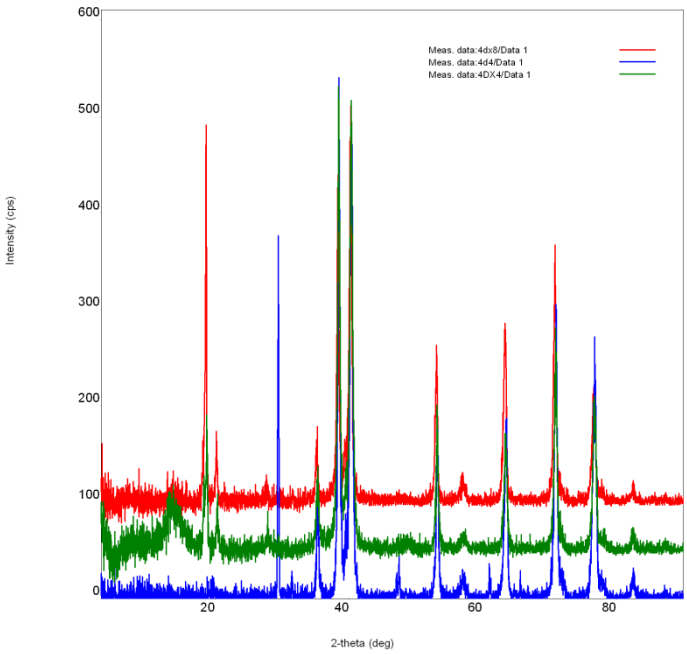

Figure 18: XRD spectra of Ti 6Al-4V (CCTC) uncoupled 4D4 [blue], AA 6061 T6 on top 4DX4 [green], Ti 6Al-4V on-top 4DX8 [red].

Spectra produced by the Ti 6Al-4V samples indicated Ti with peaks at 35.1, 38.3, 40.2, 53.2, 63.4, 70.9, 76.7, 82.5, with 57.1 likely from the alloying substance. Uncoupled sample displayed additional unidentified peaks at 29.5 and 47.6; the coupled samples also resulted in unidentified extra peaks at 18.7 and 20.2 and 13.9, and 18.8 for 4DX4 and 4DX8 respectively. The peaks at 18.7 and 18.8 could be indicative of TiO.

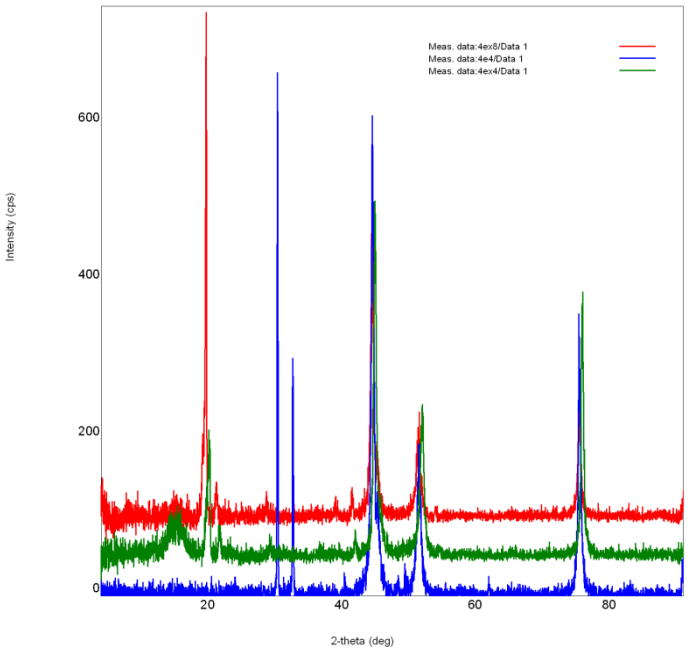

Figure 19: XRD spectra of 316 SS samples (CCTC) uncoupled 4E4 [blue], AA 6061 T6 on top 4EX4 [green], 316 SS on-top 4EX8 [red].

The peaks in the spectra at 43.4, 50.5, 74.6 for the 316 stainless steel samples match the stainless steel composition. Additionally, on the uncoupled sample produced peaks at 29.3 and 31.6, suspected to be $CaCO_3$ while the peaks on the coupled samples at approximately 19.0 and 40.5 may be from $Al(OH)_3$. On 4EX8, peak at 14.3 was not identified.

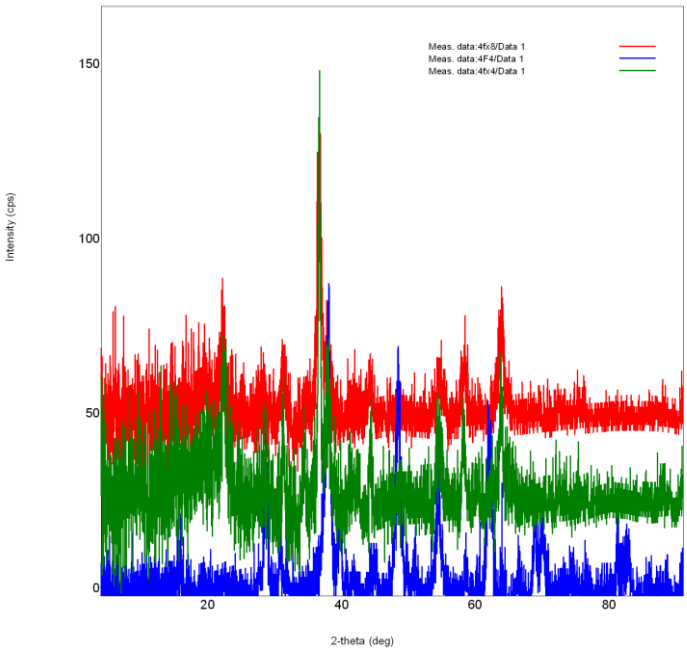

Figure 20: XRD spectra of 1018 steel samples (CCTC) uncoupled 4F4 [blue], AA 6061 T6 on top 4FX4 [green],1018 steel on-top 4FX8 [red].

1018 steel produced spectra that indicates Lepidocrocite with peaks at 27.7, 37.0, 38.8, 47.5, 53.3, 67.7, 69.0 for the uncoupled sample. Both coupled samples produced peaks that are similar to goethite at 21.3, 35.6, 53.7, 57.3, 52.7.

4.2.3 3-D Profilometry

3.2.3.1 Copper

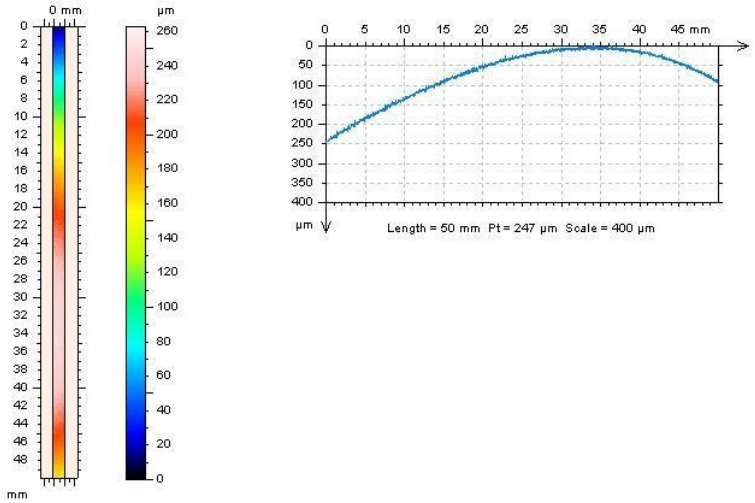

Figure 21: Surface Roughness of pure Cu at Lyon Arboretum (uncoupled 1C2). LEFT: Area spectra. RIGHT: Depths along length of sample.

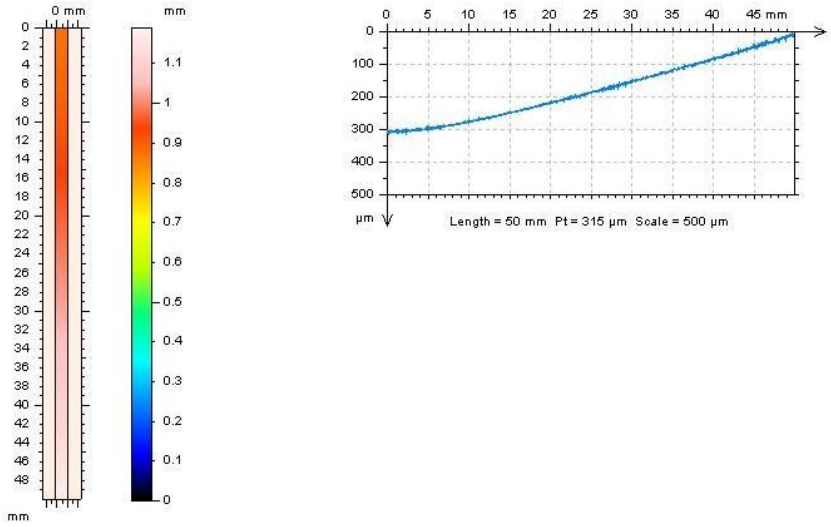

Figure 22: Surface Roughness of pure Cu at Lyon Arboretum (pure Cu on-top 1CL2). LEFT: Area spectra. RIGHT: Depths along length of sample.

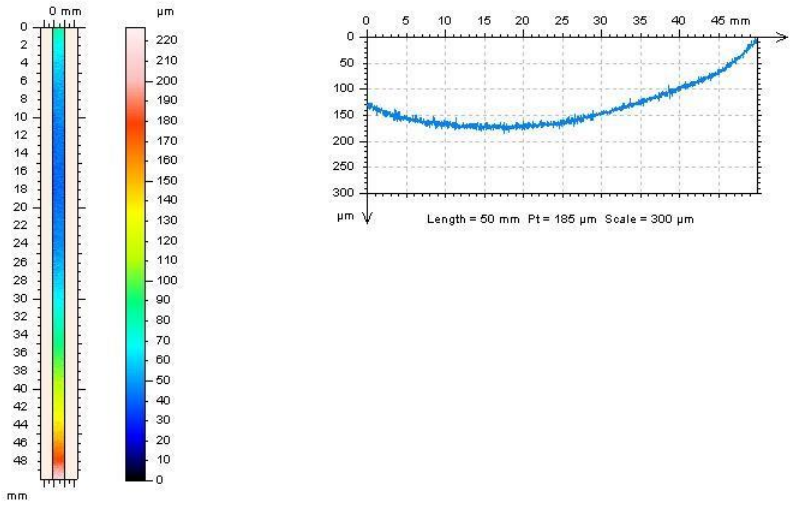

Figure 23: Surface Roughness of pure Cu at Lyon Arboretum (AA 6061-T6 on-top 1CX3). LEFT: Area spectra. RIGHT: Depths along length of sample.

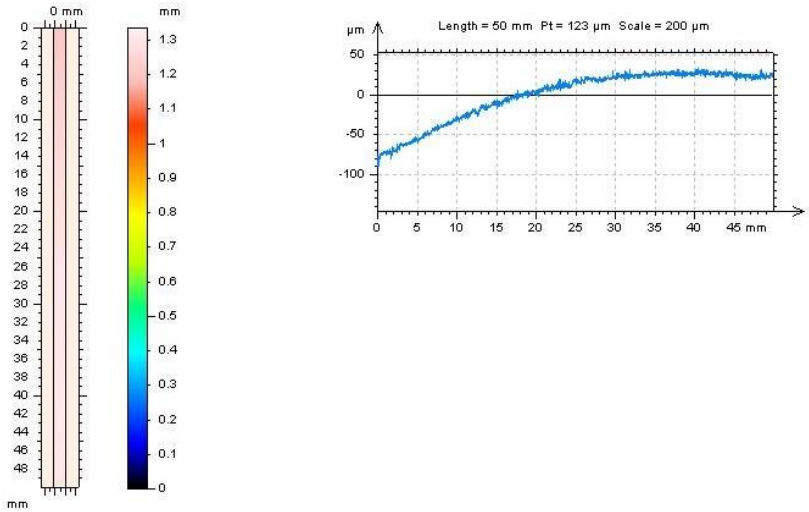

Figure 24:Surface Roughness of pure Cu at Lyon Arboretum (pure Cu on-top 1CX7). LEFT: Area spectra. RIGHT: Depths along length of sample.

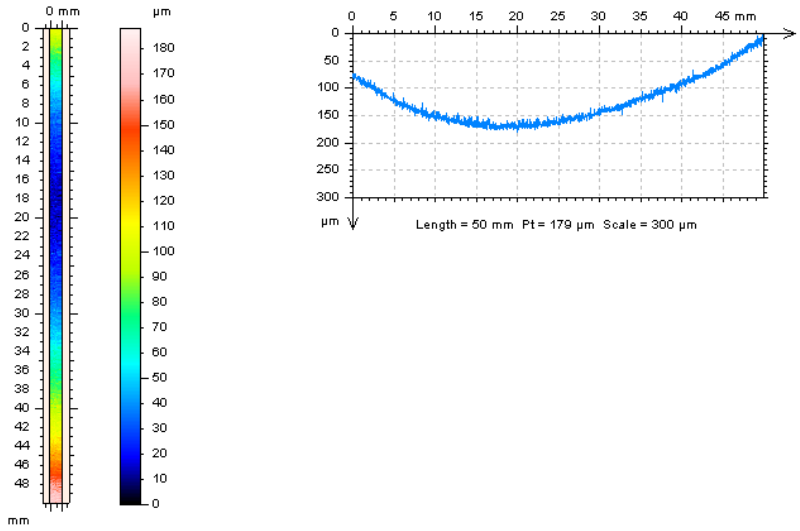

Figure 25: Surface Roughness of pure Cu at MCBH (uncoupled 2C3). LEFT: Area spectra. RIGHT: Depths along length of sample.

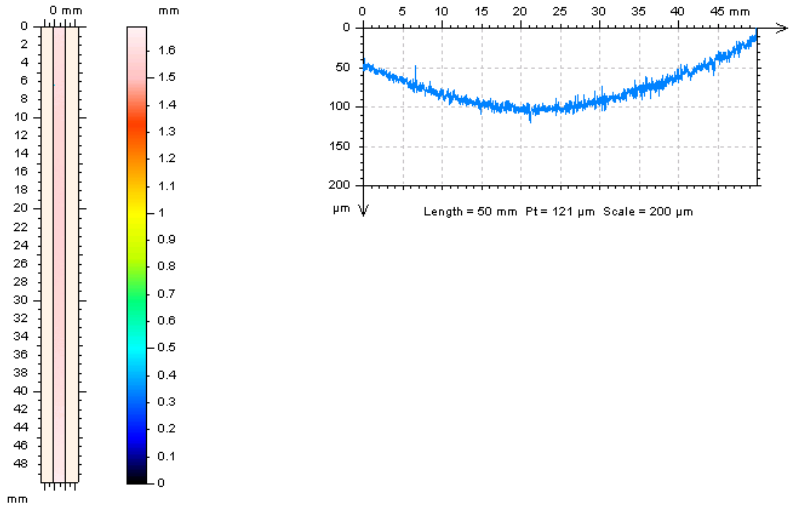

Figure 26: Surface Roughness of pure Cu at MCBH (pure Cu on-top 2CL3). LEFT: Area spectra. RIGHT: Depths along length of sample.

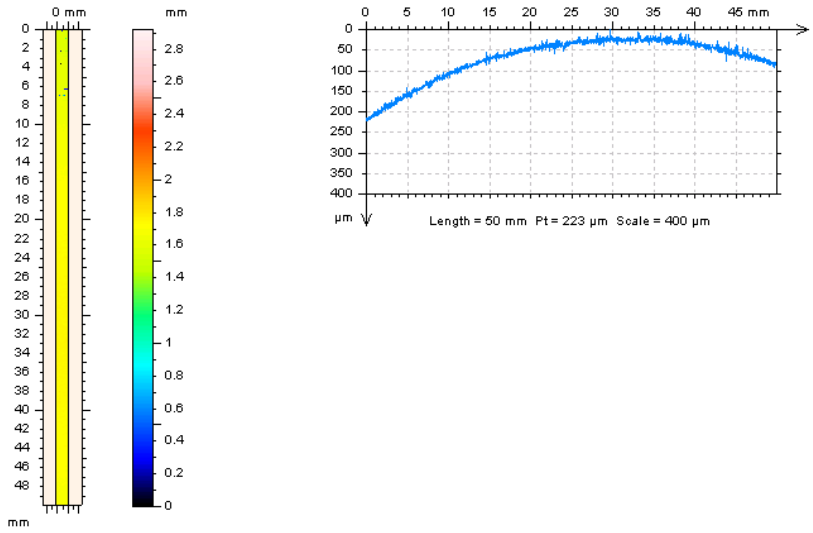

Figure 27:Surface Roughness of pure Cu at MCBH (AA 6061-T6 on-top 2CX3). LEFT: Area spectra. RIGHT: Depths along length of sample.

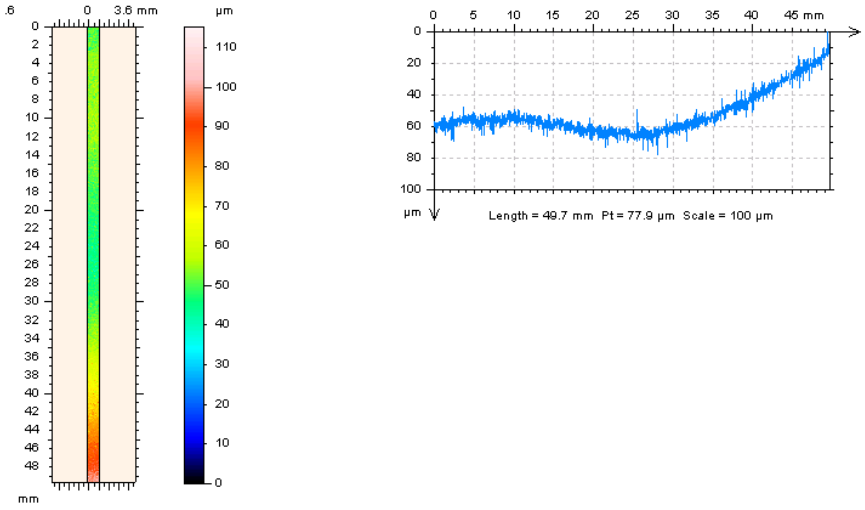

Figure 28: Surface Roughness of pure Cu at MCBH (pure Cu on-top 2CX5). LEFT: Area spectra. RIGHT: Depths along length of sample.

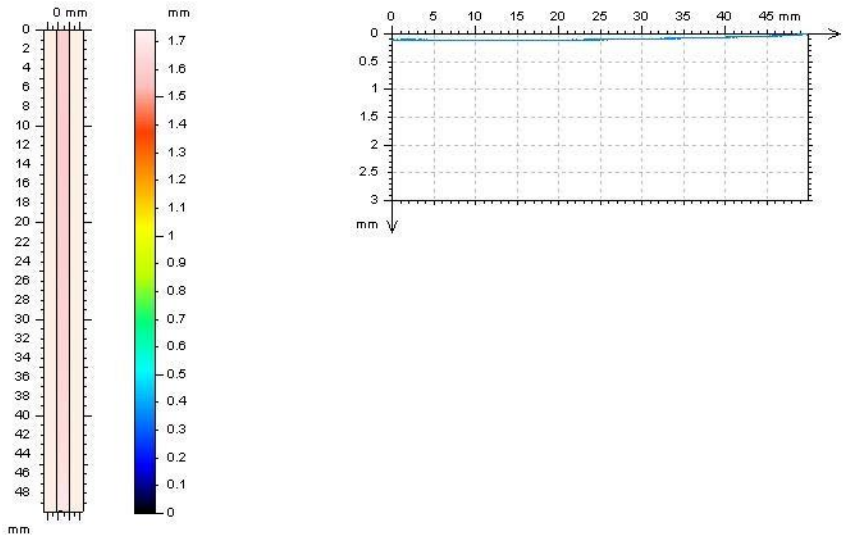

Figure 29: Surface Roughness of pure Cu at Kilauea (uncoupled 3C3). LEFT: Area spectra. RIGHT: Depths along length of sample.

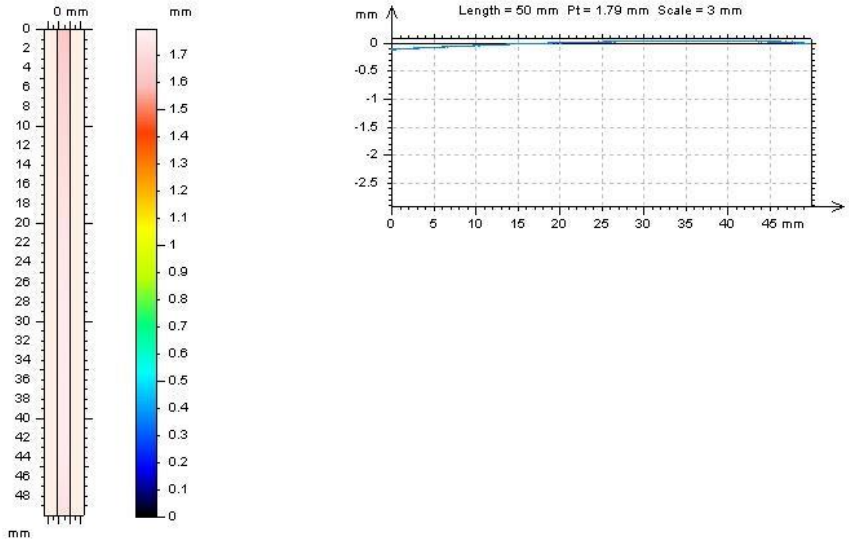

Figure 30: Surface Roughness of pure Cu at Kilauea (pure Cu on-top 3CL1). LEFT: Area spectra. RIGHT: Depths along length of sample.

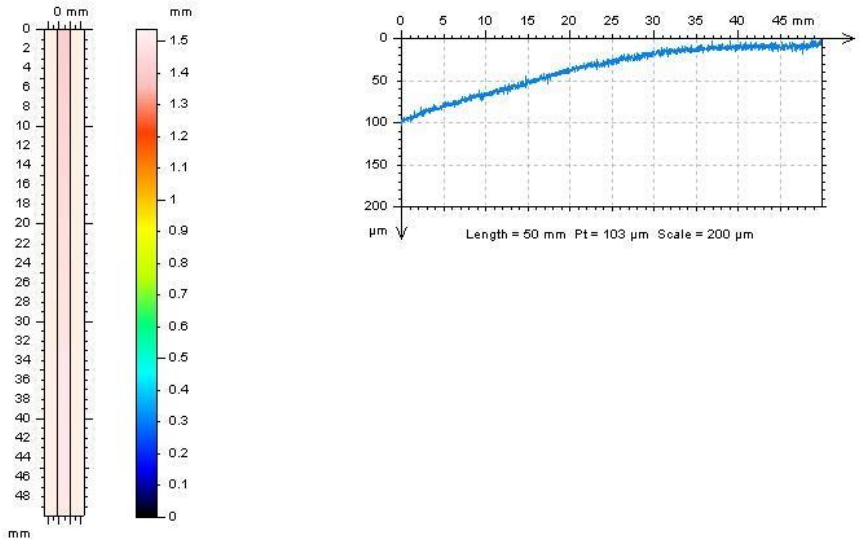

Figure 31: Surface Roughness of pure Cu at Kilauea (AA 6061-T6 on-top 3CX3). LEFT: Area spectra. RIGHT: Depths along length of sample.

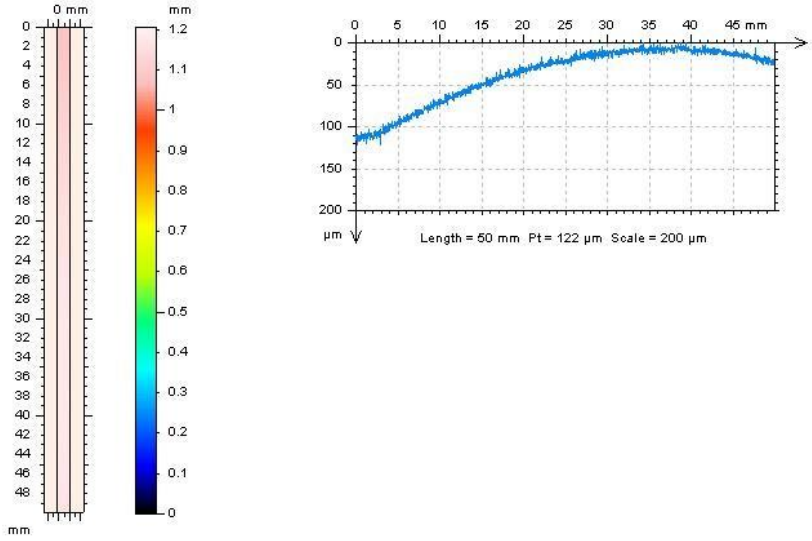

Figure 32: Surface Roughness of pure Cu at Kilauea (pure Cu on-top 3CX7). LEFT: Area spectra. RIGHT: Depths along length of sample.

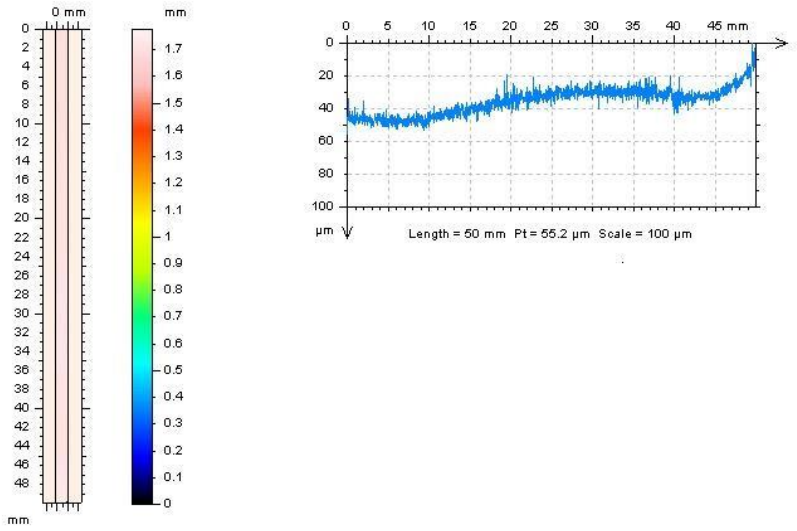

Figure 33: Surface Roughness of pure Cu at CCTC (uncoupled 4C1). LEFT: Area spectra. RIGHT: Depths along length of sample.

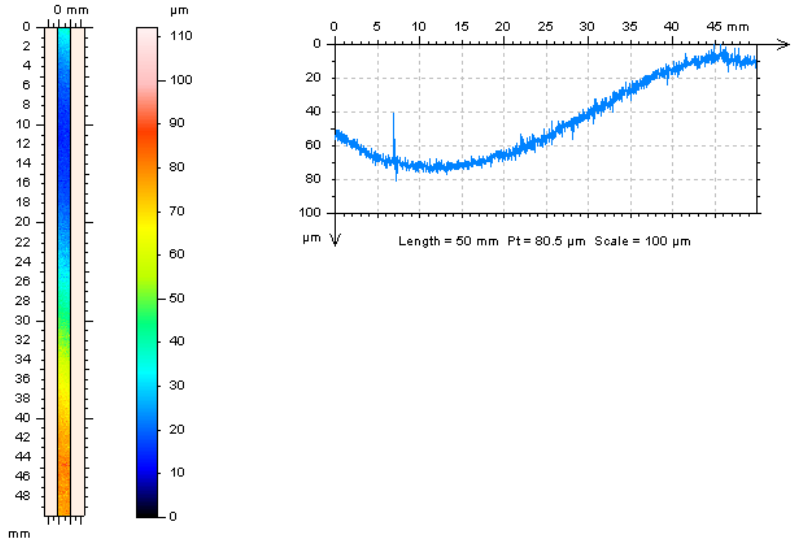

Figure 34: Surface Roughness of pure Cu at CCTC (AA 6061-T6 on-top 4CL3). LEFT: Area spectra. RIGHT: Depths along length of sample.

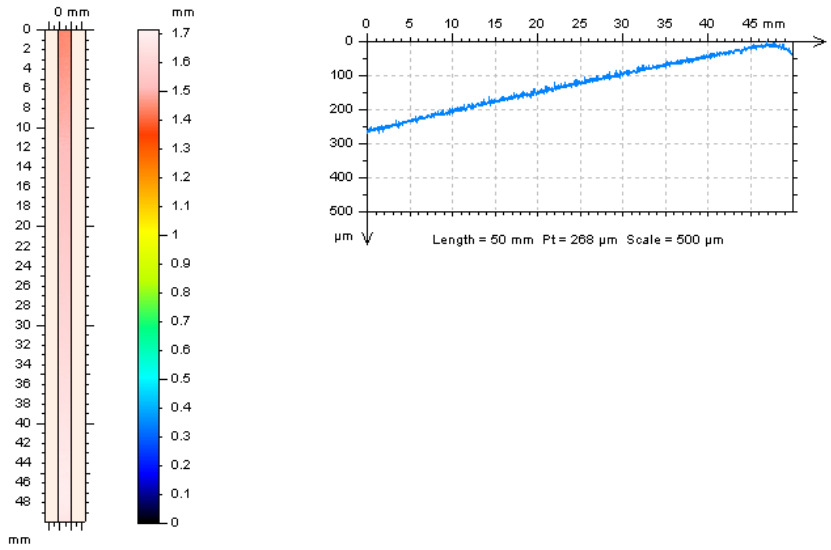

Figure 35: Surface Roughness of pure Cu at CCTC (pure Cu on-top 4CL6). LEFT: Area spectra. RIGHT: Depths along length of sample.

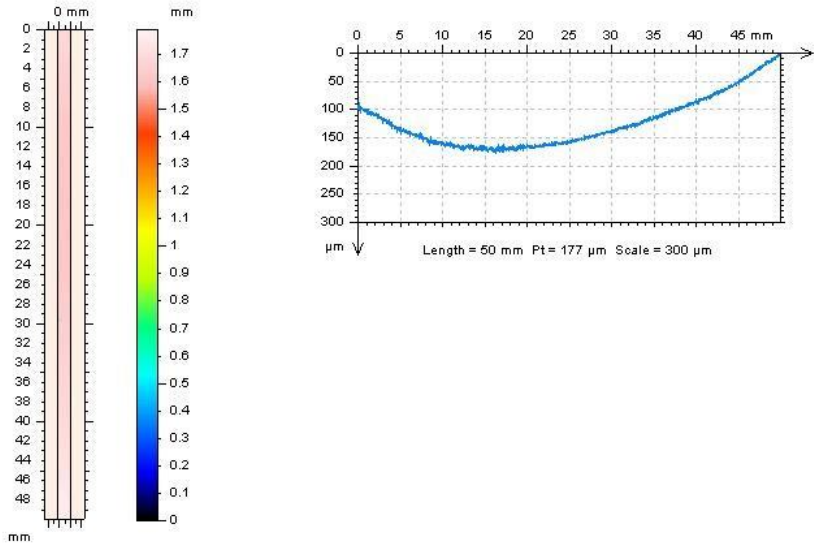

Figure 36: Surface Roughness of pure Cu at CCTC (AA 6061-T6 on-top 4CX3). LEFT: Area spectra. RIGHT: Depths along length of sample.

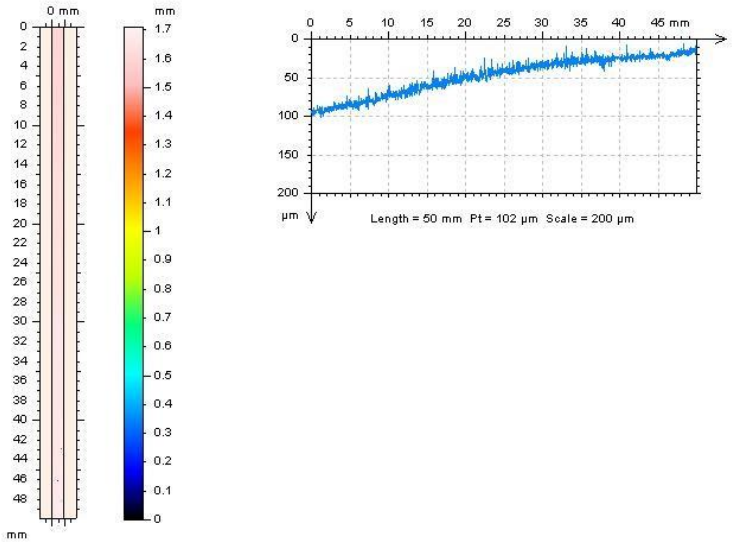

Figure 37: Surface Roughness of pure Cu at CCTC (pure Cu on-top 4CX7). LEFT: Area spectra. RIGHT: Depths along length of sample.

3.2.3.2 Silver

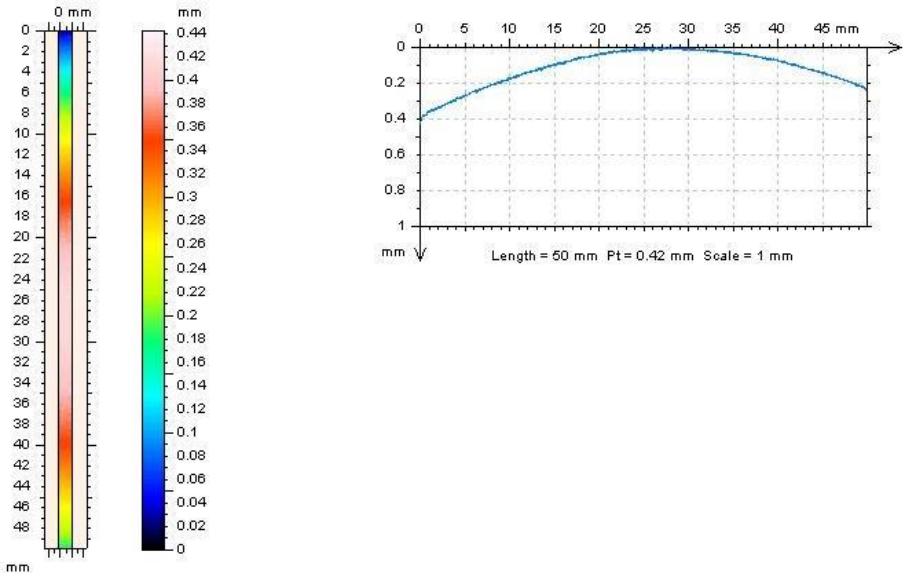

Figure 38: Surface Roughness of pure Ag at Lyon Arboretum (uncoupled 1B1). LEFT: Area spectra. RIGHT: Depths along length of sample.

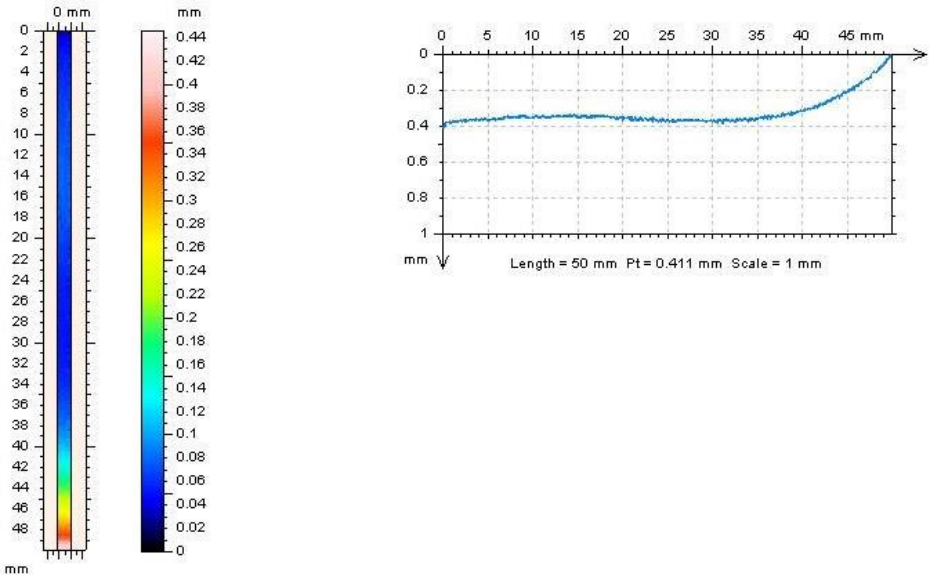

Figure 39: Surface Roughness of pure Ag at Lyon Arboretum (pure Ag on-top 1BL1). LEFT: Area spectra. RIGHT: Depths along length of sample.

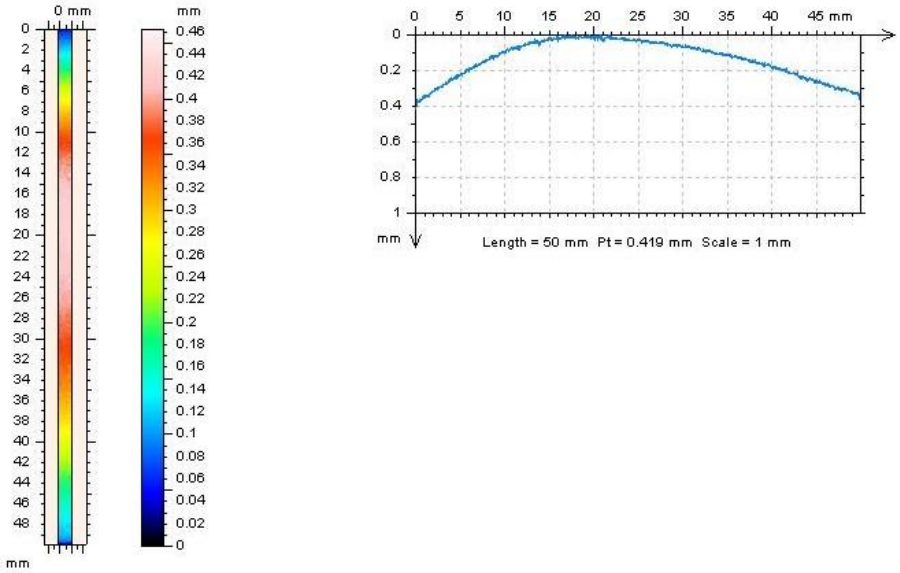

Figure 40: Surface Roughness of pure Ag at Lyon Arboretum (AA 6061-T6 on-top 1BX2). LEFT: Area spectra. RIGHT: Depths along length of sample.

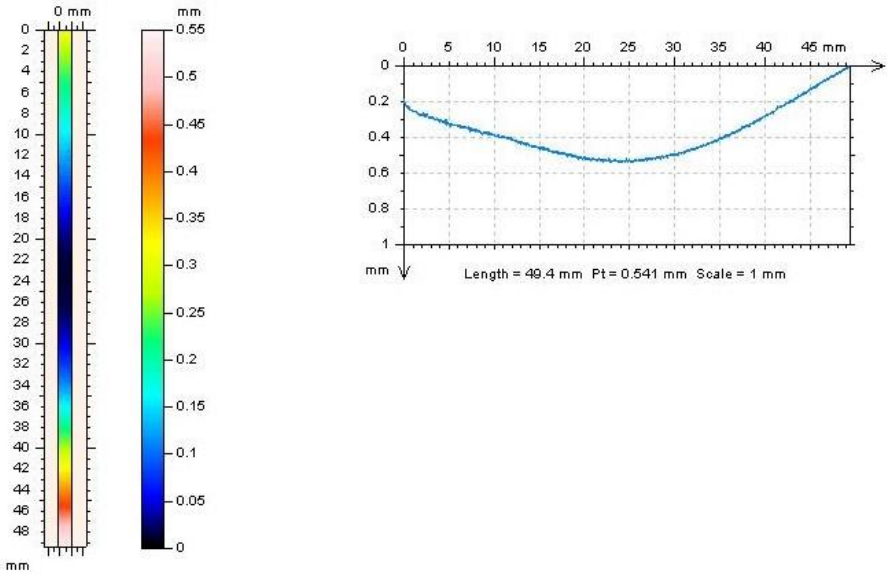

Figure 41: Surface Roughness of pure Ag at Lyon Arboretum (pure Ag on-top 1BX7). LEFT: Area spectra. RIGHT: Depths along length of sample.

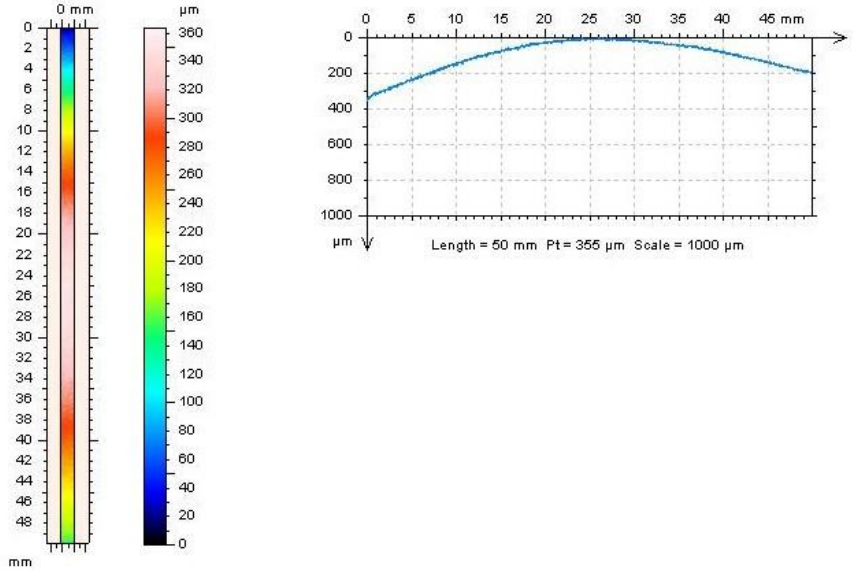

Figure 42: Surface Roughness of pure Ag at MCBH (uncoupled 2B3). LEFT: Area spectra. RIGHT: Depths along length of sample.

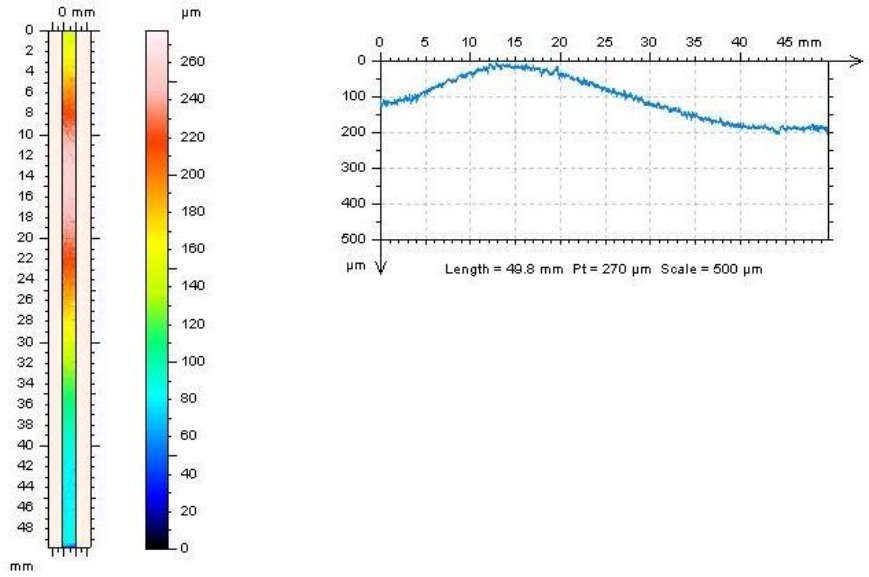

Figure 43: Surface Roughness of pure Ag at MCBH (pure Ag on-top 2BL2). LEFT: Area spectra. RIGHT: Depths along length of sample.

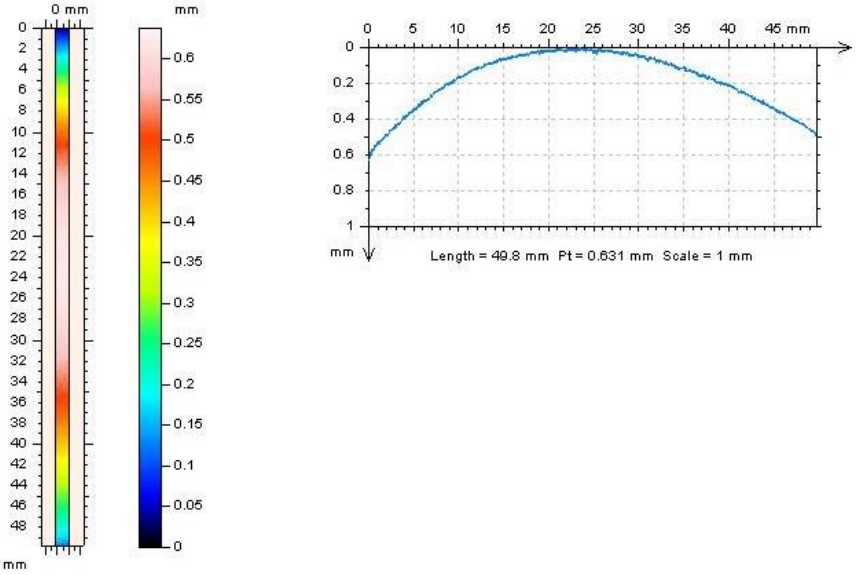

Figure 44: Surface Roughness of pure Ag at MCBH (AA 6061-T6 on-top 2BX1). LEFT: Area spectra. RIGHT: Depths along length of sample.

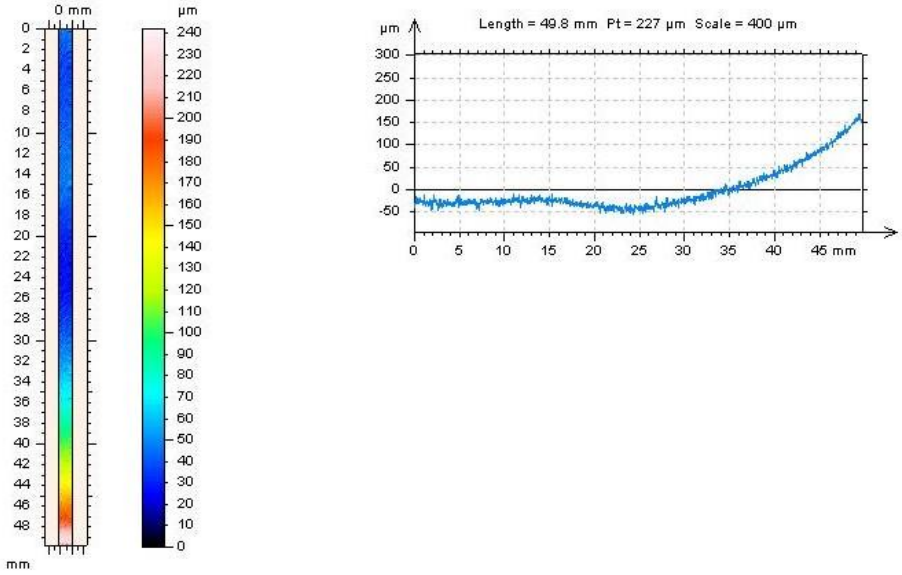

Figure 45: Surface Roughness of pure Ag at MCBH (pure Ag on-top 2BX5). LEFT: Area spectra. RIGHT: Depths along length of sample.

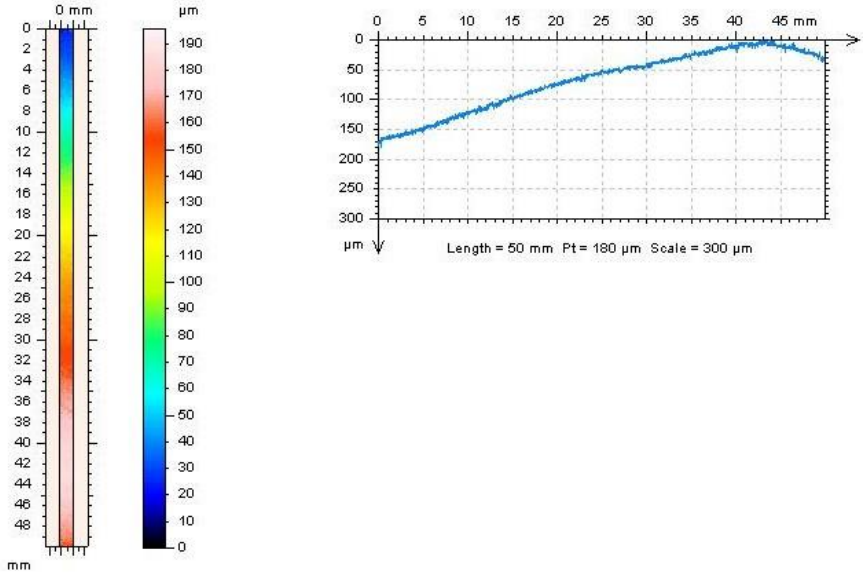

Figure 46: Surface Roughness of pure Ag at Kilauea (uncoupled 3B1). LEFT: Area spectra. RIGHT: Depths along length of sample.

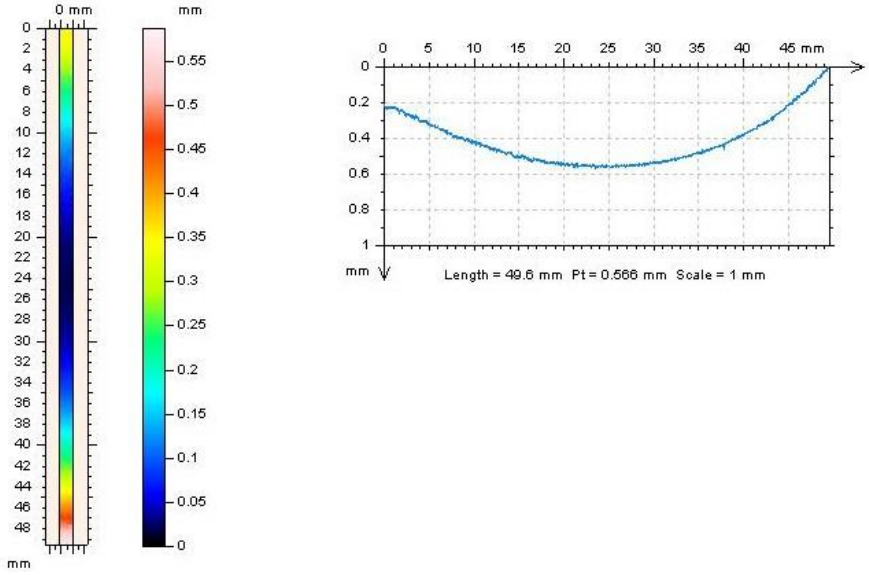

Figure 47: Surface Roughness of pure Ag at Kilauea (pure Ag on-top 3BL3). LEFT: Area spectra. RIGHT: Depths along length of sample.

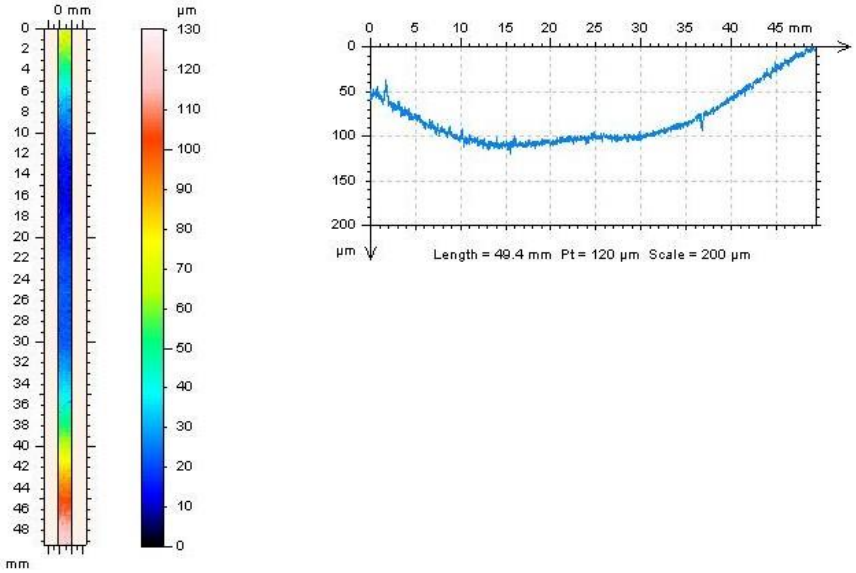

Figure 48: Surface Roughness of pure Ag at Kilauea (AA 6061-T6 on-top 3BX3). LEFT: Area spectra. RIGHT: Depths along length of sample.

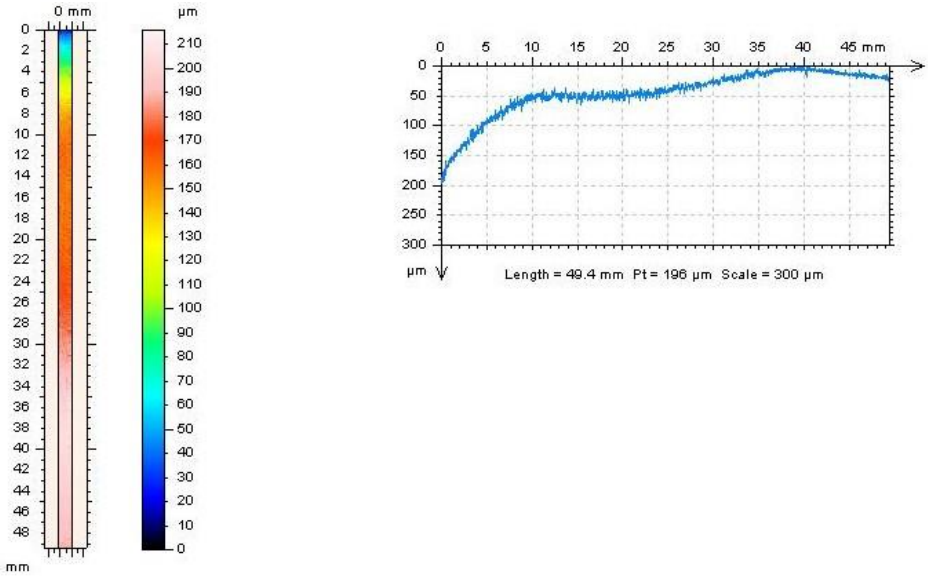

Figure 49: Surface Roughness of pure Ag at Kilauea (pure Ag on-top 3BX7). LEFT: Area spectra. RIGHT: Depths along length of sample.

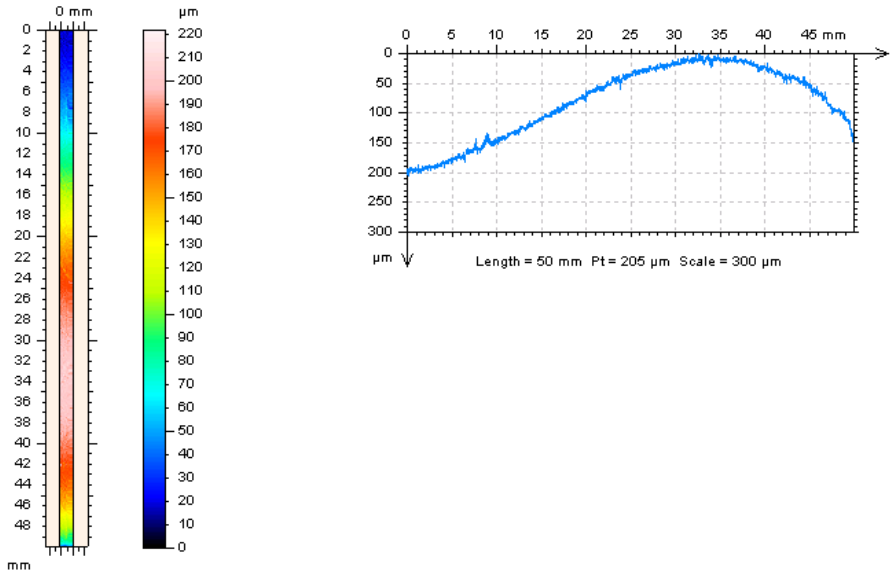

Figure 50: Surface Roughness of pure Ag at CCTC (uncoupled 4B2). LEFT: Area spectra. RIGHT: Depths along length of sample.

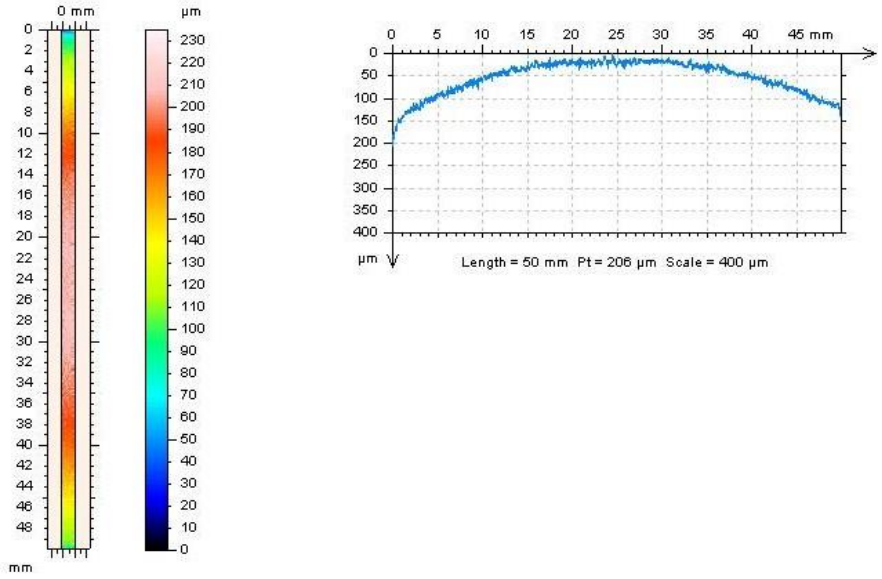

Figure 51: Surface Roughness of pure Ag at CCTC (AA 6061-T6 on-top 4BL1). LEFT: Area spectra. RIGHT: Depths along length of sample.

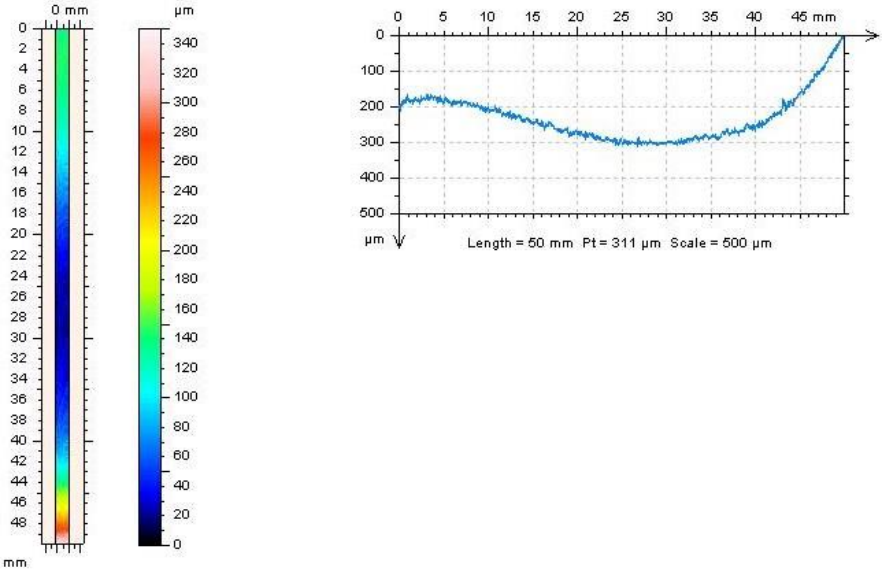

Figure 52: Surface Roughness of pure Ag at CCTC (pure Ag on-top 4BL6). LEFT: Area spectra. RIGHT: Depths along length of sample.

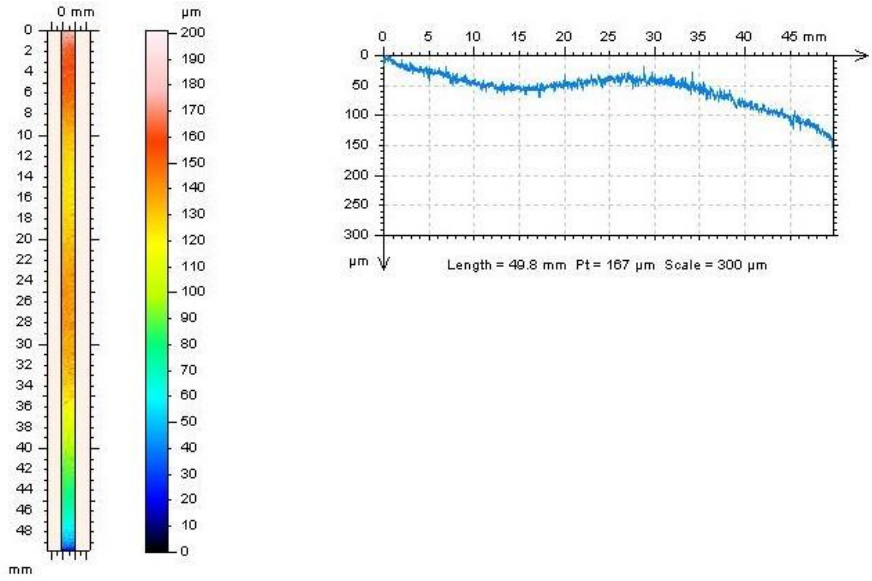

Figure 53: Surface Roughness of pure Ag at CCTC (AA 6061-T6 on-top 4BX2). LEFT: Area spectra. RIGHT: Depths along length of sample.

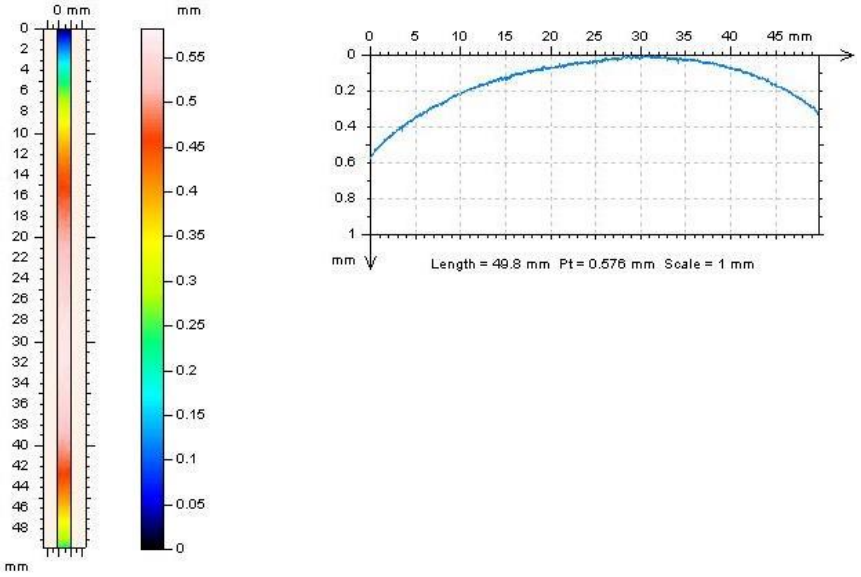

Figure 54: Surface Roughness of pure Ag at CCTC (pure Ag on-top 4BX5). LEFT: Area spectra. RIGHT: Depths along length of sample.

3.2.3.3 Titanium

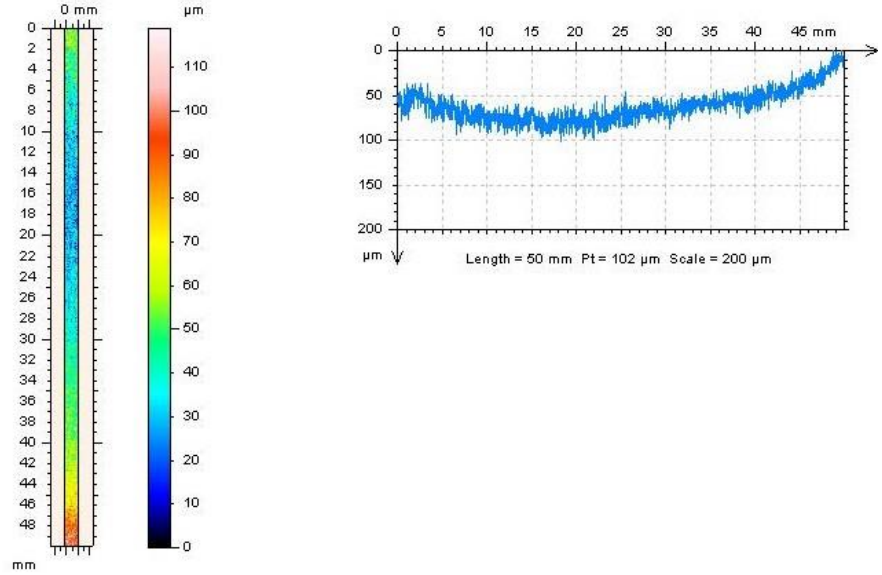

Figure 55: Surface Roughness of Ti 6Al-4V at Lyon Arboretum (uncoupled 1D2). LEFT: Area spectra. RIGHT: Depths along length of sample.

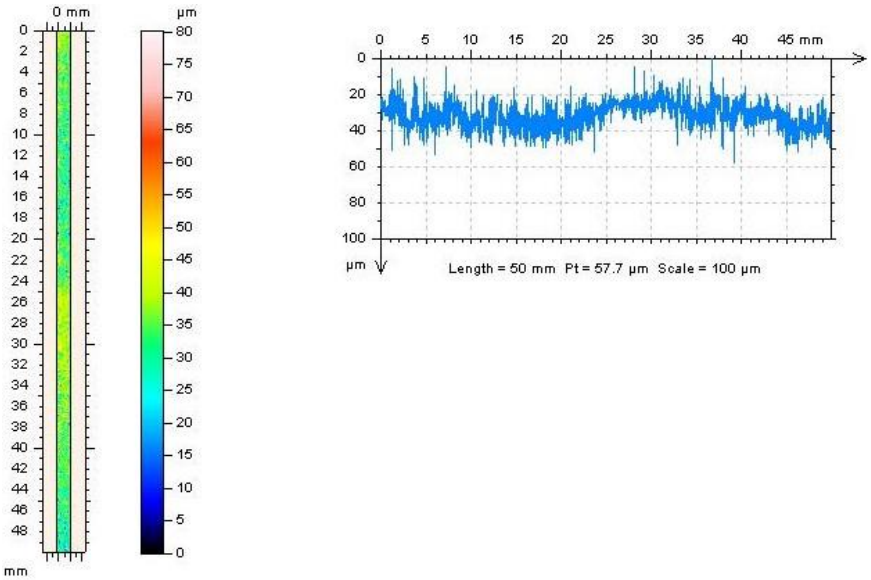

Figure 56: Surface Roughness of Ti 6Al-4V at Lyon Arboretum (Ti 6Al-4V on-top 1DL1). LEFT: Area spectra. RIGHT: Depths along length of sample.

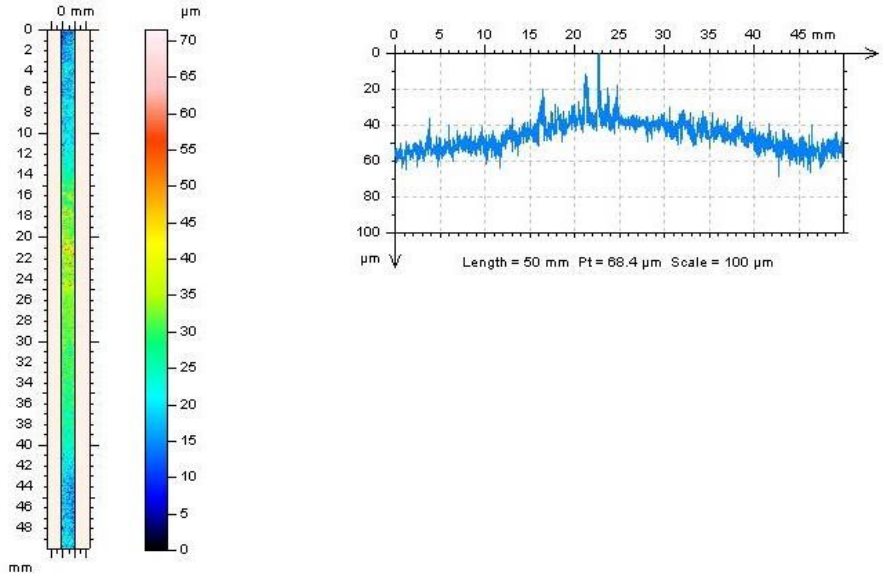

Figure 57: Surface Roughness of Ti 6Al-4Vat Lyon Arboretum (AA 6061-T6 on-top 1DX2). LEFT: Area spectra. RIGHT: Depths along length of sample.

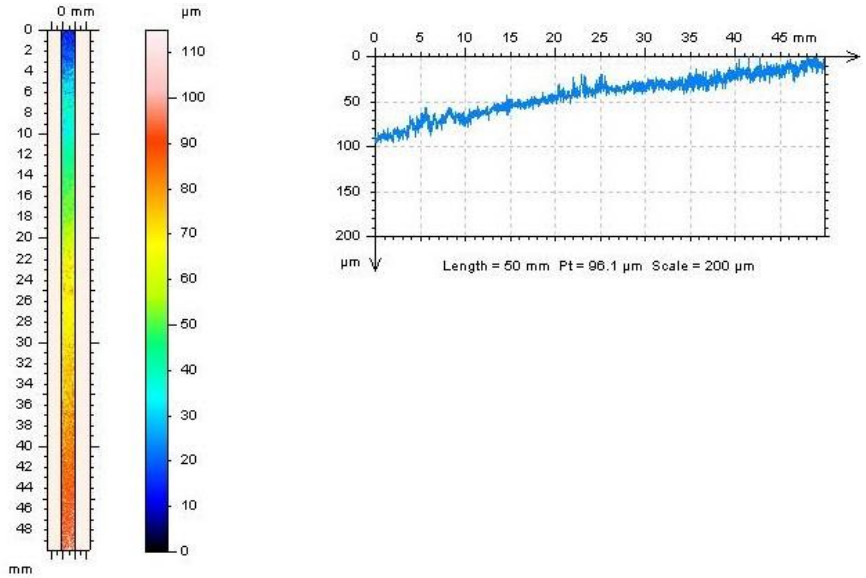

Figure 58: Surface Roughness of Ti 6Al-4V at Lyon Arboretum (Ti 6Al-4V on-top 1DX7). LEFT: Area spectra. RIGHT: Depths along length of sample.

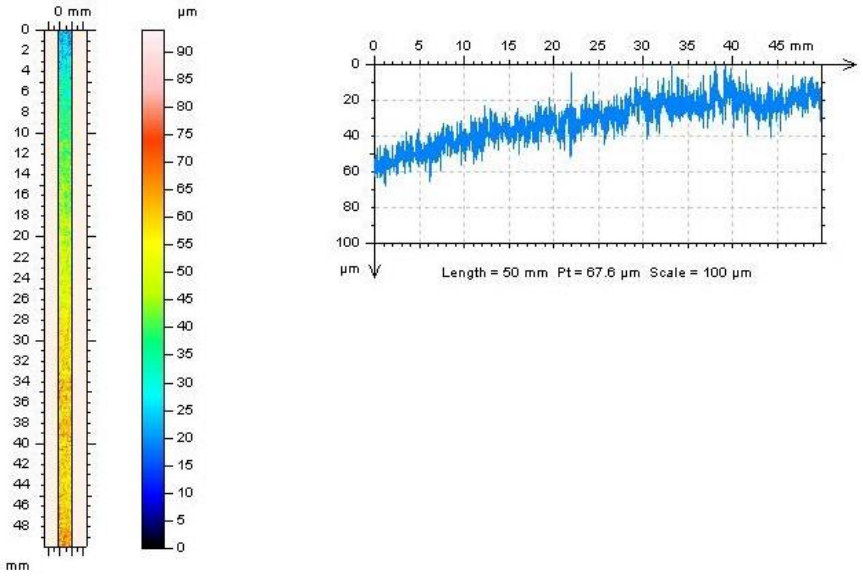

Figure 59: Surface Roughness of Ti 6Al-4V at MCBH (uncoupled 3D1). LEFT: Area spectra. RIGHT: Depths along length of sample.

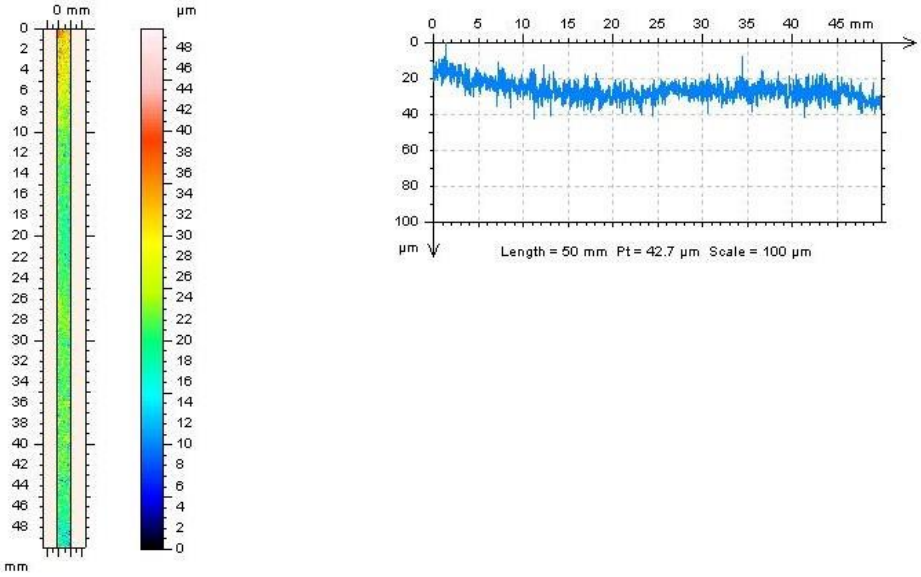

Figure 60: Surface Roughness of Ti 6Al-4V at MCBH (Ti 6Al-4V on-top 3DL3). LEFT: Area spectra. RIGHT: Depths along length of sample.

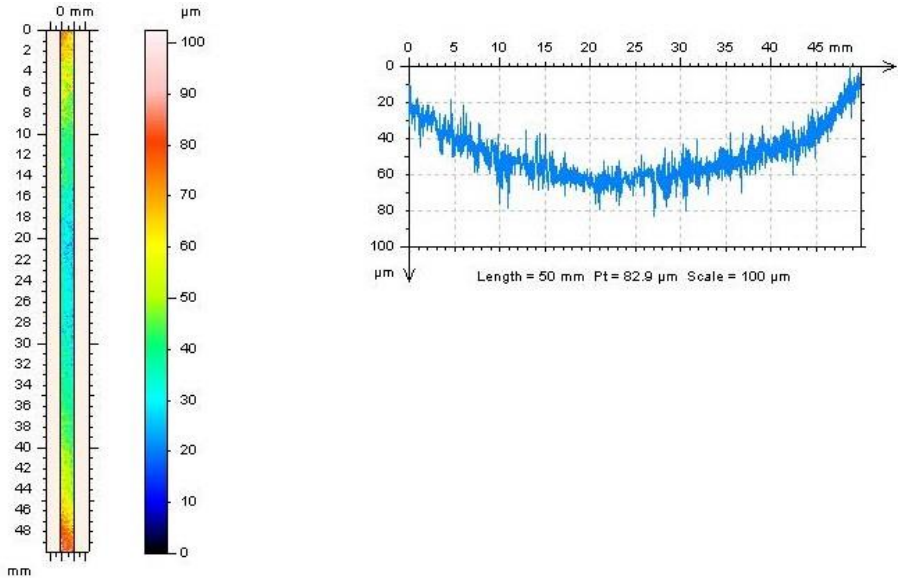

Figure 61: Surface Roughness of Ti 6Al-4V at MCBH (AA 6061-T6 on-top 3DX2). LEFT: Area spectra. RIGHT: Depths along length of sample.

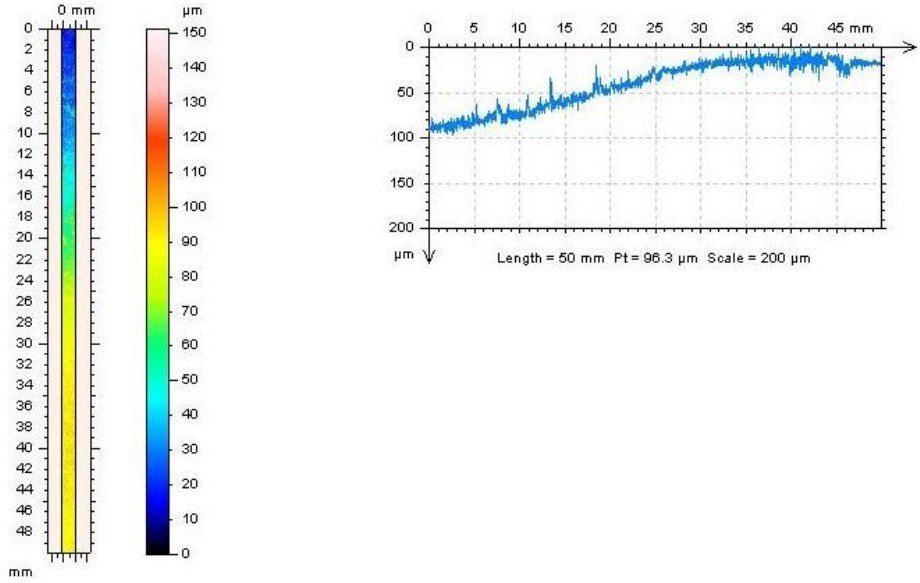

Figure 62: Surface Roughness of Ti 6Al-4V at MCBH (Ti 6Al-4V on-top 3DX6). LEFT: Area spectra. RIGHT: Depths along length of sample.

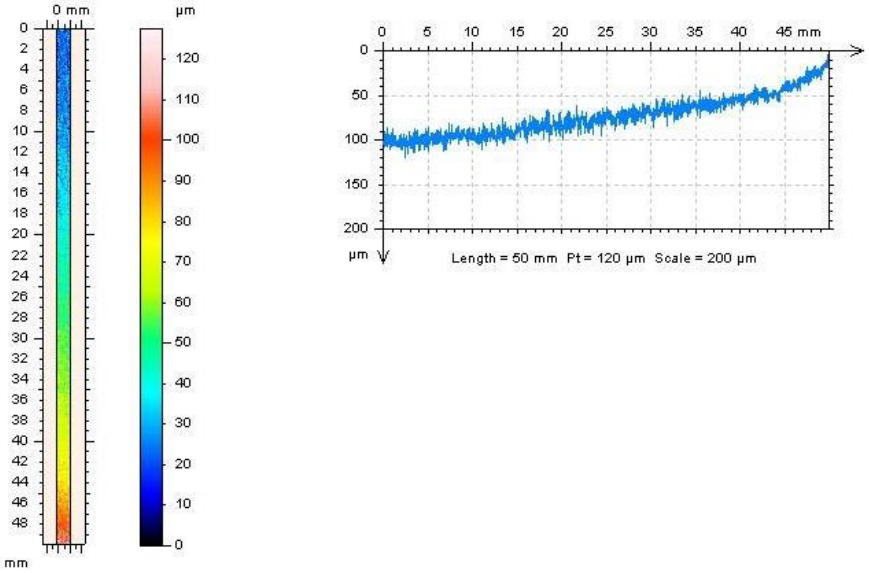

Figure 63: Surface Roughness of Ti 6Al-4Vi at Kilauea (uncoupled 2D2). LEFT: Area spectra. RIGHT: Depths along length of sample.

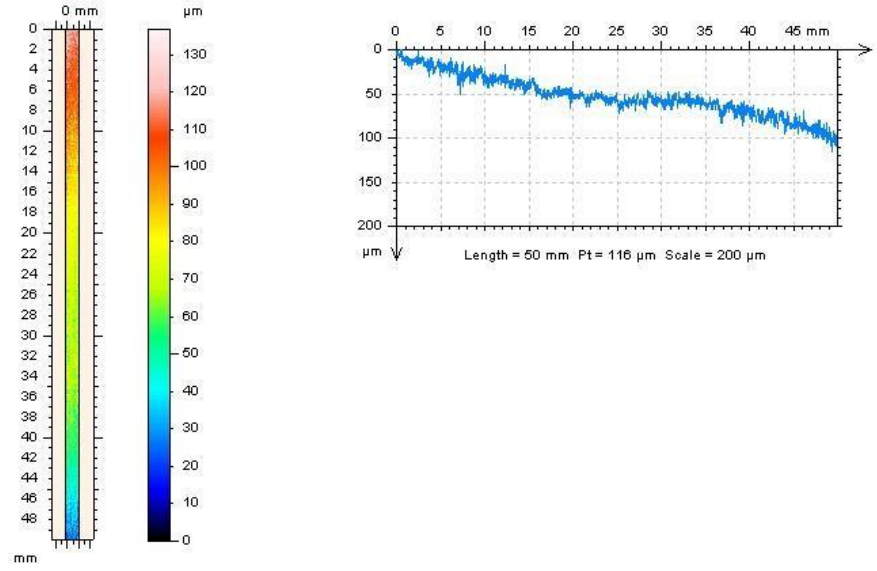

Figure 64: Surface Roughness of Ti 6Al-4V at Kilauea (Ti 6Al-4V on-top 2DL2). LEFT: Area spectra. RIGHT: Depths along length of sample.

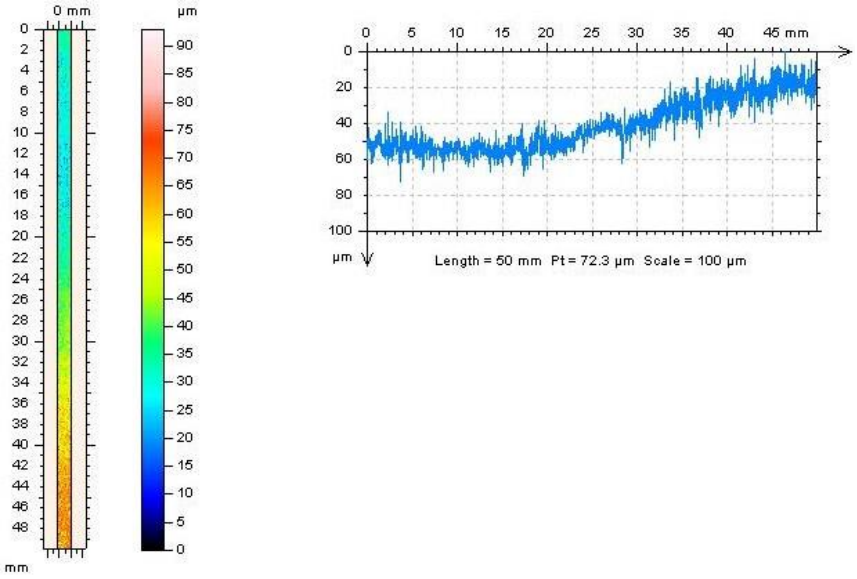

Figure 65: Surface Roughness of Ti 6Al-4V at Kilauea (Ti 6Al-4V on-top 2DL3). LEFT: Area spectra. RIGHT: Depths along length of sample.

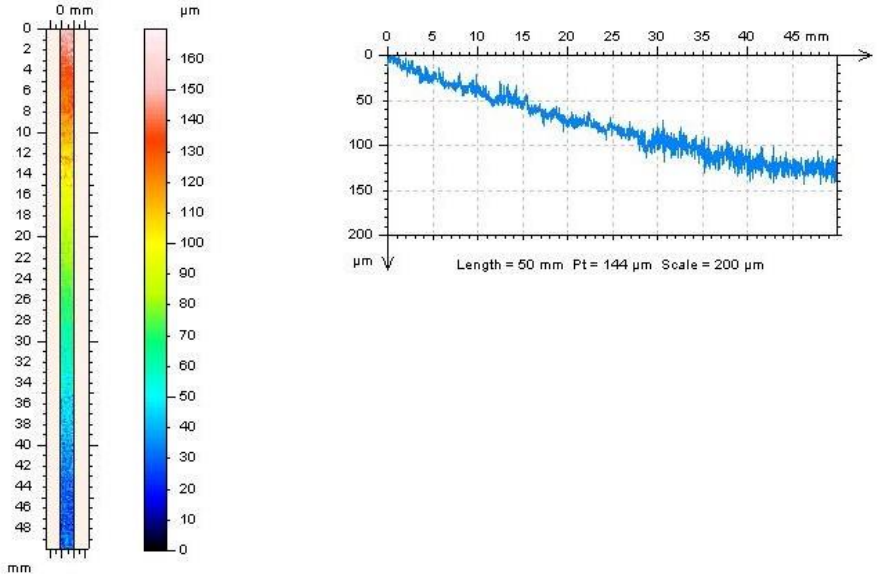

Figure 66: Surface Roughness of Ti 6Al-4V at Kilauea (AA 6061-T6 on-top 2DX1). LEFT: Area spectra. RIGHT: Depths along length of sample.

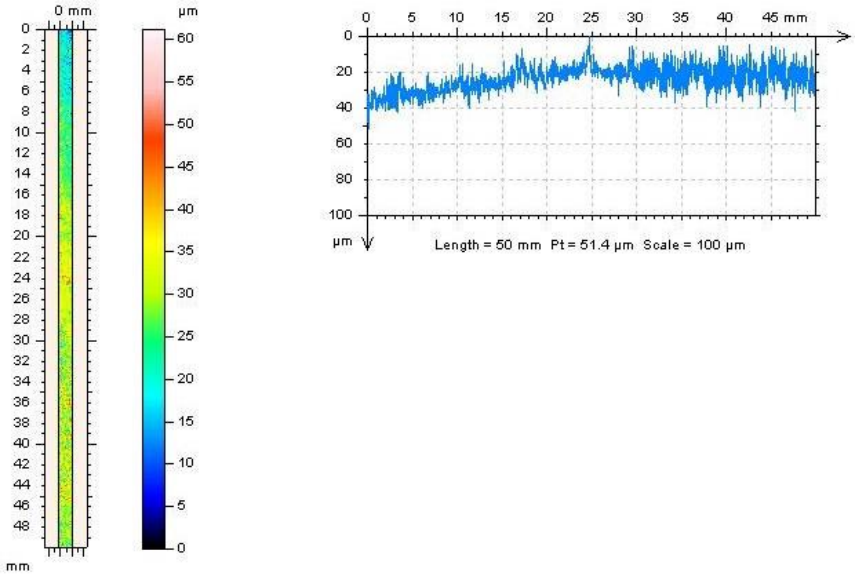

Figure 67: Surface Roughness of Ti 6Al-4V at Kilauea (Ti 6Al-4V on-top 2DX6). LEFT: Area spectra. RIGHT: Depths along length of sample.

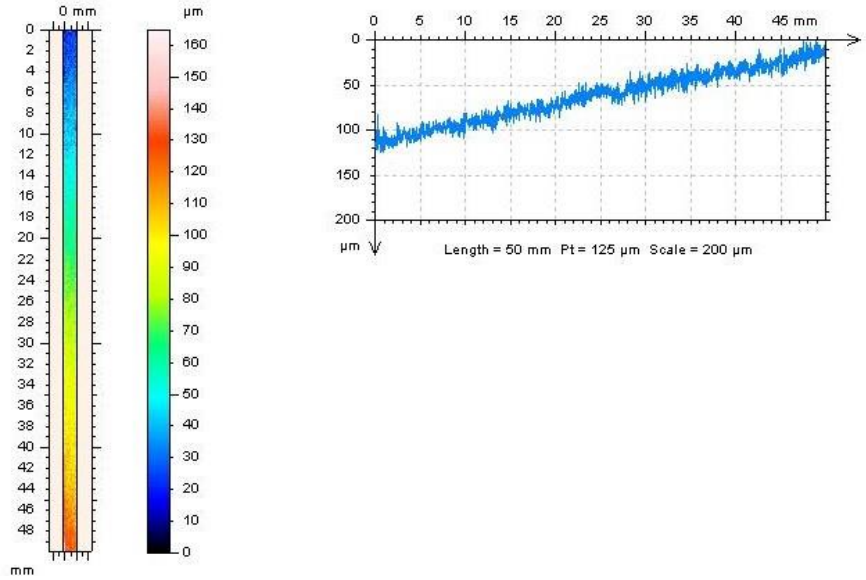

Figure 68: Surface Roughness of Ti 6Al-4V at CCTC (uncoupled 4D1). LEFT: Area spectra. RIGHT: Depths along length of sample.

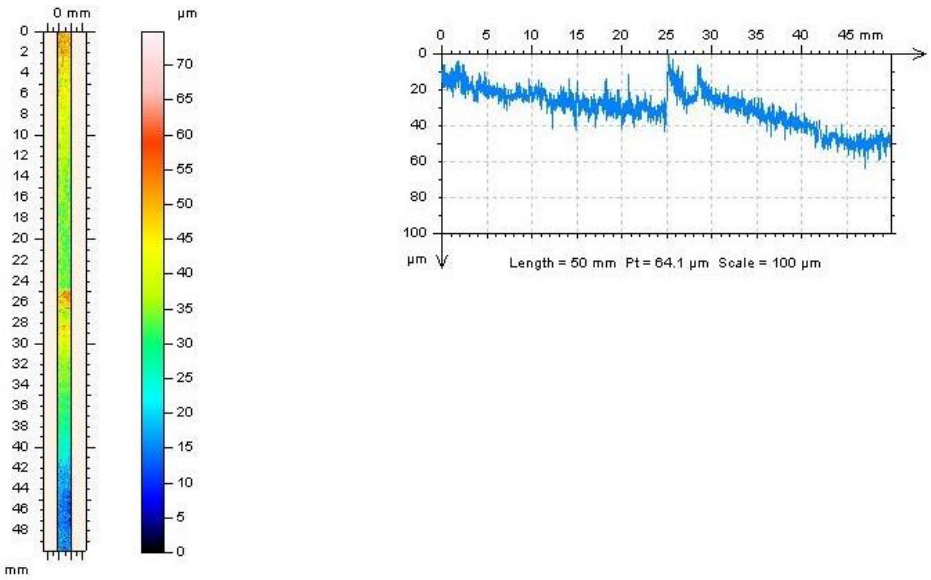

Figure 69: Surface Roughness of Ti 6Al-4V at CCTC (AA 6061-T6 on-top 4DL3). LEFT: Area spectra. RIGHT: Depths along length of sample.

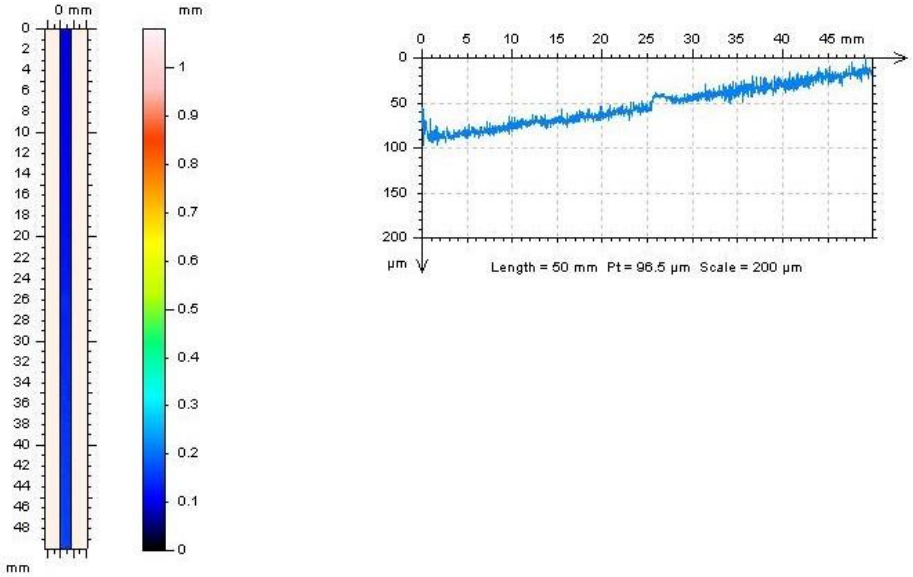

Figure 70: Surface Roughness of Ti 6Al-4V at CCTC (Ti 6Al-4V on-top 4DL6). LEFT: Area spectra. RIGHT: Depths along length of sample.

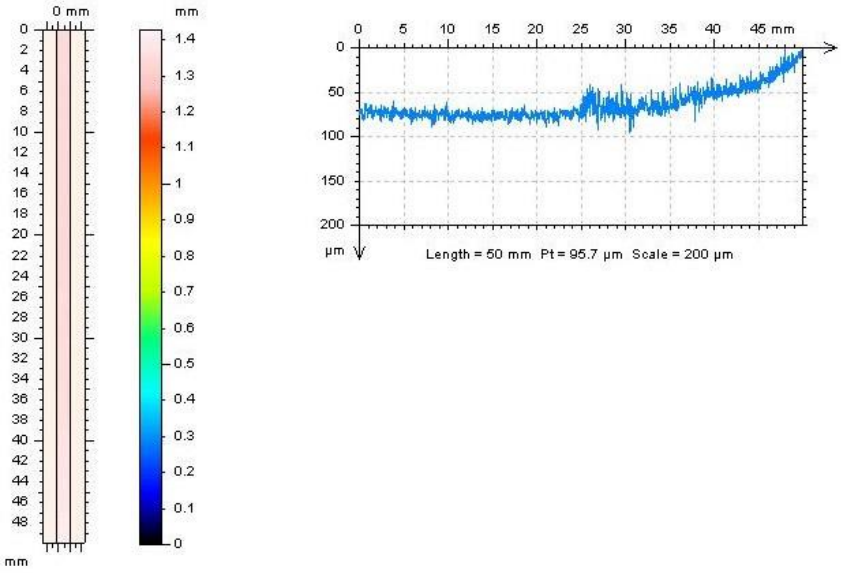

Figure 71: Surface Roughness of Ti 6Al-4V at CCTC (AA 6061-T6 on-top 4DX2). LEFT: Area spectra. RIGHT: Depths along length of sample.

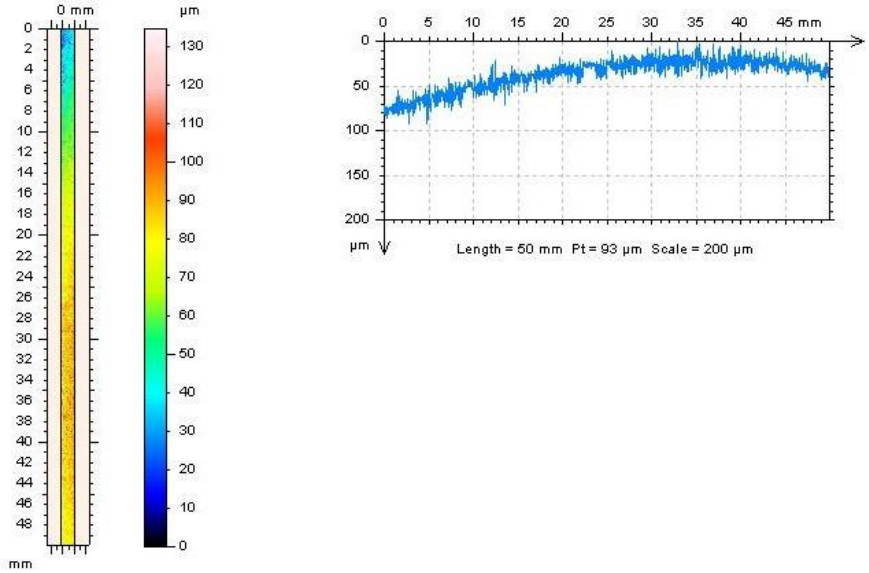

Figure 72: Surface Roughness of Ti 6Al-4V at CCTC (Ti 6Al-4V on-top 4DX5). LEFT: Area spectra. RIGHT: Depths along length of sample.

3.2.3.4 316 Stainless Steel

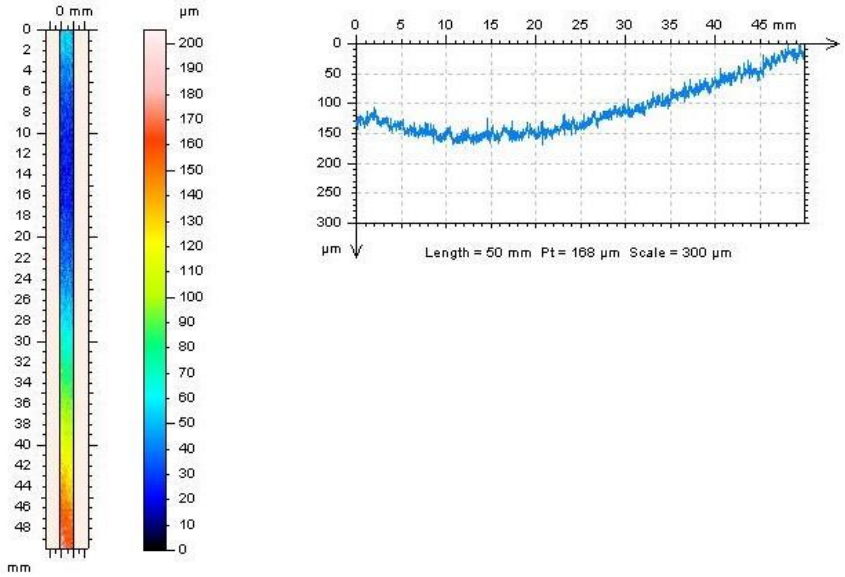

Figure 73: Surface Roughness of 316 SS at Lyon Arboretum (uncoupled 1E1). LEFT: Area spectra. RIGHT: Depths along length of sample.

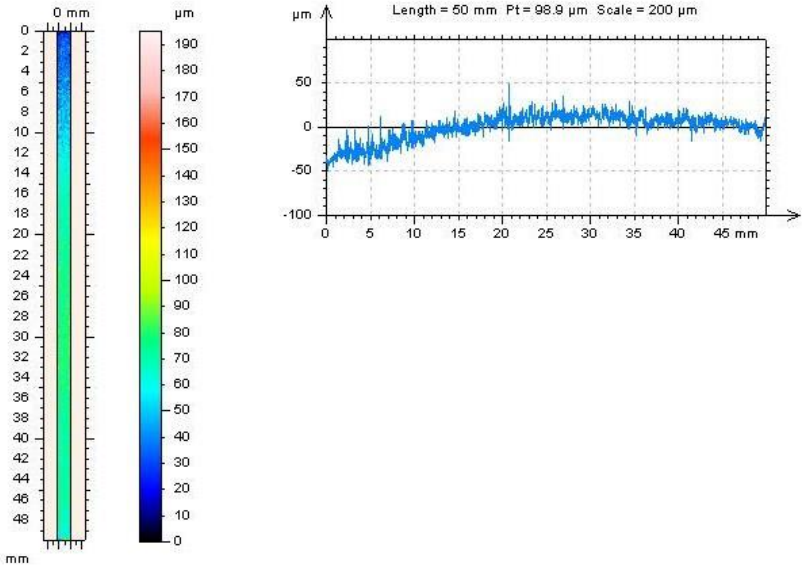

Figure 74: Surface Roughness of 316 SS at Lyon Arboretum (316 SS on-top 1EL1). LEFT: Area spectra. RIGHT: Depths along length of sample.

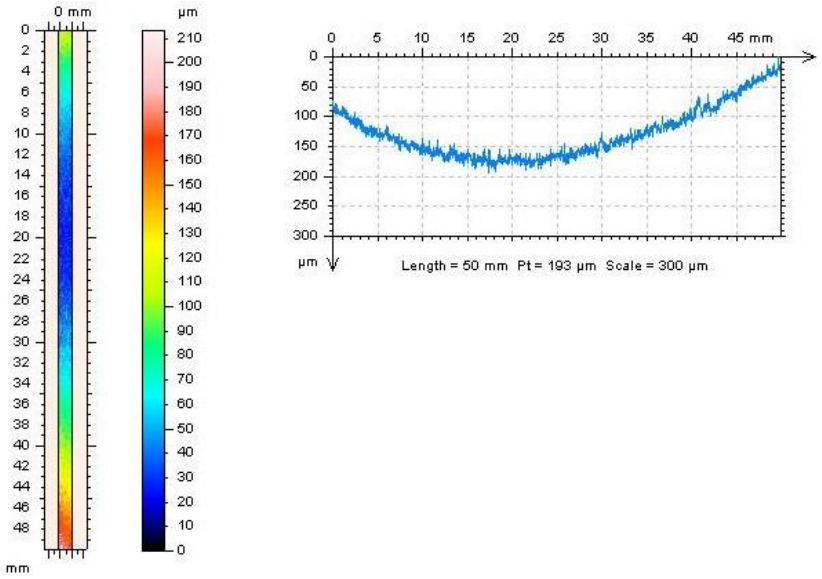

Figure 75: Surface Roughness of 316 SS at Lyon Arboretum (AA 6061-T6 on-top 1EX3). LEFT: Area spectra. RIGHT: Depths along length of sample.

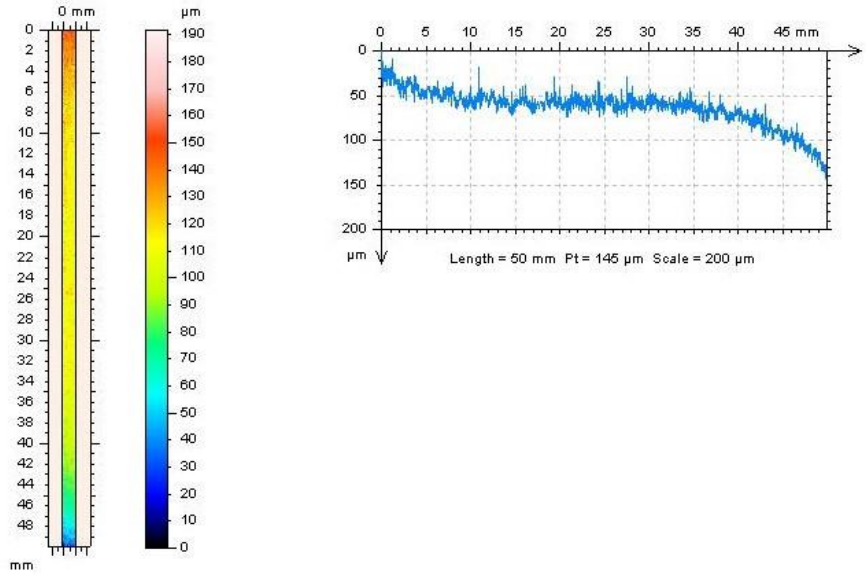

Figure 76: Surface Roughness of 316 SS at Lyon Arboretum (316 SS on-top 1EX6). LEFT: Area spectra. RIGHT: Depths along length of sample.

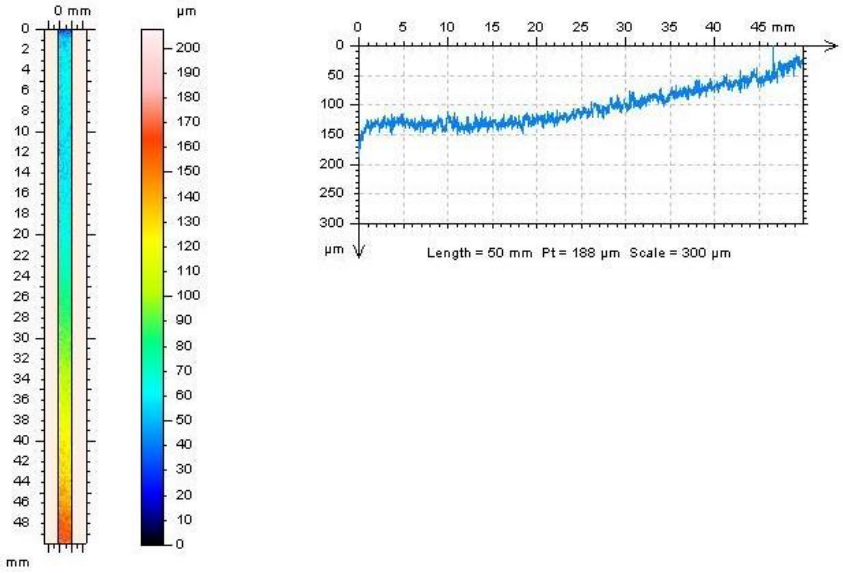

Figure 77: Surface Roughness of 316 SS at MCBH (uncoupled 2E3). LEFT: Area spectra. RIGHT: Depths along length of sample.

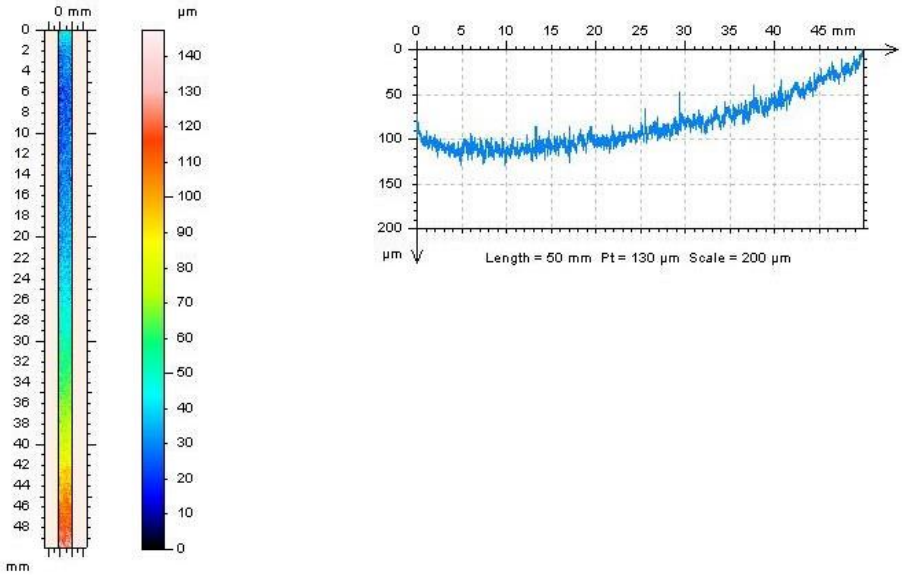

Figure 78: Surface Roughness of 316 SS at MCBH (316 SS on-top 2EL3). LEFT: Area spectra. RIGHT: Depths along length of sample.

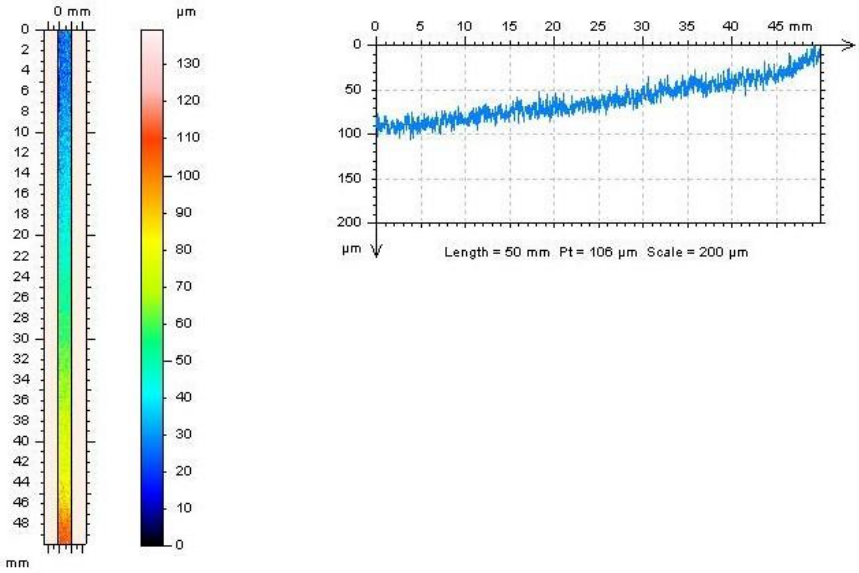

Figure 79: Surface Roughness of 316 SS at MCBH (AA 6061-T6 on-top 2EX2). LEFT: Area spectra. RIGHT: Depths along length of sample.

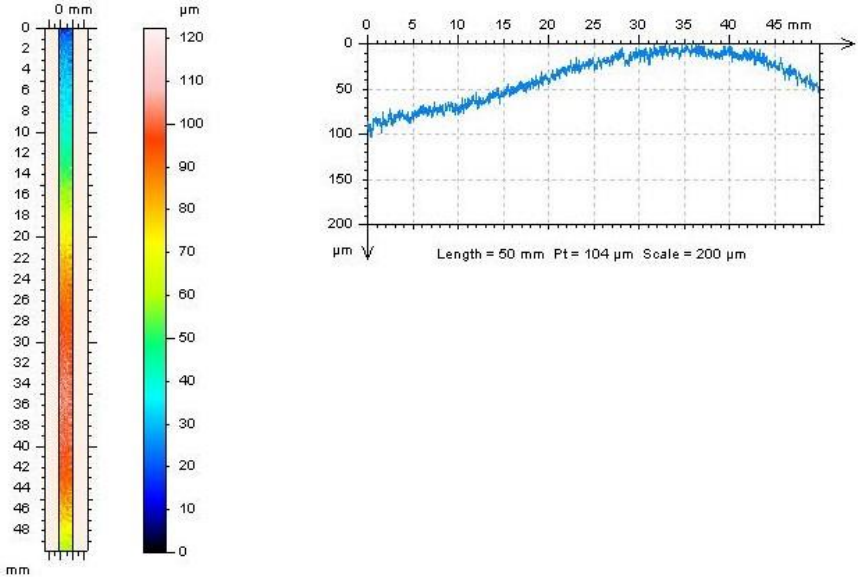

Figure 80: Surface Roughness of 316 SS at MCBH (316 SS on-top 2EX5). LEFT: Area spectra. RIGHT: Depths along length of sample.

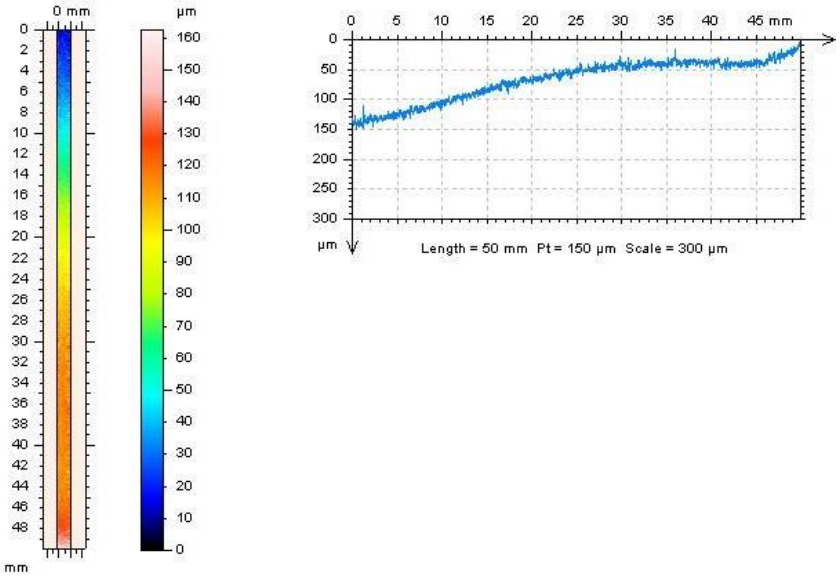

Figure 81: Surface Roughness of 316 SS at Kilauea (uncoupled 3E1). LEFT: Area spectra. RIGHT: Depths along length of sample.

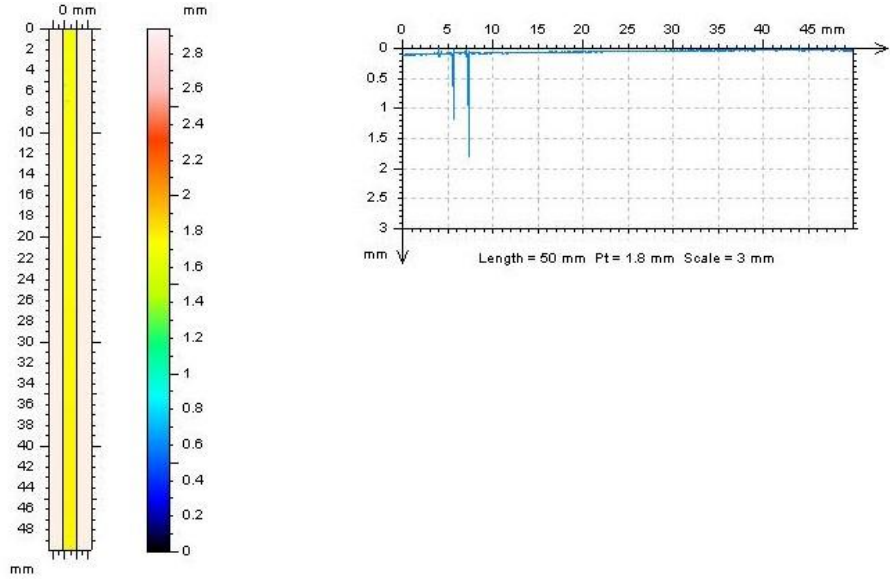

Figure 82: Surface Roughness of 316 SS at Kilauea (316 SS on-top 3EL3). LEFT: Area spectra. RIGHT: Depths along length of sample.

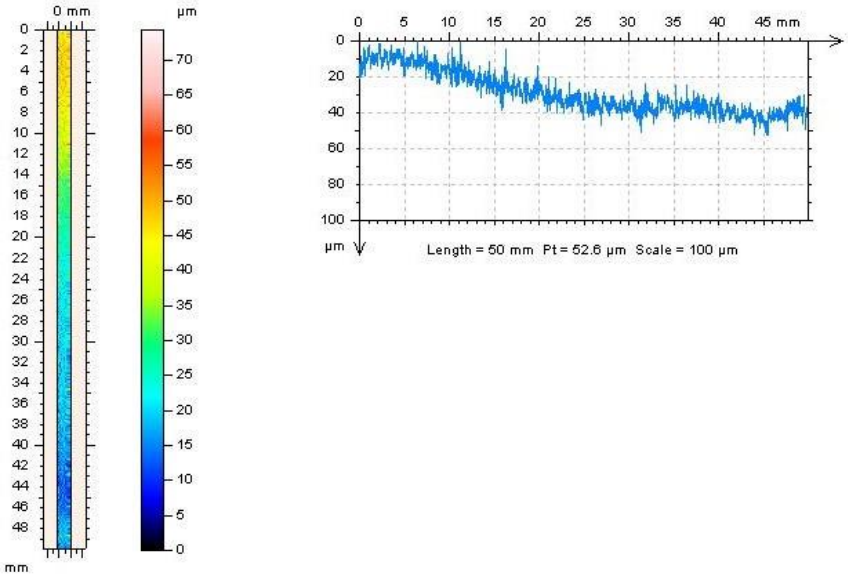

Figure 83: Surface Roughness of 316 SS at Kilauea (AA 6061-T6 on-top 3EX1). LEFT: Area spectra. RIGHT: Depths along length of sample.

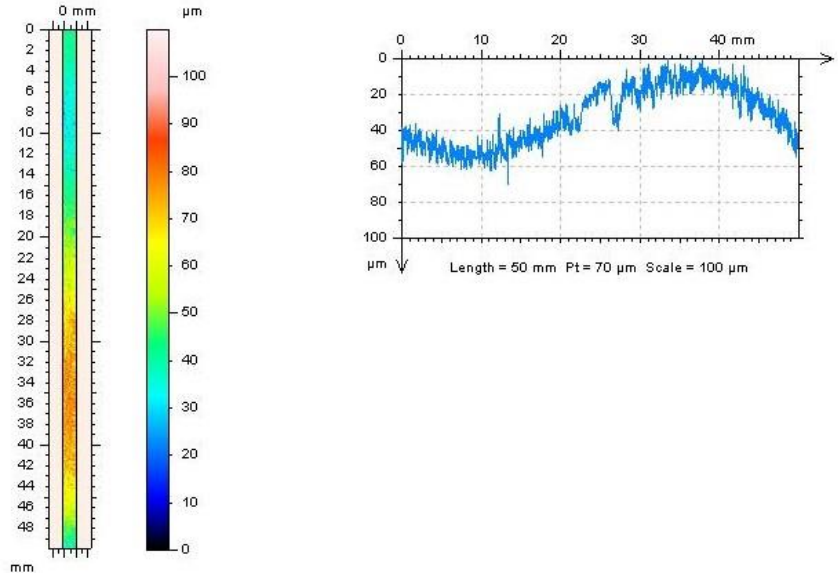

Figure 84: Surface Roughness of 316 SS at Kilauea (316 SS on-top 3EX7). LEFT: Area spectra. RIGHT: Depths along length of sample.

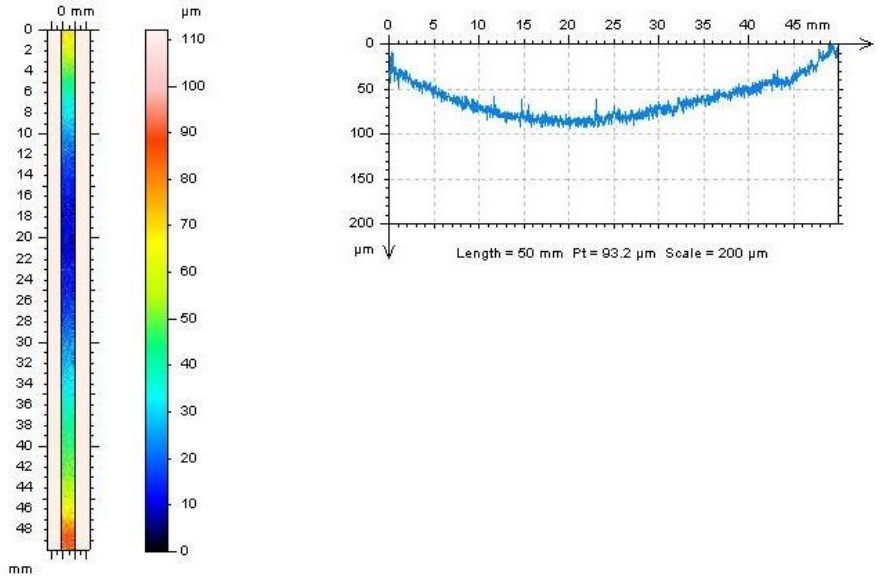

Figure 85: Surface Roughness of 316 SS at CCTC (uncoupled 4E3). LEFT: Area spectra. RIGHT: Depths along length of sample.

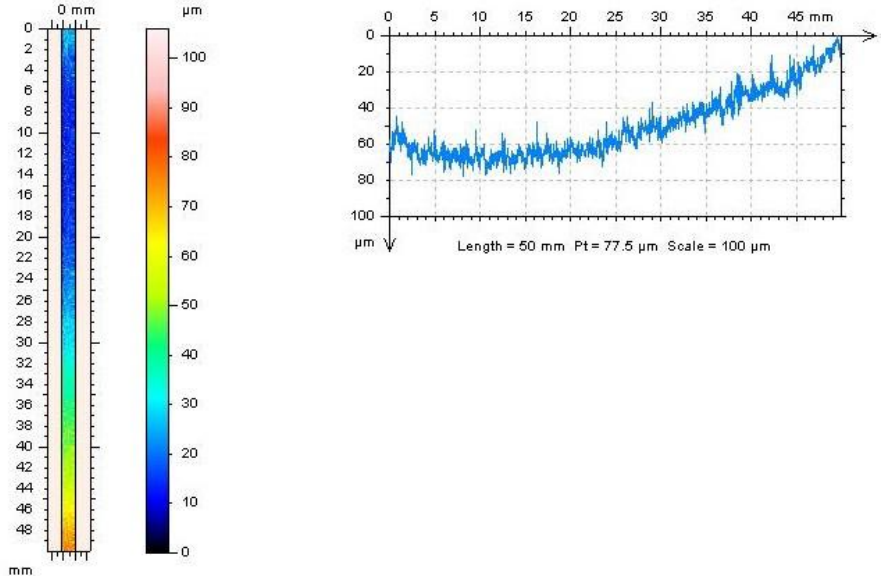

Figure 86: Surface Roughness of 316 SS at CCTC (AA 6061-T6 on-top 4EL1). LEFT: Area spectra. RIGHT: Depths along length of sample.

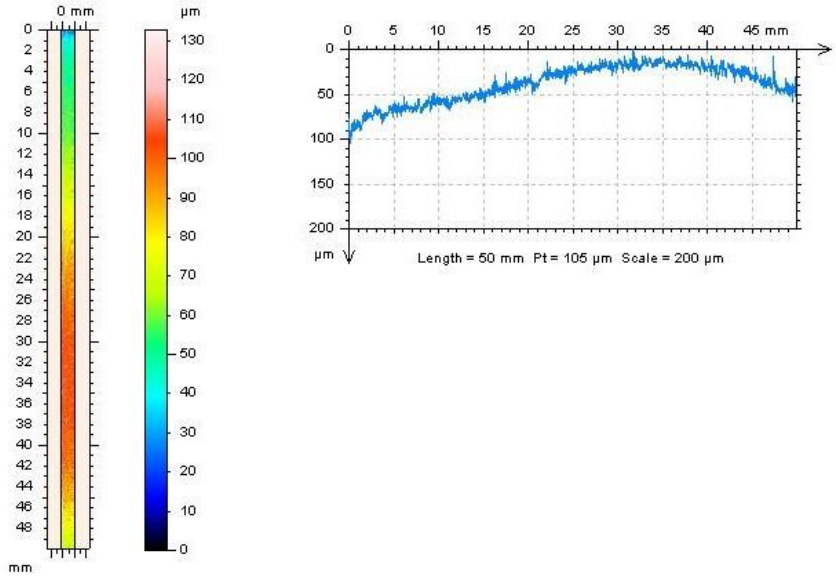

Figure 87: Surface Roughness of 316 SS at CCTC (316 SS on-top 4EL6). LEFT: Area spectra. RIGHT: Depths along length of sample.

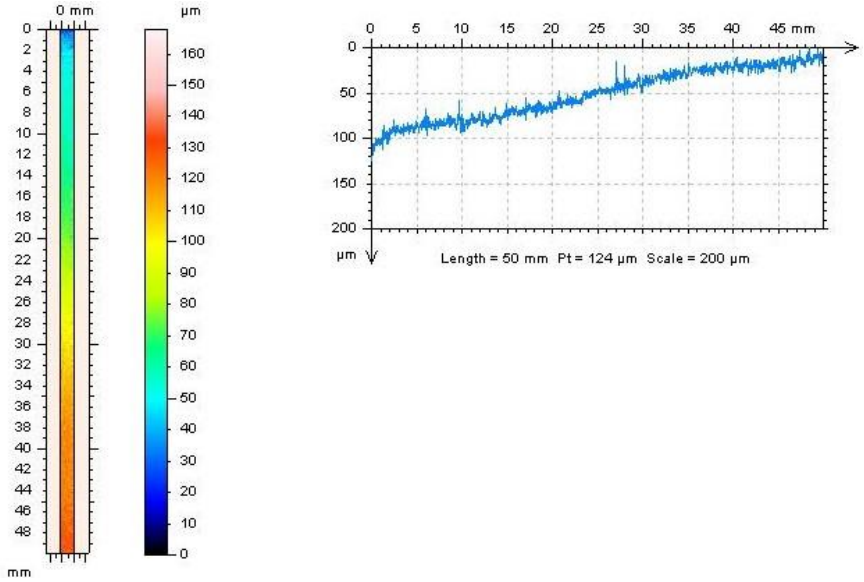

Figure 88: Surface Roughness of 316 SS at CCTC (AA 6061-T6 on-top 4EX2). LEFT: Area spectra. RIGHT: Depths along length of sample.

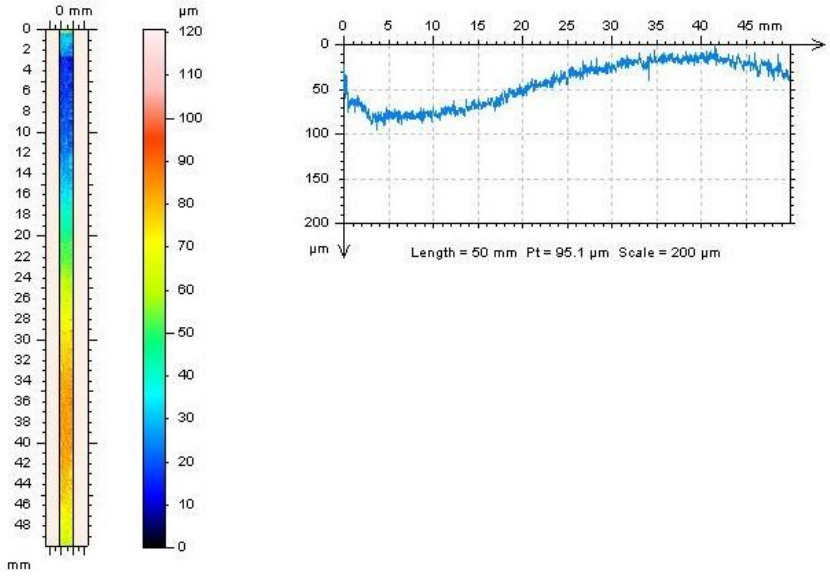

Figure 89: Surface Roughness of 316 SS at CCTC (316 SS on-top 4EX6). LEFT: Area spectra. RIGHT: Depths along length of sample.

3.2.3.5 1018 Steel

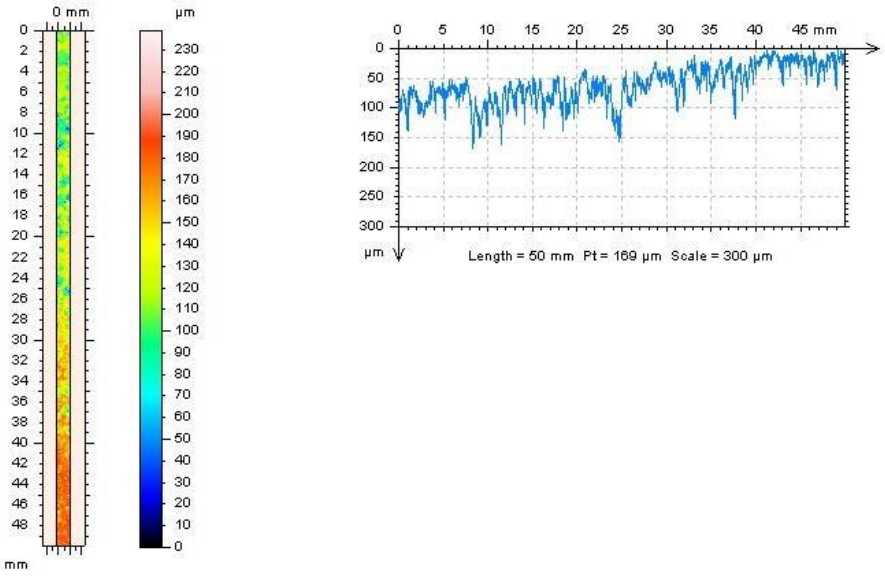

Figure 90: Surface Roughness of 1018 steel at Lyon Arboretum (uncoupled 1F3). LEFT: Area spectra. RIGHT: Depths along length of sample.

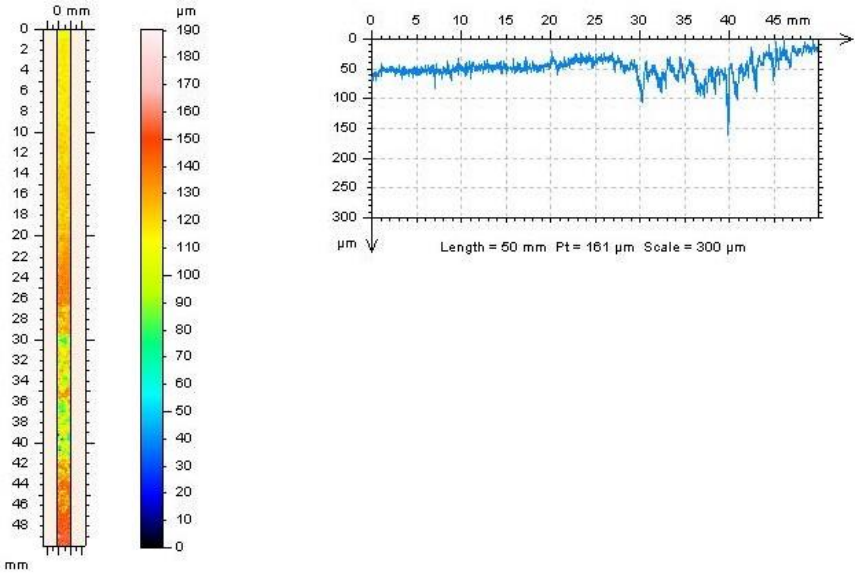

Figure 91: Surface Roughness of 1018 steel at Lyon Arboretum (1018 steel on-top 1FL3). LEFT: Area spectra. RIGHT: Depths along length of sample.

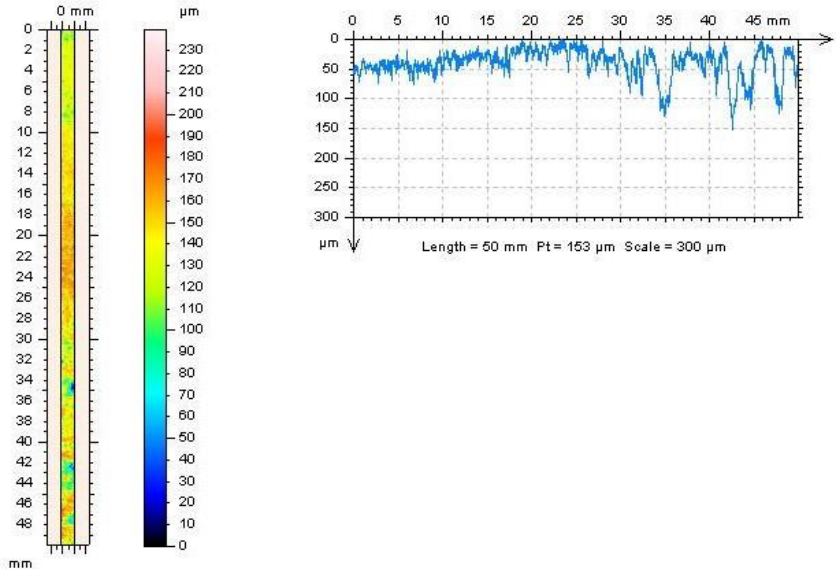

Figure 92: Surface Roughness of 1018 steel at Lyon Arboretum (AA 6061-T6 on-top 1FX3). LEFT: Area spectra. RIGHT: Depths along length of sample.

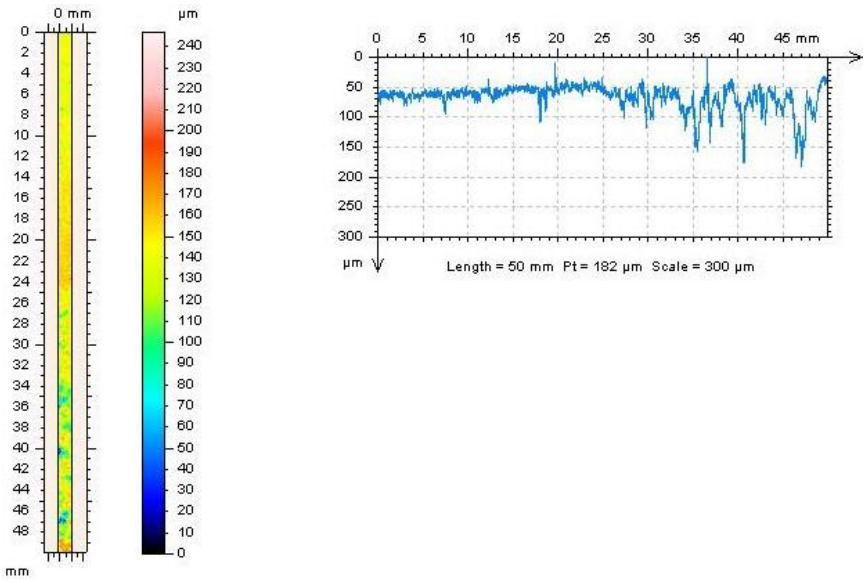

Figure 93: Surface Roughness of 1018 steel at Lyon Arboretum (1018 steel on-top 1FX7). LEFT: Area spectra. RIGHT: Depths along length of sample.

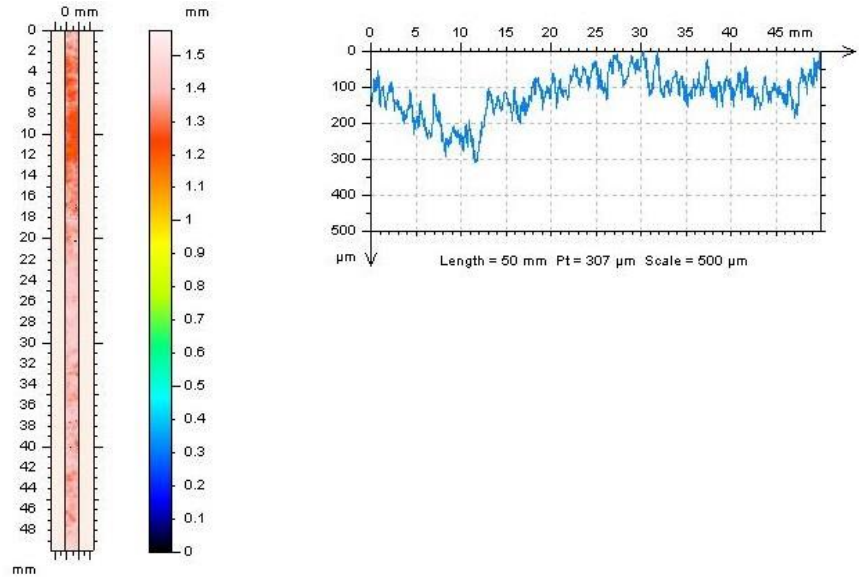

Figure 94: Surface Roughness of 1018 steel at MCBH (uncoupled 2F2). LEFT: Area spectra. RIGHT: Depths along length of sample.

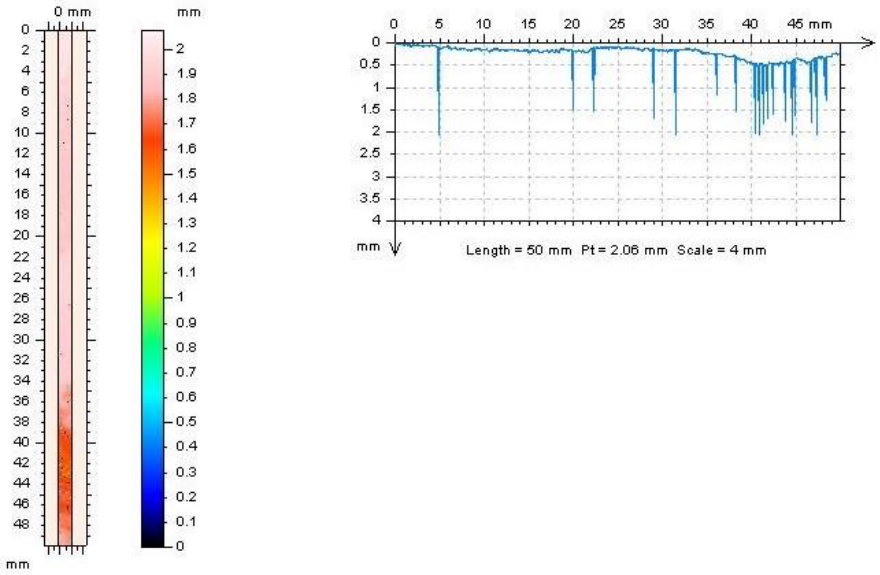

Figure 95: Surface Roughness of 1018 steel at MCBH (1018 steel on-top 2FL3). LEFT: Area spectra. RIGHT: Depths along length of sample.

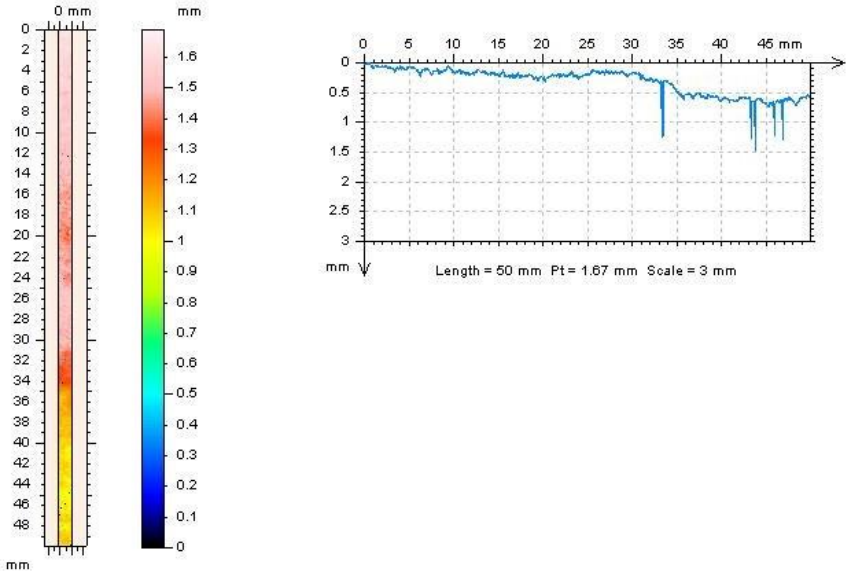

Figure 96: Surface Roughness of 1018 steel at MCBH (AA 6061-T6 on-top 2FX3). LEFT: Area spectra. RIGHT: Depths along length of sample.

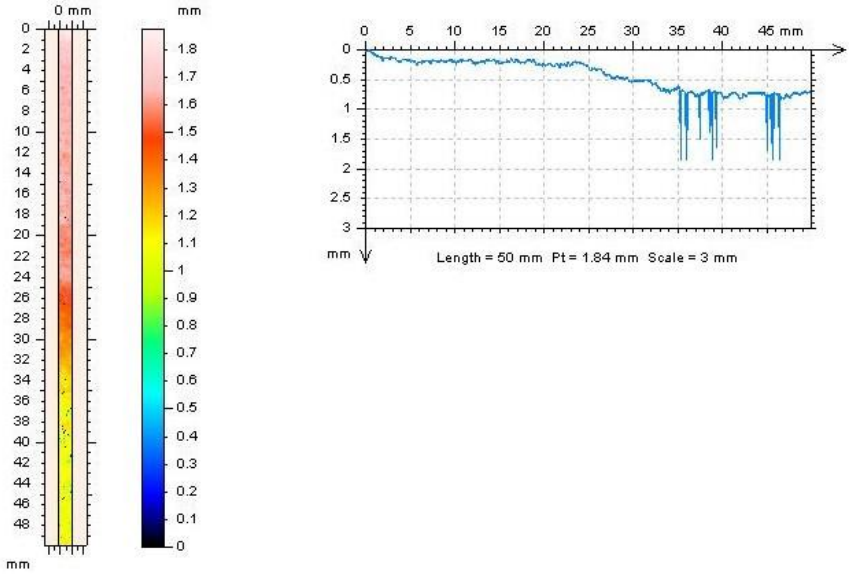

Figure 97: Surface Roughness of 1018 steel at MCBH (1018 steel on-top 2FX7). LEFT: Area spectra. RIGHT: Depths along length of sample.

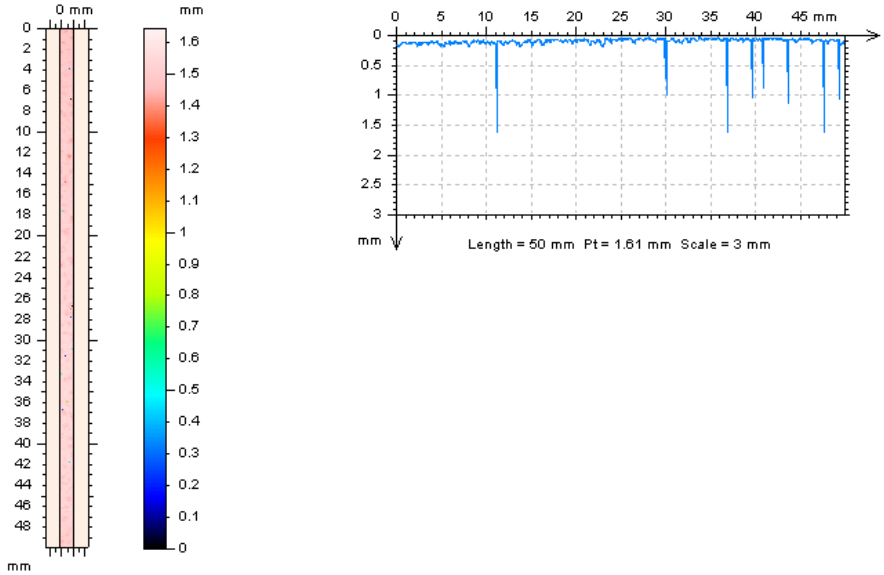

Figure 98: Surface Roughness of 1018 steel at Kilauea (uncoupled 3F1). LEFT: Area spectra. RIGHT: Depths along length of sample.

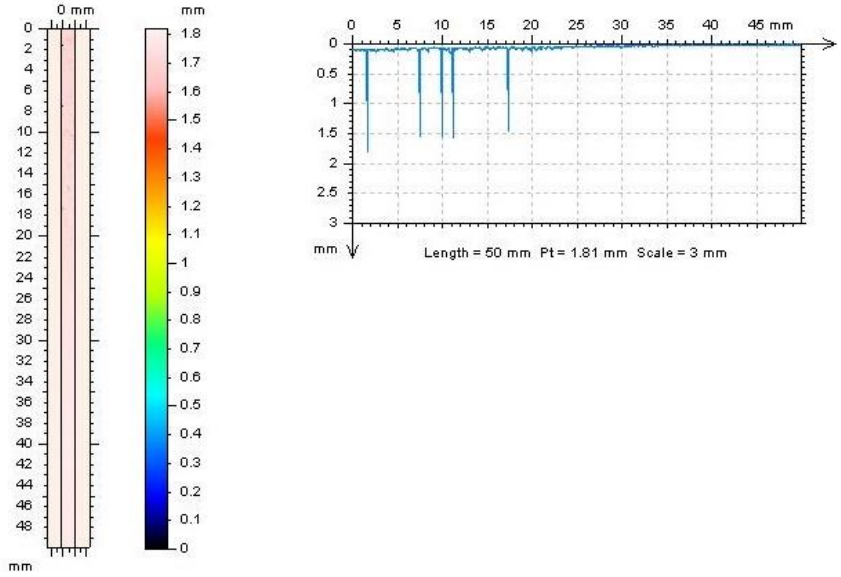

Figure 99: Surface Roughness of 1018 steel at Kilauea (1018 steel on-top 3FL1). LEFT: Area spectra. RIGHT: Depths along length of sample.

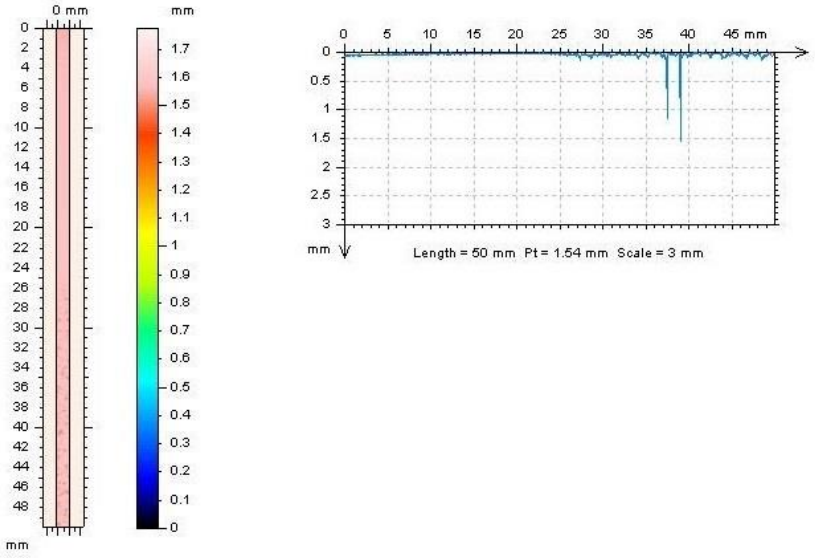

Figure 100: Surface Roughness of 1018 steel at Kilauea (AA 6061-T6 on-top 3FX2). LEFT: Area spectra. RIGHT: Depths along length of sample.

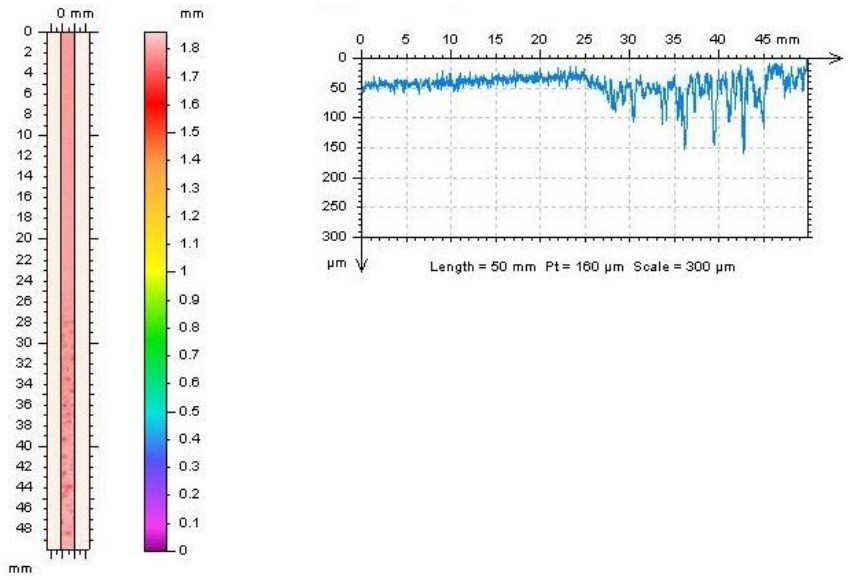

Figure 101: Surface Roughness of 1018 steel at Kilauea (1018 steel on-top 3FX7). LEFT: Area spectra. RIGHT: Depths along length of sample.

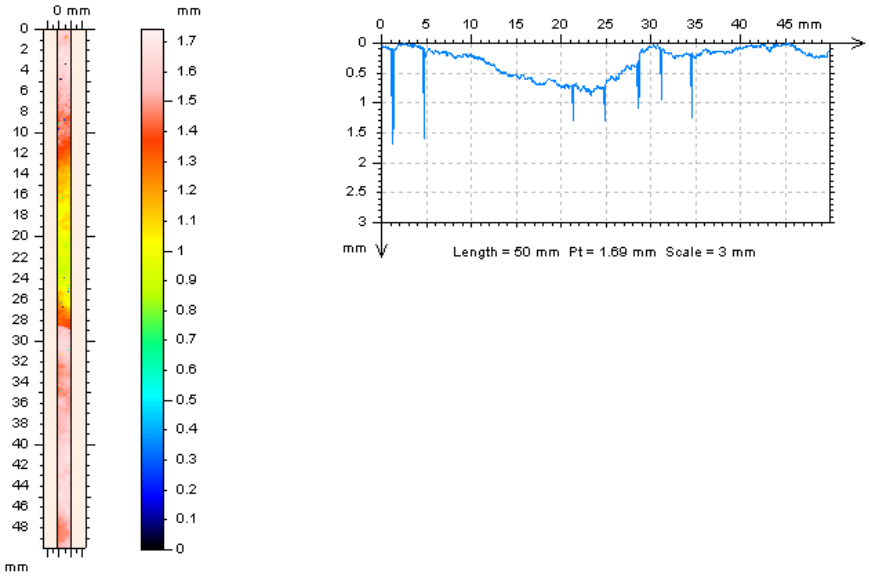

Figure 102: Surface Roughness of 1018 steel at CCTC (uncoupled 4F2). LEFT: Area spectra. RIGHT: Depths along length of sample.

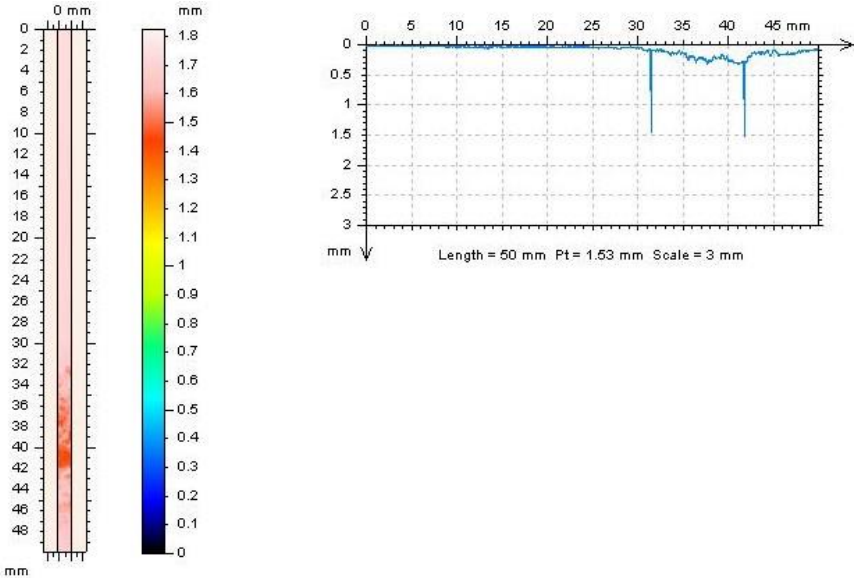

Figure 103: Surface Roughness of 1018 steel at CCTC (AA 6061-T6 on-top 4FL2). LEFT: Area spectra. RIGHT: Depths along length of sample.

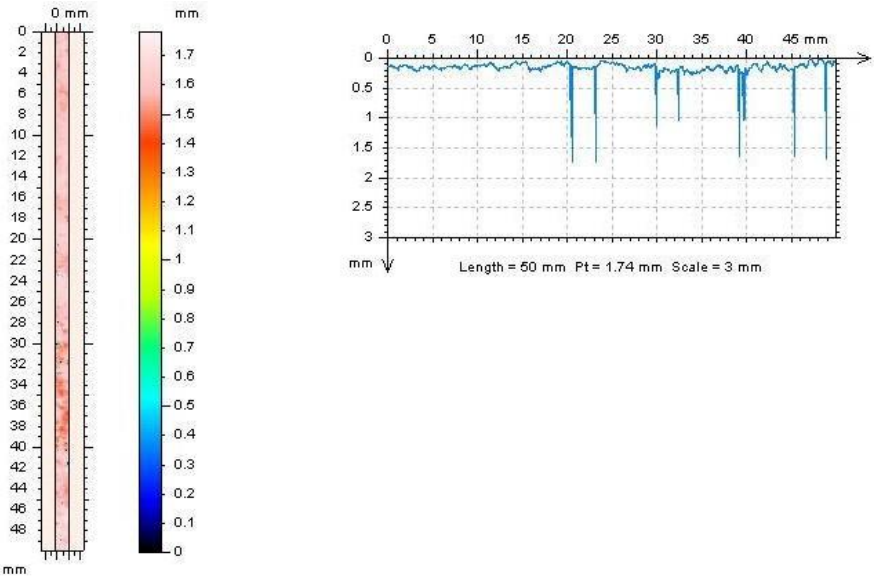

Figure 104: Surface Roughness of 1018 steel at CCTC (1018 steel on-top 4FL6). LEFT: Area spectra. RIGHT: Depths along length of sample.

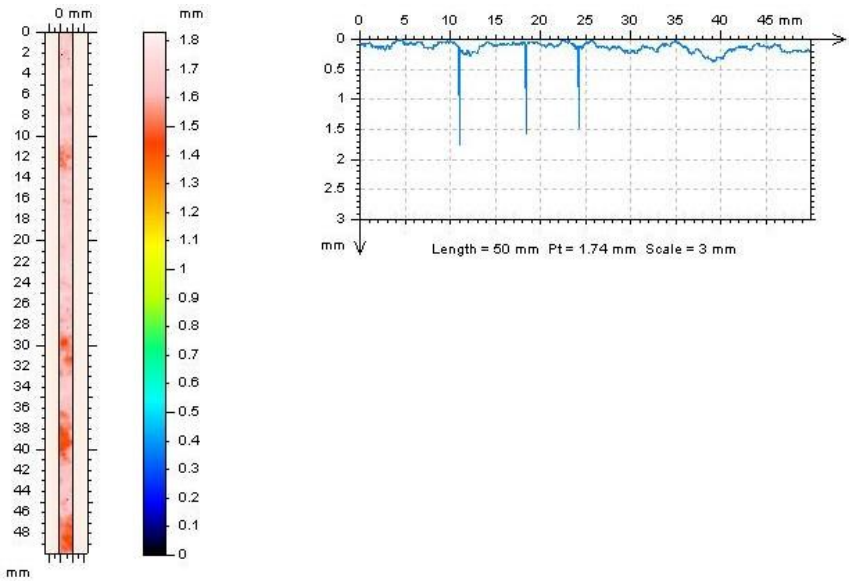

Figure 105: Surface Roughness of 1018 steel at CCTC (AA 6061-T6 on-top 4FX3). LEFT: Area spectra. RIGHT: Depths along length of sample.

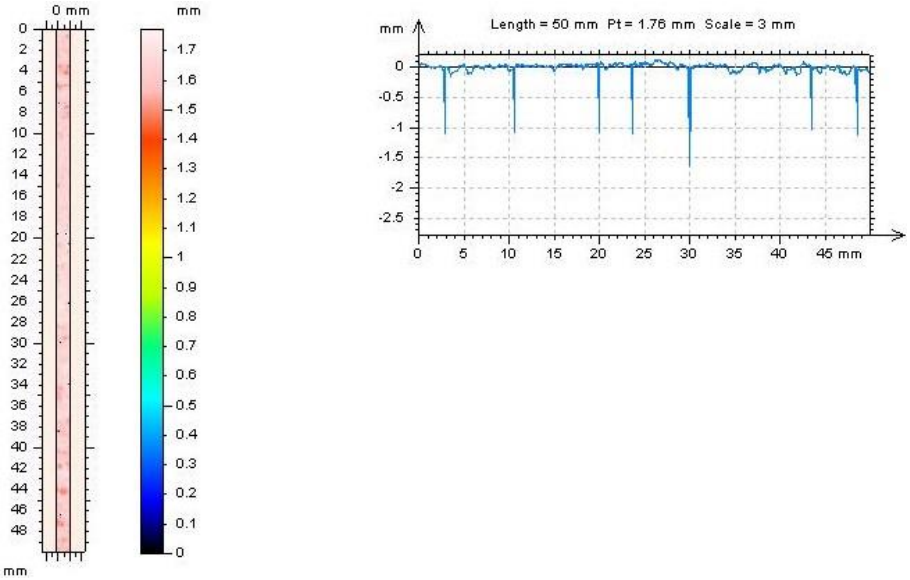

Figure 106: Surface Roughness of 1018 steel at CCTC (1018 steel on-top 4FX5). LEFT: Area spectra. RIGHT: Depths along length of sample.

5 Discussion

5.1 Within site: MCBH, Kilauea, Lyon Arboretum, CTCC

The environmental impact on corrosion in various exposure sites and controls was of interest in this study. Each site provided insight on corrosion rates by various corrosive aggressors, such as chlorides, sulfates, and the effects of simulated long-term exposure.

5.1.1 Lyon Arboretum

Lyon Arboretum is a rainforest environment that is best characterized by the natural, organic materials and humid, wet climate. The location is far from the ocean which minimizes chlorides in the environment. Thus, this location was expected to have the lowest corrosion rates, due to halogens, across the board. Based on the penetration rates calculated in

Table 2 through Table 6, the Lyon Arboretum generated the lowest or one of the lowest penetration rates. Based on those penetration rates, the general ranking from smallest to largest is Ti 6Al-4V <316 stainless steel< pure Ag<pure Cu< 1018 steel. From the XRD analysis, the spectra produced for all samples in this location show that majority of the similar peaks with coupled spectra indicating peaks indicative of its own metal/alloy. With pure Cu, Ti 6Al-4V , and 316 stainless steel, an additional peak at 18.5 was part of the spectra and likely $Al(OH)_3$ contributed from contamination of the anode (Al) onto the cathode.

5.1.2 Marine Corp Base Hawaii

Exposure to the MCBH, a location high in chlorides (Cl^-), samples are in a highly corrosive environment. The chlorides could induce pitting that normally occurs for passivating alloys such as Ti 6Al-4V and 316 stainless steel. Because of this, the expectation is that the exposed specimen would show signs of chlorides on the surface as well more corrosion products (i.e., oxides).

5.1.3 Kilauea

Kilauea Volcano park exposes specimens to an environment high in sulfur, due to the release of sulfur-dioxide – a natural occurrence for volcanoes – resulting in acid rain. The expectation was to see evidence of sulfur-containing products on the surface of the samples as well as reduced amount of oxide buildup (due to acid etching) that were scanned using the XRD. However, the only species that resulted in a by product of sulfur was Cu in the form of copper sulfite. The pure Ag samples showed traces of AgCl on its surface due to airborne chlorides from the coastline. Similar to the other locations, Ti 6Al-4V showed the least amount of mass loss followed by 316 stainless steel, pure Cu, pure Ag, and 1018 steel.

5.1.4 Cyclic Corrosion Test Chamber

The CCTC simulates highly corrosive environment through a series of spraying of a saltonto the samples and drying cycles. Due to the various salt mixtures that were utilized, sodium bicarbonate and calcium carbonate precipitate were not unusual or unexpected. Despite this expectation, the only species that demonstrated peaks for $CaCO_3$ was pure Ag and 316 Stainless Steel. The other three species exhibited corrosion by-product in their resulting spectra; and all but 1018 steel produced a peak at approximately 18.5 that again is suspected to be caused by contamination of Al. The penetration rate rating was the same as the other three sites.

5.2 Comparison Between Sites

Further comparison and analysis was done for each of the metals and alloys of interest. Each metal and alloy was assessed individually both quantitatively and qualitatively.

5.2.1 Copper

The pure copper samples experienced a small amount of mass loss due to corrosion. The samples exposed to the MCBH had a blue-ish surface (patina), indicative of corrosion of copper, on the areas that were not covered by either the fastener or the AA6061-T6 sample. Visually, it appears as if the entire surface of those samples at the MCBH had severe corrosion, however, the penetration rate at this site was about half of the GM 9540P. In Figure 6, the Cu exposed to MCBH showed evidence of not just Cu, but CuO and patina that can be seen in Table 9 with the speckles of black (CuO) and blue (patina) in the crevice area. At Kilauea, these samples showed evidence of brochantite (Cu_4SO_4 $(OH)_6$) from the XRD spectra and seen by the darker layer shown in Table 10. The CCTC, Table 11, visually showed the uncoupled sample with a very dark black layer and coupled samples with those same black and blue speckles as MCBH.

The same blue hued patina is visually observed on the AA6061-T6 coupons seen in Table 24, Table 25, and Table 27. Thus, it is likely that the unidentified peaks at approximately 18.5-19.0 on the XRD spectra for Cu at Lyon Arboretum, MCBH, and CCTC are attributed to $Al(OH)_3$ cross-contamination.

The calculated penetration rates found that the locations that produced the lowest to highest rates are as follows: Lyon Arboretum, Kilauea, MCBH, and CCTC, which could be indication that Cu is more susceptible to chlorides rather than acid rain. Also, since the pure copper was coupled to AA 6061-T6, environments that depolarize or corrode AA 6061-T6 will likely make the AA 6061-T6 a more efficient sacrificial anode for the copper.

5.2.2 Silver

Silver being the most noble of the metals did experience a lower corrosion rate than its noble counterpart, pure Cu. However, pure Ag did not fair as well as the 316 stainless steel and Ti 6Al-4V samples. The XRD spectra demonstrate how readily pure Ag will react with the environment to produce AgCl. However, from Table 12 through Table 15, the samples show evidence of a black patina that is more likely a silver sulfide. Silver sulfide XRD peaks, however, were unable to be identified. The couples did demonstrate a decrease in the resulting penetration rate, about half the uncoupled rate.

5.2.3 Ti 6Al-4V

Ti 6Al-4V alloy resulted in the least corrosion for all test sites. In fact, all but the uncoupled Kilauea samples had gained mass, resulting in negative penetration rates as seen in Table 4 . The cleaned samples showed signs of product on the interfacial side despite having been cleaned ultrasonically. From Table 44 through Table 47, the samples that were coupled to

AA6061-T6 without a logger exhibited the most surface variation. Further comparison can be drawn that the Lyon Arboretum produced the least visually affected coupons whereas the MCBH showed more signs of interaction between the two metals for the natural environments. The CCTC resulted in coupons that were the most visually affected by the coupling and chamber for all configurations and specifically in the non-interfacial surfaces. The coupons that were coupled to AA6061-T6 with the logger showed little to no effect on the overlapping surfaces for all sites. This can be attributed to the insulating piece that was placed between the two surfaces that prevented direct metal-to-metal contact between the Ti 6Al-4V and the AA 6061-T6 (these samples were still galvanically coupled through the logger).

5.2.4 316 Stainless Steel

316 stainless steel had the second least amount of corrosion rate. In addition, the peaks displayed in the XRD spectra of Figure 4, Figure 9, Figure 15, and Figure 19 were consistent and indicated the alloy. However, for MCBH did have potential signs of NaCl that could be cause for the higher penetration rates at MCBH compared to the other three locations. The 3D profilometry reaffirmed that the surfaces of the 316 stainless steel sample were smooth and that pitting was not a major concern in corrosion of this species.

5.2.5 1018 Steel

1018 steel demonstrated the highest corrosion rate quantitatively. Similarly, Table 52 through Table 55 show the severe pitting that the samples underwent throughout each site. Interestingly, the cleaned samples that were exposed to Kilauea showed a clear delineation of the crevice where it was coupled with AA6061-T6 and where the fastener had contacted with the surface for all orientations of the coupling. The corrosion was more severe outside of the crevice. After those surfaces were cleaned, the topography was rather smooth in the crevice area;

whereas, that of the samples exposed to the other three sites was more extreme with peaks and divots throughout the surface of the sample. Furthermore, from Table 6, the penetration rates of the coupons at Kilauea were the smallest, though the uncoupled penetration rate was higher than that of the Lyon Arboretum. The results from the three other test sites also show history of the crevice area as well as the fastener contact. However, the distinction is less defined as it was for Kilauea and the orientations with the logger showed a more distinctive crevice area. This is likely attributed to the set up, with the insulating material that was placed between the two metals. In addition, the resulting corrosion on the 1018 steel samples from each site other than Kilauea demonstrated massive and uneven corrosion. From Figure 98 through Figure 101, the cleaned samples show a topography with depths that range from 150 microns to 2mm. The large depths can be seen visually, especially when the samples are viewed from the side. The surfaces can be characterized as rough and erratic.

Consistently across all four test sites, from Table 6, the samples with greatest to least penetration rate corresponded to the coupled without logger AA6061-T6 on top, coupled without logger 1018 steel on top, and coupled with logger 1018 steel on top, in that order.

The corresponding AA 6061-T6 couples also shows signs of contamination on the surface of the metal. From Table 32 through Table 35**Error! Reference source not found.**, the AA 6061-T6 samples were found to have the reddish hued corrosion byproduct on the surface, indicative of transference of the rust onto the aluminum.

5.3 Analysis of Corrosion Rates and Predictions

The determination of the corrosion of coupled metals was investigated. Calculations were made to predict the corrosion rate of the coupled samples based on the corrosion rates of the uncoupled samples and the orientation and exposure area.

$$CR_{predicted} = \frac{CR_{uncoupled,actual}\alpha_{exposed}}{\alpha_{total}} \quad \text{(Eq. 7)}$$

where $CR_{uncoupled,\ actual}$ is the measured CR for the uncoupled sample, $\alpha_{exposed}$ is the surface area of the sample without the crevice area, and α_{total} is the total surface area of the sample. The equation above indicates that the region inside of the crevice of the cathode material is not corroding and the region outside of the crevice corrodes at the same rate of the uncoupled coupon.

$$Predicted\ CR\ Ratio = \frac{CR_{actual}}{CR_{predicted}} \quad \text{(Eq. 8)}$$

The resulting ratios of the predicted corrosion rates to the actual measured corrosion rates are shown in the following tables. If the ratio is close to unity, that indicated that the crevice region of the cathode was cathodically protected by the anode AA6061-T6, and the regions outside of the crevice corroded at the normal rate of the uncoupled coupon. If the actual-to-predicted ratio is much greater than unity, that could indicate that the cathode metal was subjected to crevice corrosion in the contact region with the AA6061-T6, or the region outside of the crevice corroded at a rate greater than that of the uncoupled coupon. If the actual-to-predicted ratio is much less than unity, that could indicate that the cathode metal was not subjected to crevice corrosion in the contact region with the AA6061-T6, and the region outside of the crevice also corroded at a rate less than that of the uncoupled coupon.

Table 56: Ratio of predicted to actual penetration rate of pure Cu coupled to AA6061-T6.

	Coupled with logger	Coupled without logger

Exposure site	AA 6061-T6 on top 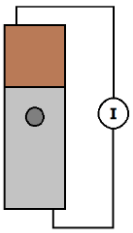	Cu on top 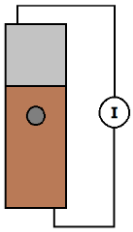	AA 6061-T6 on top 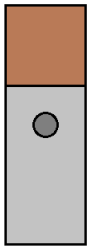	Cu on top 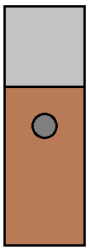
CCTC	5.77E-01	6.01E-01	4.70E-01	4.11E-01
MCBH		5.39E-01	5.46E-01	5.98E-01
LA		4.80E-01	3.37E-01	4.59E-01
KIL		5.46E-01	5.28E-01	5.07E-01

Table 57: Ratio of predicted to actual penetration rate of pure Ag coupled to AA 6061-T6.

Exposure site	Coupled with logger		Coupled without logger	
	AA 6061-T6 on top	Pure Ag on top	AA 6061-T6 on top	Pure Ag on top
	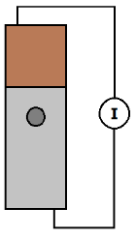	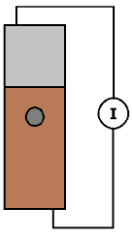	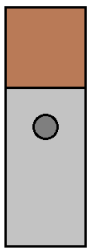	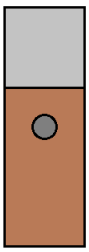
CCTC	6.83E-01	5.08E-01	1.68E+00	9.57E-01
MCBH		4.42E-01	2.88E-01	3.33E-01
LA		2.95E-01	2.39E-01	2.88E-01
KIL		2.58E-01	3.01E-01	2.60E-01

Table 58: Ratio of predicted to actual penetration rate of Ti 6Al-4V coupled to AA 6061-T6.

Exposure site	Coupled with logger		Coupled without logger	
	AA 6061-T6 on top	Ti 6Al-4V on top	AA 6061-T6 on top	Ti 6Al-4V on top
	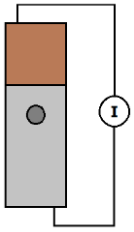	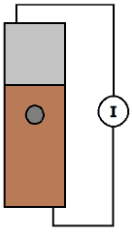	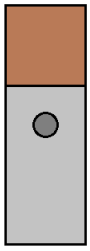	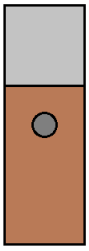
CCTC	7.38E+00	3.62E+00	1.67E+01	5.61E+00
MCBH		8.53E+00	2.82E+01	3.46E+01
LA		1.84E+00	1.54E+01	7.93E+00
KIL		CR/0	CR/0	CR/0

Table 59: Ratio of predicted to actual penetration rate of 1018 steel coupled to AA 6061-T6.

Exposure site	Coupled with logger		Coupled without logger	
	AA 6061-T6 on top	1018 steel on top	AA 6061-T6 on top	1018 steel on top
	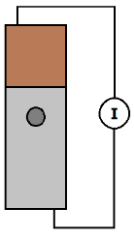	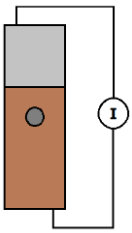	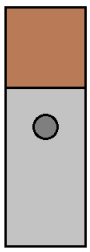	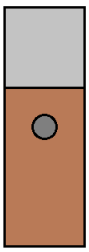
CCTC	5.12E-01	5.80E-01	7.26E-01	6.71E-01
MCBH		5.19E-01	5.84E-01	5.33E-01
LA		1.28E+00	1.36E+00	1.35E+00
KIL		7.56E-01	8.12E-01	7.86E-01

Table 60: Ratio of predicted to actual penetration rate of 316 SS coupled to AA 6061-T6.

Exposure site	Coupled with logger		Coupled without logger	
	AA 6061-T6 on top	316 SS on top	AA 6061-T6 on top	316 SS on top
	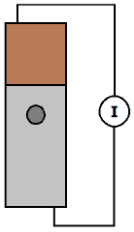	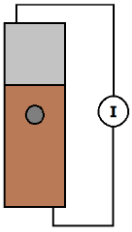	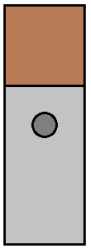	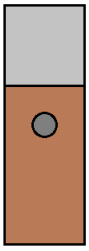
CCTC	1.18E+00	7.40E-01	8.87E-01	5.92E-01
MCBH		1.40E-01	1.95E+02	-1.14E+01
LA		1.24E+00	1.24E+00	1.66E+00
KIL		1.04E+00	8.87E-01	7.40E-01

The predicted ratios yielded values that were in the range of 0.1 to 10, within one order of magnitude from unity, with the exception of the coupled 316 stainless steel samples without a logger and Ti 6Al-4V samples without loggers. The 316 stainless steel samples without a logger at MCBH produced both the highest and lowest values—195, two order of magnitudes above unity, and -11.4, the only negative ratio produced. Simultaneously, 316 stainless steel had resulting ratios for the other three sites (Lyon Arboretum, Kilauea, and CCTC) that were overall closest to unity. The 1018 steel ratios produced were overall closest to unity within ±0.5, and smaller than unity for all but the Lyon Arboretum samples. Conversely, the predicted ratios of Ti 6Al-4V were the farthest away from equating to one—with MCBH samples ratios much larger than unity. This can be attributed to crevice corrosion or that the area past the crevice area corroded at a higher rate than the uncoupled sample. In addition, due to the zero corrosion rate of the uncoupled samples at Kilauea, any corrosion would produce a ratio infinitely large. Thus, the very large values for Ti 6Al-4V may also be a product of the cleaning, as it may be inconsistent or ineffective.

The noble metals, pure Cu and pure Ag, produced ratios that were less than one, except pure Ag without a logger at CCTC. Pure Cu produced the most consistent ratios across all four sites at approximately 0.5. The samples without a logger at CCTC had smaller ratios than their coupled with logger counterparts. This result could be a result of AA 6061-T6 sacrificing itself, as the ratios both differed by at least 0.1. Pure silver, however, yielded predicted ratios that were larger for the samples without the logger than those with the logger, at CCTC. The other three environmental test sites resulted in small ratios, less than 0.5. This could be a result of the AA 6061-T6 effectively protecting the pure Ag samples.

Generally, the samples without loggers had values smaller than unity that could be attributed to a lower corrosion rate of the area outside the crevice area—that could imply that the cathodic protection of AA 6061-T6 extended beyond the crevice region. Those samples that had raios larger than unity could have experienced higher crevice corrosion, potentially from the cross contamination with AA 6061-T6 or a higher corrosion rate of the outside region compared to the uncoupled sample.

6 Conclusion

The effect of galvanic corrosion of the AA 6061-T6 was found to have generally decreased the penetration rates of the cathodic metals and alloys it was coupled to. The species that best illustrated the cathodic protection by the AA6061-T6 was 1018 steel, as the corrosion rates for all coupled orientations was less than the uncoupled corrosion rates. The results from coupled Ti 6Al-4V samples yielded negative corrosion rates, which implied that the Ti 6Al-4V gained weight rather than loss weight. The uncoupled samples also returned negative corrosion rates that may be attributed to the inability of the cleaning procedure (ultrasonic cleaning for Ti 6Al-4V) to remove a buildup of surface oxide. Generally, the orientation of the couples did affect the corrosion rates. For instance, nearly all the couples with AA6061-T6 on top produced more corrosion of the cathode than those that had the cathode oriented on top for those exposed to Kilauea and CCTC. The calculated average penetration rates produced a hierarchy in ascending order starting with Ti 6Al-4V , followed by 316 stainless steel, pure Ag, pure Cu, and finally, 1018 steel with the highest rates, for all four locations.

The four locations studied provided insight on the corrosion byproduct and the readiness of these chemical reactions. The macroscopic and XRD analysis provided evidence of the following: corrosion products at Lyon Arboretum were primarily oxides and hydroxides due to the availability of oxygen and water. At MCBH, chlorides, oxides, hydroxides, and carbonates were identified resulting from the exposure to airborne sea salt. At Kilauea, the high levels of sulfur dioxide and sulfates, and moderate levels of chlorides (due to the proximity to the sea) yielded corrosion products of varying compositions: sulfate, oxide, chloride, and hydroxide. Finally, CCTC revealed similar products to MCBH with the evidence of calcium carbonate from

the salt spray utilized in the procedure. The corrosion products align with the expectations from the availability of the corrosive aggressors (i.e., Cl^-, SO_4^{2-}).

Surface analysis portrayed the effects of pitting corrosion and contamination by Al. 3-D profilometry showed the resulting surface roughness after the exposed samples were cleaned. Notably, 1018 steel samples, primarily at Kilauea showed severe pitting in the non-interfacial region for those coupled samples. For the sample that had the logger attached, the resulting smooth surface of the interfacial side indicated the insulating piece and crevice shielded the region from sulfur dioxide. The coupled samples without the logger also resulted in a smoother surface in the crevice region than the exposed surfaces, though the crevice did indicate more inconsistencies and roughness than that of the logger sample. The 3-D profilometry results from the other species displayed the smoothness of the surface, though not flat. The macroscopic scans further validate the types of corrosion products on both the uncoupled and coupled samples. Particular attention to the interfacial region showed signs of those previously mentioned corrosion product that are identified by color characteristics. Similarly, many of those same corrosion products were then identified on the interfacial area of those associated AA6061-T6 coupons.

Finally, the attempt to predict the corrosion rates based on the theory provided for cathodic protection. The 1018 steel species produced ratios that were overall the closest to unity, while pure Cu resulted in ratios not near unity but consistent across all sites. Interestingly, the ratios calculated for the Ti 6Al-4V samples produced the least accurate predicted corrosion rates to actual at the CCTC. In addition, Ti 6Al-4V also produced a corrosion rates that were infinitely larger than the predicted rates at Kilauea. Most of the predicted corrosion rate ratios produce, aside from Ti 6Al-4V, were smaller than unity. Therefore, it is assumed that the areas not in

contact with the anode did not corrode and that the area outside of the crevice region corroded at a rate less than its uncoupled counterpart. This modeled behavior could be a result of cathodic protection—where AA 6061-T6 acts as a sacrificial anode and its protection goes beyond the assumed region—that is, the crevice. The disparities in the predicted ratios from unity may signify that there are other actions taking place beyond the assumptions of cathodic protection, galvanic corrosion, and local corrosion.

References

[1] NACE International, "Galvanic Corrosion," 13 February 2018. [Online]. Available: https://www.nace.org/Corrosion-Central/Corrosion-101/Galvanic-Corrosion/.

[2] F. W. Gibbs, "Encyclopedia Britannica," 2018. [Online]. Available: https://www.britannica.com/biography/Sir-Humphry-Davy-Baronet. [Accessed 11 March 2018].

[3] R. W. Revie and H. H. Uhlig, Corrosion and Corrosion Control, Hoboken: John Wiley & Sons, Inc., 2008.

[4] D. P. Doyle and T. E. Wright, "Quantitative Assessment of Atmospheric Galvanic Corrosion," in *Galvanic Corrosion, ASTM STP 978*, Philadelpia, H.P. Hack, Ed., American Society for Testing and Materials, 1988, pp. 161-173.

[5] F. Masnfeld and J. Kenkel, "Galvanic corrosion of aluminum alloys. II. Effect of solution composition," *Corrosion Science,* vol. 15, no. 3, pp. 183-98, 1975.

[6] R. Francis, "Galvanic corrosion of high alloy stainless steels in sea water," *British Corrosion Journal,* vol. 29, no. 1, p. 53, 1994.

[7] K. Quiambao, "Galvanic Corrosion of Aluminum Coupled to Passivating and Non-passivating Alloys," Honolulu, 2016.

[8] ASM Aerospace Specification Metals, "ASM Material Data Sheet," MatWeb, LLC., [Online]. Available: http://asm.matweb.com/search/SpecificMaterial.asp?bassnum=MQ316Q. [Accessed May 2018].

[9] ASM Aerospace Spcification Metals, "ASM Material Data Sheet," MatWeb, LLC., [Online]. Available: http://asm.matweb.com/search/SpecificMaterial.asp?bassnum=mtp641. [Accessed May 2018].

[10] MatWeb Material Property Data, "AISI 1018 Steel, cold drawn," MatWeb, LLC., 2018. [Online]. Available: http://www.matweb.com/search/DataSheet.aspx?MatGUID=3a9cc570fbb24d119f08db22a53e2421&ckck=1. [Accessed May 2018].